



No.15

JLCA

NEWS LETTER

Life-Cycle Assessment Society of Japan

LIME2

Life-cycle Impact assessment Method based on Endpoint modeling

Chapter 2 : Characterization and Damage Evaluation Methods

2.1 Ozone layer depletion

2.2 Global warming

2.3 Acidification

LIME2

Life-cycle Impact assessment Method based on Endpoint modeling

Chapter 2 Characterization and Damage Evaluation Methods

2.1 Ozone layer depletion

2.2 Global warming

2.3 Acidification

written and edited by

Dr.Norihiro ITSUBO

(Associate Professor, Faculty of Environmental and Information Studies,
Tokyo City University)

Dr. Atsushi INABA

(Professor, Faculty of Engineering, Kogakuin University)

Chapter II

Characterization and Damage Evaluation Methods

Contents

2.1	Ozone layer depletion	1
2.1.1	What phenomenon is ozone layer destruction?	1
(1)	Cause of ozone layer destruction	1
(2)	Endpoints of ozone layer destruction	3
2.1.2	Characterization of ozone layer depletion	5
(1)	Existing characterization factors for ozone layer depletion	5
(2)	Characterization factor of ozone layer destruction under LIME	6
2.1.3	Damage assessment from ozone layer destruction	7
(1)	Basic policy for calculation of damage factors.....	7
(2)	Examination for calculation of damage functions for all types of ODS.....	9
(3)	Relation between emission of ODS and the amount of UV-B reaching the ground.	9
(4)	Human health: damage functions for skin cancer.....	16
(5)	Human health: damage functions for cataract	18
(6)	Primary production: damage functions for the terrestrial ecosystem	20
(7)	Primary production: damage functions for the aquatic ecosystem	21
(8)	Social assets: damage functions for agricultural production	24
(9)	Social assets: damage functions for wood production.....	25
(10)	Arrangement of damage functions of ozone layer destruction and damage factors	25
2.1.4	Procedure for impact assessment of ozone layer destruction	27
2.2	Global warming	31
2.2.1	What phenomenon is global warming?	31
(1)	Cause of global warming	32
(2)	Endpoints of global warming.....	33
2.2.2	Characterization of global warming	38
(1)	Characterization factors for global warming	38
(2)	Characterization factors for global warming under LIME	39

2.2.3	Damage assessment of global warming.....	40
(1)	Basic policy for calculation of damage factors.....	41
(2)	Calculation of temperature change due to GHG emissions.....	51
(3)	Human health: damage function for heat stress.....	53
(4)	Human health: damage function for infection	55
(5)	Human health: damage function for disaster damage.....	57
(6)	Human health: damage function for malnutrition/starvation.....	57
(7)	Social assets: damage function for agricultural production.....	59
(8)	Social assets: damage function for energy consumption	62
(9)	Social assets: damage function for land loss	66
(10)	Regionality in the damage function for global warming	69
(11)	Arrangement of the damage functions for global warming.....	70
2.2.4	Procedure for impact assessment of global warming	74
 2.3	Acidification	80
2.3.1	What phenomenon is acidification?.....	80
(1)	Cause of acidification	80
(2)	Endpoints of acidification.....	82
2.3.2	Characterization of acidification.....	83
(1)	Characterization factor for acidification under the existing LCA method.....	83
(2)	Characterization factor for acidification under LIME	85
2.3.3	Damage assessment of acidification	90
(1)	Basic policies for damage factor calculation and uncertainty assessment.....	90
(2)	Primary production: damage functions for terrestrial primary production.....	94
(3)	Social assets: damage function for fishery production.....	101
(4)	Social assets: damage functions for wood production.....	107
(5)	Social assets: damage functions for materials	107
(6)	Damage factors for acidification.....	108
2.3-4	Procedure for impact assessment of acidification	110

Chapter II

Characterization and Damage Evaluation Methods

2.1 Ozone layer depletion

2.1.1 What phenomenon is ozone layer destruction?

(1) Cause of ozone layer destruction

Ozone (O_3) is a gaseous body made from combination of three oxygen atoms. Ninety percent of the ozone in the atmosphere exists in the stratosphere (WMO 1999). However, there is no clearly defined layer as associated with the name stratospheric ozone layer. The stratospheric ozone layer is a layer that lies about 15 to 50 km high in the stratosphere and where the density of ozone is relatively high. The density of ozone is the highest at an altitude of about 20 to 25 km (Ogura 1999).

Because ultraviolet rays from the sun are strong in the stratosphere, an oxygen molecule absorbs ultraviolet rays and photo-dissociates into two oxygen atoms. These oxygen atoms combine with other oxygen molecules into ozone. Meanwhile, an ozone molecule absorbs ultraviolet rays and photo-dissociates into an oxygen molecule and an oxygen atom. That is, ozone absorbs ultraviolet rays during both processes of formation and resolution. This effect is more conspicuous when ultraviolet rays have a shorter wavelength and higher energy. As the wavelength of ultraviolet rays become shorter, ultraviolet rays give stronger damage to living things, which can live on the earth because the stratospheric ozone layer blocks ultraviolet rays with a short wavelength. If the atmosphere were compressed under standard conditions (0°C , 1 atmosphere), the thickness between the surface of the earth and the ceiling would be about 8 km. Ozone would occupy only 3 mm of the thickness (Asakura et al, 1995). However, because this is a result of ozone's absorption of ultraviolet rays through the processes of formation and resolution, it is useless to worry so long as the thickness of the ozone layer is maintained.

However, the emergence of ozone-depleting substances (ODSs) completely changed the condition of the stratospheric ozone layer. When hydrogen that is an element of hydrocarbon is partially or completely substituted with fluorine (F), chlorine (Cl), bromine (Br) or iodine (I), a hydrocarbon is changed to a halocarbon. Halocarbon that contains Cl, Br, or I can become an ODS (Table 2.1-1). ODSs exist in the natural world, such as methyl chloride (CH_3Cl). However, ODSs that have strong impact are artificial substances – especially, chlorofluorocarbons (hereinafter referred to as “CFCs”) and bromofluorocarbons (hereinafter referred to as “Halons”). Because CFCs and others have industrially excellent characteristics, such as non-combustibility, low toxicity, low thermal conductance, volatility, liquefiability, and low surface tension, they were consumed in large amounts as cooling media, blowing agents, detergent solvents, sprays, extinguishing agents, etc. Later, however, it became clear that CFCs emitted into the atmosphere are not resolved in the troposphere, reach the stratosphere by the global atmospheric circulation, and are resolved by strong ultraviolet rays in the stratosphere, resulting in the liberation of Cl and Br. Cl atoms and Br atoms liberated from ODS catalytically resolve O_3 molecules one after another. As a result, ozone decreases in the stratosphere. This is called ozone layer depletion. However, the actual chemical reaction occurring in the stratosphere is more complex. For details of the cause of

formation of the so-called ozone hole, see existing materials (Fuwa et al. 2002; Environment Agency's Global Environmental Department 1995).

As ozone decreases in the stratosphere, more ultraviolet rays reach the ground. Ultraviolet rays have a wavelength of 100 to 400 nm and are divided into UV-C (a short wavelength of 100 to 290 nm), UV-B (a medium wavelength of 290 to 320 nm), and UV-A (a long wavelength of 320 to 400 nm) (the range of wavelengths for UV-B is that used for photobiology (Ichihashi et al. 2000)). Because UV-C has a short wavelength, greatly influences living things, and is highly absorbed in the atmosphere, it hardly reaches the ground, even if the amount of stratospheric ozone were to decrease to 10% the amount at present (Asakura et al, 1995). On the other hand, because UV-A is hardly absorbed by ozone, the intensity on the ground scarcely changes even if the amount of stratospheric ozone decreases. That is, the ultraviolet ray whose intensity increases on the ground as a result of ozone layer destruction is UV-B. Because UV-B has strong adverse impact on living things, such as giving damage to DNA, there is concern that an increase in UV-B may have harmful impact on various endpoints, such as human health and the ecosystem (Figure 2.1-1).

Table 2.1-1: Types of halocarbons

Type of substance		Examples of substance			
Generic name	ODS	Examples of substance	ODP (UNEP 2000)	GWP (100 years) (WMO 1999)	Atmospheric lifetime (Years) (WMO 1999)
Fluorocarbon	Chlorofluorocarbon (CFC)	○	CFC-11 CFC-12	1.0 0.82	4600 10600
	Bromofluorocarbon (Halon)	○	Halon-1211 Halon-1301	5.1 12.0	1300 6900
	Hydrochlorofluorocarbon (HCFC)	○	HCFC-22 HCFC-123	0.034 0.012	1700 120
	Hydrobromofluorocarbon (HBFC)	○	HBFC-22B1	0.74	470
	Perfluorocarbon (PFC)	×	CF ₄ C ₂ F ₆	- -	5700 11900
	Hydrofluorocarbon (HFC)	×	HFC-23 HFC-125	- -	12000 3400
	Chlorocarbon	○	CCl ₄ CH ₃ CCl ₃	1.2 0.1	1800 140
Bromocarbon		○	CH ₃ Br	0.6	5
					0.7

- ODS ○: With ozone depleting capability, ×: Without ozone depleting capability
- ODP: Ozone depleting potential (relative value when the ozone depleting capability of CFC-11 is 1). The source is UNEP (2000).
- GWP (100 years): Global warming potential (relative value when the 100-year greenhouse effect of CO₂ is 1). The source is WMO (1999).
- Atmospheric lifetime: the amount of a substance in the atmosphere at a certain point of time less annual loss. The source is WMO (1999).
- ODP for HCFC-123 is the value for a typical isomer (CHCl₂CF₃).
- There are various other substances, such as those including iodine, and both chlorine and bromine.

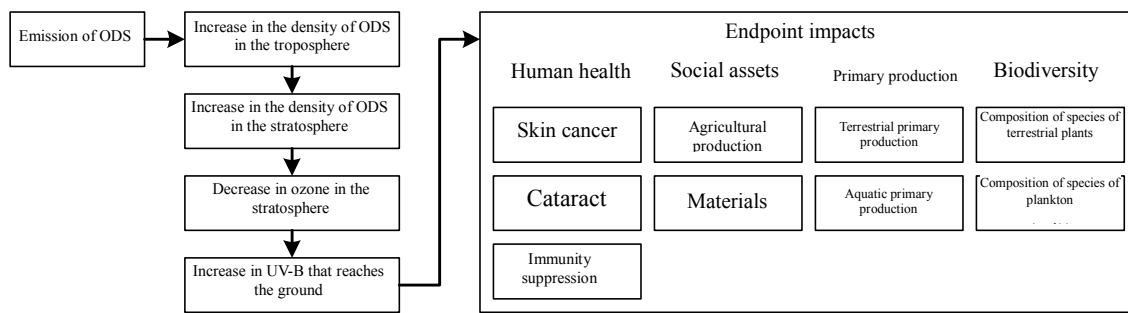


Figure 2.1-1: Cause of ozone layer destruction

(2) Endpoints of ozone layer destruction

a Human health

Although exposure to ultraviolet rays creates vitamin D, it has harmful impact on the skin, eyes, and immune system. The impact of ultraviolet rays can be divided into acute lesions, which appear several hours after exposure and disappear two to three days after, and chronic lesions, which are caused as a result of repeated exposure over a long time (Table 2.1-2). It is especially of concern that ozone layer destruction may cause skin cancer and cataract, both of which are chronic lesions. Although ozone layer destruction is said to have important impact on the immune system, quantitative data are scarce.

UV-B has strong impact on surface skin and inner skin, but does not reach subcutaneous tissues. UV-B gives damage to the DNA of skin cells by inducing photochemical reactions. Usually, however, damage disappears because of living bodies' defense mechanisms (repair of DNA and apoptosis of abnormal cells). However, repeated exposure over a long time increases the probability of mutating cells and increasing the number of mutated cells, eluding the living body's defense mechanism. This may lead to skin cancer. Melanocytes, basal cells, produce melanin mainly through exposure to UV-A. Because melanin absorbs ultraviolet rays, it is one of the important defense protectors against ultraviolet rays. Therefore, the degree of possibility of suffering skin cancer differs according to skin color. Among Caucasians, skin cancer caused by exposure to ultraviolet rays is a common cancer. According to an epidemiological survey (Ferlay et al. 1997), Caucasians' morbidity of skin cancer is about ten times that of members of the Asians and black races.

The crystalline lens of an eye mainly consists of crystalline, special water-soluble protein that has high transparency and refractivity. Although the transparency of a crystalline lens decreases with age, exposure to ultraviolet rays causes polymer coagulation of crystalline protein and worsens the opacity of the lens. If opacity worsens to the extent that the sight is damaged, a cataract occurs, which in the worst case may cause blindness. According to an epidemiological survey (Sasaki et al. 1999), the ratio of persons who suffer opacity of crystalline lenses is higher in lower latitudes, which indicates that there is a positive correlation between the intensity of ultraviolet rays and the morbidity of a cataract. However, according to an epidemiological survey conducted in Hokkaido, Noto, and Okinawa (Sasaki et al. 1999), there is no significant difference between the intensity of ultraviolet rays and the degree of opacity. This seems to be because actual exposure to ultraviolet rays differs depending on differences in climatic conditions and living habits. For example, exposure to ultraviolet rays is caused by not only sunlight but also snow reflection

in snow-covered areas, while people in subtropical areas do not often go out during the time when the solar altitude is high.

Table 2.1-2: Impact of ultraviolet rays on human health

Part	Typical acute lesions	Typical chronic lesions
Skin	<ul style="list-style-type: none"> • Sunburn (accompanied by red spots and pain; caused by UV-B exposure; excessive sunburn becomes a burn or vesicles) • Sunshine allergy 	<ul style="list-style-type: none"> • Photoaging (pigment freckles, pigmented nevus, (light) elastic fiber degeneration) <Light> • Intraepidermal cancer (solar keratosis, etc.) ↓ • Invasive cancer (squamous cell carcinoma, basal cell carcinoma, malignant melanoma, skin cancer) <Heavy>
Eye	<ul style="list-style-type: none"> • Actinic keratitis (a typical case is snow blindness; caused by UV-B exposure) • Solar conjunctivitis 	<ul style="list-style-type: none"> • Cataract (cortical: white turbidity on the surface of a crystalline lens; nuclear: white turbidity at the center of a crystalline lens; one of the causes is long exposure to ultraviolet rays) • Conjunctival lesions, such as pterygium and pinguecula
Immune system	<ul style="list-style-type: none"> • Impact on immunocompetent cells (disappearance or decreased function of epidermal Langerhans cells, lymphocytes, epidermal keratinocytes, or natural killer cells) 	<ul style="list-style-type: none"> • Decline in immune function (it becomes easier to suffer various infectious diseases; a cancer may occur due to a decline in the function to control cancers.)

- Arranged based on the Environment Agency's Global Environmental Department (1995) and Ichihashi et al (2000).

b Impact on the ecosystem

UV-B exposure also has impacts on the ecosystem. At the level of cells, impacts include damage to DNA, obstruction to photosynthesis, abnormal metabolism, and induction to apoptosis.

Although sunlight is essential for plants' photosynthesis, ultraviolet rays included in sunlight is harmful to plants. Because, unlike animals, plants cannot actively avoid ultraviolet rays, terrestrial plants in particular have developed a defense mechanism against ultraviolet rays. An example is the synthesis of antioxidant substances, such as vitamin C. However, UV-B exposure may cause obstruction to the growth of leaves, a harmful impact on reproduction, a decline in dry matter production, a decline in the height of grass, occurrence of chlorosis, an impact on competition due to differences in sensitivity to ultraviolet rays among plant species, etc. Even if the impact is small at the level of individual plant, the total impact may become enormous. Because there are many research cases concerning the impact of UV-B exposure on plants, many qualitative data have been gained concerning each plant species' sensitivity to UV-B (Krupa et al. 1989). However, because the impacts of other factors are strong, it is difficult to assess the impact of UV-B exposure only.

Although it can be thought that the impact of ultraviolet rays on terrestrial animals is similar to that on human health, concrete information is scarce.

Because water absorbs ultraviolet rays well, it is harder for aquatic organisms to receive the impact of ultraviolet rays than terrestrial organisms. However, because water also absorbs visible light necessary for photosynthesis, photosynthesis is active on the surface of oceans and fresh water, where visible light is affluent. Therefore, the nearer the surface, the stronger the impact of ultraviolet rays is. The impact of ultraviolet rays on phytoplankton includes repression of growth, a decline in survival rate, and obstruction to photosynthesis, while the impact of ultraviolet rays on zooplankton also includes a decline in the survival rate and a decline in egg production. At the field level also, a positive correlation has been found between a decrease in stratospheric ozone in the South Pole region and a decrease in the size of krill population (Naganobu et al. 1999).

c Impact on social assets

Ultraviolet rays also have impact on farm products. Although the impact of ultraviolet rays on farm products is similar to that on plants, repression of growth, a decline in yield, and changes in the sensitivity to pathogens and harmful insects are important impacts related to food production. Ultraviolet rays also cause the deterioration, color degradation, and denaturalization of plastic and other materials used in agriculture, resulting in a decline in their strength and a reduction in their useful lives.

2.1.2 Characterization of ozone layer depletion

(1) Existing characterization factors for ozone layer depletion

In LCA so far, the midpoint approach has been mainly adopted for the assessment of ozone layer destruction. Under this approach, a total of products of the inventory of each ODS by the characterization factor for the ODS is calculated and the relative size is assessed.

The indicator that has been frequently used in LCA as a characterization factor of ozone layer destruction is ozone layer destruction potential (ODP) (Solomon et al. 1992). ODP has been adopted for the World Meteorological Organization's (WMO)'s "Scientific Assessment of Ozone Layer Destruction" (WMO 1999) (hereinafter referred to as the "WMO Scientific Assessment") and the "Montreal Protocol on Substances That Deplete the Ozone Layer" (UNEP 2000) (hereinafter referred to as the "Montreal Protocol").

ODP is a result of standardization of the volume of ozone depleted in a certain period after emission of CFC-11, a typical ODS, for a certain period.

$$ODP_T(X) = \int_0^T \delta[O_3](X, t) / \delta[O_3](CFC-11, t) dt \quad (2.1-1)$$

In this equation, ODPT (X) is ODP during the period T for the type X of ODS. $\delta[O_3]$ (X, t) and $\delta[O_3]$ (CFC-11, t) are the volume of ozone depleted at the point of time t by the emission of the unit volume of X and CFC-11 respectively at the point of time 0.

If T is infinite, ODP (ODP^∞) is the ozone depleting capability in the whole period between the emission of X and its disappearance from the atmosphere standardized by CFC-11's ability (WMO 1992). This ODP has been adopted internationally; for example, by the Montreal Protocol.

Meanwhile, because atmospheric lifetime varies among ODS species, ODP differs depending on the integration period – that is, the way of dividing T. This is called time-dependent ODP (Fuwa et al. 2002). This is the same way of thinking as setting three levels (20, 100, and 500 years) for the integration period in global warming potential (GWP), which is used in the field of global warming. When time-dependent ODP is used, even if ODP_{∞} is similar, it is possible to assess separately the impact of ODS species with a short atmospheric lifetime and a strong ozone depleting capability and the impact of ODS species with a long atmospheric lifetime and a weak ozone depleting capability.

Although time-dependent ODP is recommended as a characterization factor of ozone layer destruction in some cases (Nichols et al. 1996), ODP_{∞} is usually used for LCA. It is inferred that this followed international trends.

(2) Characterization factor of ozone layer destruction under LIME

For LIME, we also adopted ODP as the characterization factor of ozone layer destruction. However, because there are several sets of materials for the setting of ODP, we held discussions about the integration period and the sources of ODP as follows and, under LIME, we recommended ODP_{∞} presented in the WMO Scientific Assessment (Asakura et al. 1995) as the characterization factor of ozone layer destruction. The characterization factor is as shown in Appendix 1.

a Integration period

If all the impacts of the emission of ODS are to be taken into consideration, a longer integration period is desirable. However, ODP is greatly different from GWP in that no GWP for an indefinite integration period has been publicly announced, while ODP presented by international organizations is that for an indefinite integration period.

If an integration period is longer, the fluctuation of environmental conditions and the uncertainty of ODP become greater. If the uncertainty of ODP_{∞} is so great as not to be used, ODP_{∞} should not be recommended. However, because the atmospheric lifetime of CFC, which is relatively long, is several decades, and because ODP_{∞} has been presented in the WMO Scientific Assessment (WMO 1999), which has been verified repeatedly, ODP_{∞} can be thought to be so reliable as to be used for LCA. Therefore, ODP_{∞} with an indefinite integration period has been recommended for LIME.

b Sources of ODP

There are two sources of ODP_{∞} : the WMO Scientific Assessment (WMO 1999) and the Montreal Protocol (UNEP 2000). The WMO Scientific Assessment summarizes the latest scientific knowledge. Although its scientific grounds for calculation are clear, it only shows ODP for some types of ODSs. On the other hand, the Montreal Protocol (UNEP 2000), whose purpose is to regulate ODSs internationally, does not show grounds for calculation, but specifies ODP for many types of ODSs. In addition, even if two ODSs are of the same type, the value of ODP is not necessarily the same for both.

With regard to an ODS that contains many types of substances, LCA has so far dealt with typical ODSs. Therefore, instead of increasing the number of types of ODSs, giving priority to an increase in the reliability of ODP for types of ODSs that can be covered by LCA, we

recommended ODP presented in the WMO Scientific Assessment (WMO 1999) as the characterization factor for LIME.

2.1.3 Damage assessment from ozone layer destruction

(1) Basic policy for calculation of damage factors

Under LCA, the midpoint approach that uses ODP as the characterization factor has so far been the main impact assessment method for ozone layer destruction. However, because damage cannot be concretely calculated by the midpoint approach, an endpoint approach is necessary for damage assessment. There are still only two LCA methods that use an endpoint approach for the assessment of ozone layer destruction: the Eco-indicator (Goedkoop et al. 2000), which was developed in Europe; and Environmental Priority Strategies (EPS) (Steen 1999). Under LIME also, we developed an ozone layer destruction assessment method that uses an endpoint approach.

Table 2.1-3: Category endpoints of ozone layer destruction and objects of calculation of damage functions

Area of protection	Category endpoints		Objects of calculation of damage functions	
Human health	Skin cancer	Malignant melanoma (MM), basal cell carcinoma (BCC), squamous cell carcinoma (SCC)	<input type="radio"/>	MM, BCC, SCC
	Cataract	Cortical cataract, nuclear cataract	<input type="radio"/>	Cataract (no distinction of type)
	Immune suppression	Impediment to immunocompetent skin cells	<input checked="" type="checkbox"/>	Scarce quantitative information
Social assets	Agricultural production	Decline in production of farm products, impact on harmful insects and pathogens, etc.	<input type="radio"/>	Agricultural production (soybean, rice, green pea, mustard)
	Wood production	Impact of decline in primary production of wood	<input type="radio"/>	Net primary productivity (NPP) of coniferous forests
	Materials	Deterioration in quality, decline in durability, etc.	<input checked="" type="checkbox"/>	Scarce quantitative information
Primary production	Terrestrial eco-system	Decline in primary production of terrestrial plants	<input type="radio"/>	NPP of coniferous forests
	Aquatic eco-system	Decline in primary production of phytoplankton	<input type="radio"/>	NPP of aquatic plankton in cold zones
Biodiversity	Terrestrial eco-system	Impact on competition among terrestrial plant species	<input checked="" type="checkbox"/>	Scarce quantitative information
	Aquatic eco-system	Impact on the structure of plankton species	<input checked="" type="checkbox"/>	Scarce quantitative information
Other	Climate	Changes in atmospheric chemicals, changes in heat balance in the atmosphere, etc.	-	Secondary impact and scarce quantitative information

LIME defines a quantitative indicator of the relation between inventory and impact on each category endpoint as a damage function and defines a set of damage functions for each area of protection as a damage factor. The category endpoints of ozone layer destruction and the objects of calculation of damage functions are as shown in Table 2.1-3. The table covers almost all important category endpoints mentioned in Section 2.1.1.

Figure 2.1-2 shows the flowchart of calculation of damage functions and damage factor. The damage functions of ozone layer destruction indicate the extent of increase in potential damage quantity with additional emission of the unit quantity of Type X of ODS. For example, if 1 kg of CFC-11 is emitted, how many additional persons will potentially suffer cataract?

An ODS about which quantitative information, such as atmospheric lifetime, can be gained was used for direct calculation of a damage function of ozone layer destruction. The calculation procedure can be summarized as follows: 1) calculating an increase in the amount of UV-B that reaches the ground as a result of emission of a unit amount of ODS, compared with the amount in the base year; 2) calculating an increase in the amount of potential damage that accompanies an increase in the unit amount of the UV-B; 3) combining these increases and calculating an increase in the amount of potential damage as a result of emission of the unit amount of the ODS; and 4) adjusting the increase by the atmospheric lifetime of the ODS. The methodology is as described in Hayashi et al. (2000, 2004).

* Substances whose damage factor cannot be calculated directly

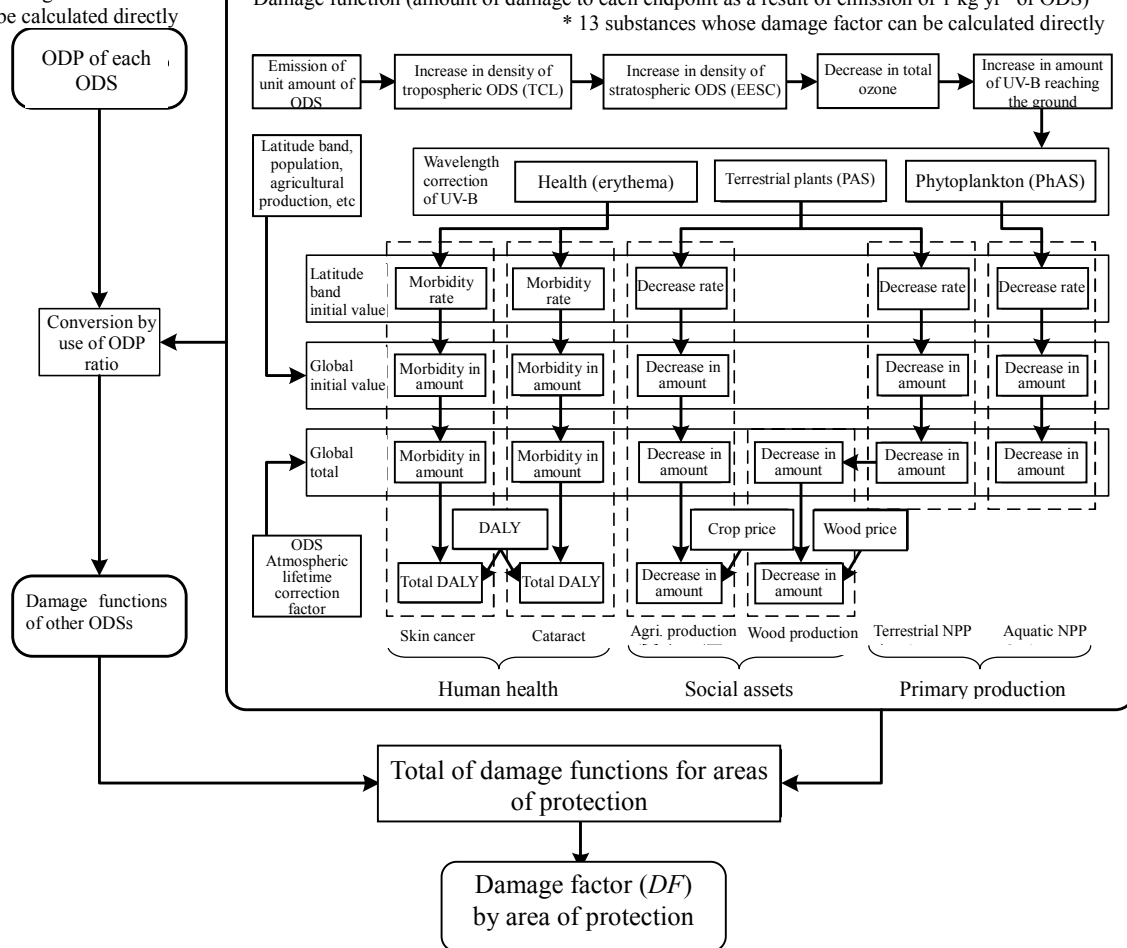


Figure 2.1-2: Flowchart of estimation of damage functions and the damage factor for ozone layer destruction

(2) Examination for calculation of damage functions for all types of ODS

The following 13 types of ODS were available for the acquisition of quantitative information, such as atmospheric lifetime, and the direct calculation of damage functions. They include the ODS used for the calculation of characterization factors.

- CFC types: CFC-11, CFC-12, CFC-113 (3 types)
- Halon types: Halon-1211, Halon-1301 (2 types)
- HCFC types: HCFC-22, HCFC-123, HCFC-124, HCFC-141b, HCFC-142b (5 types)
- Chlorocarbon types: carbon tetrachloride (CCl_4), 1,1,1- trichloroethane (1,1,1-TCE) (2 types)
- Bromocarbon type: methyl bromide (CH_3Br) (1 type)

Moreover, with regard to the types of ODS whose damage functions could not be calculated directly due to a lack of information, damage functions were calculated indirectly by the use of the ODP ratio. That is, CFC-11 (a CFC type), Halon-1211 (a Halon type) and HCFC-22 (a HCFC type and a HBFC type) were used as referential substances to calculate damage functions by multiplying the damage function of each referential substance by the ratio of the substance's ODP_{∞} corresponding to that of the ODS type in question. The source of ODP_{∞} is the Montreal Protocol (UNEP 2000). Because the ODP_{∞} of an ODS type that has a structural isomer is expressed as a range, the maximum value on the safety side was applied.

The ODP in the WMO Scientific Assessment (WMO 1999) was recommended as the characterization factor. It was possible to directly calculate the damage functions of ODS types whose characterization factors were gained. The ODP in the Montreal Protocol was used for indirect calculation of damage functions of ODS types for which ODP is not written in the WMO Scientific Assessment.

Below, we will explain the method used for directly calculating damage functions.

(3) Relation between emission of ODS and the amount of UV-B reaching the ground

a Relation between emission of ODS and tropospheric chlorine loading

We formulated a primary regression equation by using the annual global amount of CFC-11 emission (Kaye et al. 1994) as the explanatory variable and using an annual increase in the CFC-11 density converted into tropospheric chlorine loading (TCL) (Daniel et al. 1995) (Equation 2.1-2) as the objective variable (Figure 2.1-3). We regarded the inclination to be F_{TCL} , the factor for an increase in TCL as a result of emission of a unit amount of CFC-11.

$$TCL(X) = \{ nCl(X) + nBr(X) \cdot \alpha \} \cdot C_{trop}(X) \quad (2.1-2)$$

In this equation, X is ODS; nCl and nBr are the numbers of Cl and Br atoms respectively in a molecule of X ; α is the ratio of Br's ozone depleting capability to Cl's (40 to 1 (WMO 1995)); and C_{trop} is the tropospheric density of X [pptv].

With regard to FTCL of each of the 12 substances other than CFC-11, because information on global emissions and tropospheric density is insufficient, we calculated it by correcting FTCL of CFC-11 based on the molecular weight (MW) of each ODS and the numbers of Cl and Br atoms in a molecule.

$$F_{TCL}(X) = A \cdot F_{TCL}(CFC-11) \quad (2.1-3)$$

$$A = \frac{nCl(X) + nBr(X) \cdot \alpha}{MW(X)} \Bigg/ \frac{nCl(CFC-11) + nBr(CFC-11) \cdot \alpha}{MW(CFC11)}$$

However,

$$= \frac{nCl(X) + nBr(X) \cdot \alpha}{MW(X)} \Bigg/ \frac{3}{137.4} = 45.8 - \frac{nCl(X) + nBr(X) \cdot \alpha}{MW(X)}$$

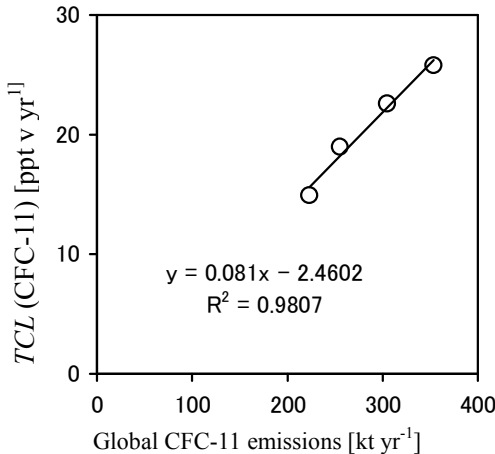


Figure 2.1-3: Relation between the global amount of CFC-11 emission and an increase in TLC

- The source for the global emissions is Kaye et al. (1994).
- Increases in TCL were calculated from results of observation by CMDL (1998).

b Relation between equivalent effective stratospheric chlorine and tropospheric chlorine loading

Stratospheric ozone is destroyed by Cl and Br liberated from ODS. The density of Cl and Br liberated from ODS is expressed as equivalent effective stratospheric chlorine (EESC) (Daniel et al. 1995) (Equation 2.1-4). X 's EESC is expressed as the product of X 's TCL and fractional chlorine release (FC) (Daniel et al. 1995).

$$EESC(X, t) = \sum_X TCL(X, t-3) \cdot FC(X) \quad (2.1-4)$$

In this equation, t is a year. TCL is three years after EESC, because it takes three years on average to transport ODS from the troposphere to the stratosphere (Environment Agency's Global Environmental Department 1995). FC is expressed by equation 2.1-5 (Daniel et al. 1995).

$$FC(X) = \left\{ \mu_{entry}(X) - \mu_{\phi z}(X) \right\} / \mu_{entry}(X) \quad (2.1-5)$$

In this equation, μ_{entry} is the density of X that enters into the stratosphere (that is, the density of near-tropopause X) and $\mu_{\phi z}$ is the density of X at latitude ϕ and at height z . FC ranges from 0 to 1. If FC is 1, this means that Cl and Br are completely liberated. FC varies according to latitude and height. In this equation, a weighted average of the density of CFC-11 in the stratosphere is calculated by weight of the average air pressure at each altitude, using observed values of CFC-11 density in the vertical direction in Japan (Environment Agency 1998) (Figure 2.1-4). The average FC of CFC-11 was calculated by substituting the weighted average into equation 2.1-5 together with the tropopause density of CFC-11. The

FCs of the other 12 substances were calculated by substituting the average FC of CFC-11 into cases where relative values of FCs of the other ODSs to the FC of CFC-11 were estimated (Daniel et al. 1995).

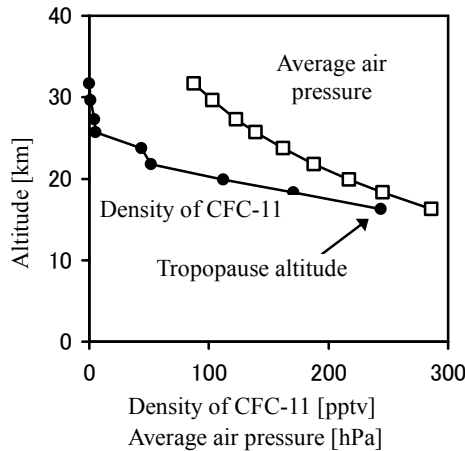
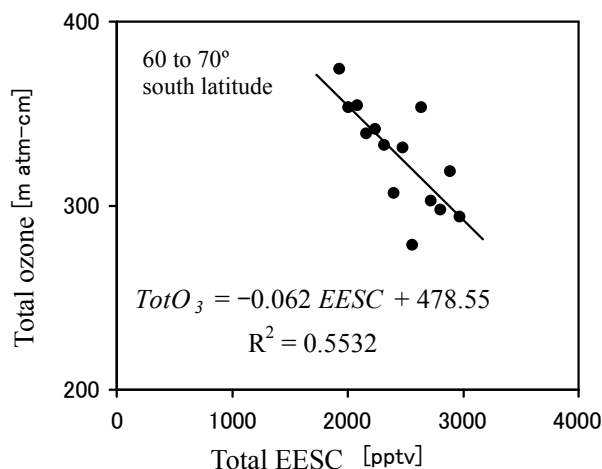


Figure 2.1-4: Relation between density of CFC-11 and altitude

- The source for the density of CFC-11 at each level of latitude is the Environment Agency (1998).
- Average air pressure was calculated based on latitude.



**Figure 2.1-5: An example of the relation between EESC and total ozone
(60 to 70 degrees south latitude; Sep. to Nov.)**

- Total EESC was based on estimation results in WMO (1999).
- Total ozone for each latitude band and each season was calculated through arrangement of satellite observed data from MacPeter, Beach (1996).

c Relation between EESC and total ozone

Total ozone is the accumulated amount of ozone between the surface of the ground and the upper edge of the atmosphere. However, because 90% of atmospheric ozone exists in the stratosphere (WMO 1999), we regarded changes in total ozone as changes in the amount of stratospheric ozone. The global distribution of total ozone (substantially, stratospheric ozone) has an inclination in the meridian direction and shows seasonal changes (Ogura 1999). Therefore, to relate EESC with total ozone, the global total is divided into ten-degree-width latitude bands (18 zones in total), and one year is divided into four seasons (March to May, June to August, September to November, and December to February).

To treat the complex ozone layer destruction mechanism in a simple manner, a group of primary regression equations was prepared with total EESC as the explanatory variable and total ozone as the objective variable for each of the ten-degree-width latitude bands, using secular changes in total EESC estimated by a numerical model (WMO 1999) and secular changes in total ozone observed by satellite (Mac Peter et al. 1996) (example: Figure 2.1-5).

d Relation between total ozone and amount of UV-B reaching the ground

If total ozone is given, the theoretical optical thickness of ozone absorption τ_{o3} can be calculated by the use of an ozone molecule's absorption cross-section of ultraviolet rays (Houghton 1986). Therefore, we converted the total ozone observed terrestrially at four points in Japan (Sapporo, Tsukuba, Kagoshima, Naha) (1995) (Japan Meteorological Agency 1998) into τ_{o3} in UV-B wavelength bands of 290 to 300 nm, 300 to 310 nm, and 310 to 320 nm.

$$A_{O_3 \lambda_1-\lambda_2} = \int_{\lambda_1}^{\lambda_2} A_{O_3}(\lambda) d\lambda \quad (2.1-6)$$

$$\tau_{O_3 \lambda_1-\lambda_2} = 6.0221367 \cdot A_{O_3 \lambda_1-\lambda_2} \cdot 10^{19} \cdot TotO_3 \cdot 10^{-2} / 22.4141 \quad (2.1-7)$$

In this equation, $A_{O_3}(\lambda)$ is the absorption cross-section [cm^2] if the wavelength of an ozone molecule is λ [nm]; $\tau_{O_3 \lambda_1-\lambda_2}$ is τ_{O_3} in the whole atmosphere within the range of wavelength from λ_1 to λ_2 (that is, the total of absorption cross-sections of all ozone molecules included in the whole vertical atmosphere with a cross-section of 1 m^2); and $TotO_3$ is the total ozone [$\text{m atm} - \text{cm}$]. In equation 2.1-7, the three items from the left of the right side indicate the optical thickness of one ozone mole, while the remaining portion indicates the number of moles of total ozone.

τ_{o3} is the optical thickness of ozone's UV-B absorption from direct solar radiation. Meanwhile, because UV-B that reaches the earth is the total solar radiation (diffused and direct) influenced by the diffusion and absorption in the whole atmosphere including ozone, τ_{o3} cannot be applied directly to this calculation. Therefore, we calculated the apparent optical thickness τ_{app} for each wavelength zone of the atmosphere, approximately applying the Lambert-Beer Law, which indicates the decline in direct solar radiation, to the decline of UV-B as total solar radiation and using the theoretical intensity of UV-B at the upper edge of the atmosphere and the intensity of UV-B observed simultaneously with the total ozone on the ground when the weather was fair (Japan Meteorological Agency 1998).

$$\tau_{app \lambda_1-\lambda_2} = (\ln I_{0 \lambda_1-\lambda_2} - \ln I_{\lambda_1-\lambda_2}) \cdot \cos ZA \quad (2.1-8)$$

Equation 2.1-11 is a variation of the Lambert-Beer Law. In this equation, I_0 and I are UV-B intensity [W m^{-2}] at the upper edge of the atmosphere and on the ground, respectively, and ZA is solar zenith angle [rad]. I_0 and $\cos ZA$ can be calculated by equations 2.1-9 and 2.1-10 (Aida 1982).

$$I_{0 \lambda_1-\lambda_2} = S_{\lambda_1-\lambda_2} \cdot (dm/d)^2 \quad (2.1-9)$$

However,

$$\begin{aligned}
 (dm/d)^2 &= 1.00011 + 0.034221 \cos \eta + 0.00128 \sin \eta \\
 &\quad + 0.000719 \cos 2\eta + 0.000077 \sin 2\eta \\
 \eta &= 2\pi \cdot (n/365) \\
 \cos ZA &= \sin \phi \sin \delta + \cos \phi \cos \delta \cos h
 \end{aligned} \tag{2.1-10}$$

In this equation, S is a solar constant [Wm^{-2}]; $(dm/d)^2$ is a sun-earth distance correction term; n is n th day of a year starting on January 1; ϕ is latitude [rad]; δ is declination of the sun [rad]; and h is an hour angle [rad] if the culmination hour is 0.

Next, we used each wavelength zone's τ_{O_3} and τ_{app} calculated from observation data at the same hour and prepared a primary regression equation for which τ_{O_3} was used as the explanatory variable and τ was used as the objective variable (Figure 2.1-6). Applying this relation to the Lambert-Beer Law, we prepared an approximate equation for the calculation of the intensity of UV-B on the ground in relation to total ozone and solar altitude.

$$I_{\lambda_1-\lambda_2} = I_{0,\lambda_1-\lambda_2} \cdot \exp(-\tau_{app,\lambda_1-\lambda_2} / \cos ZA) \tag{2.1-11}$$

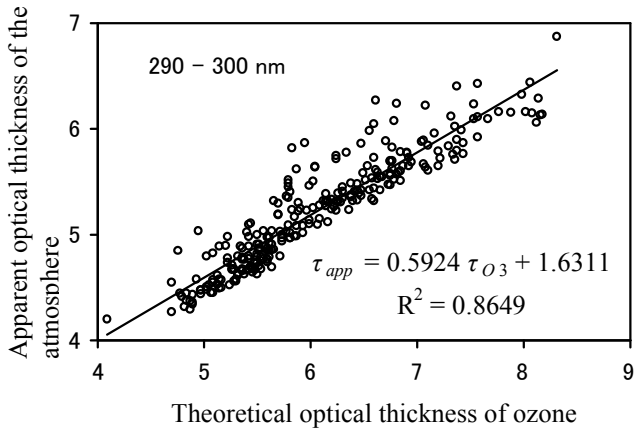


Figure 2.1-6: Relation between apparent optical thickness of the atmosphere and theoretical optical thickness of ozone

- The theoretical optical thickness of ozone was calculated from the observed amount of total ozone and the absorption cross-section of an ozone molecule.
- The apparent optical thickness of the atmosphere was calculated by applying the observed amount of total ozone, the observed intensity of ultraviolet rays on the ground, solar altitude at the time in question, etc. to the Lambert-Beer Law.

e Annual amount of UV-B in each latitude band and wavelength correction

We calculated the annual amount of UV-B on the ground in each latitude band in 1998 (the base year of 1995 plus three years needed for transporting ODS from the troposphere to the stratosphere) (Environment Agency's Global Environmental Department 1995) (the effect of clouds was not taken into consideration). Concretely, we calculated a seasonal daily average amount of UV-B in each wavelength band, multiplied the amount by the number of seasonal days to calculate an integrated seasonal amount, and totaled the integrated seasonal amounts to calculate an annual amount. Because the intensity of UV-B on the ground is greatly

influenced by atmospheric routes, we calculated the daily amount of UV-B, taking into consideration changes in solar altitude. That is, we calculated the intensity of UV-B that reached the ground at each of the ten time zones into which a half-day time H [rad], which indicates the hours from the sunrise or sunset to the culmination hour, was equally divided (11 points of time: $0.0H, 0.1H \dots 1.0H$), calculated an average intensity during the half-day time from the results, and multiplied it by the number of hours in a day to calculate the daily amount of UV-B (Figure 2.1-7). H can be calculated by equation 2.1-12 (Aida 1982).

$$H = (\pi / 2) + \arcsin(\tan \phi \tan \delta) \quad (2.1-12)$$

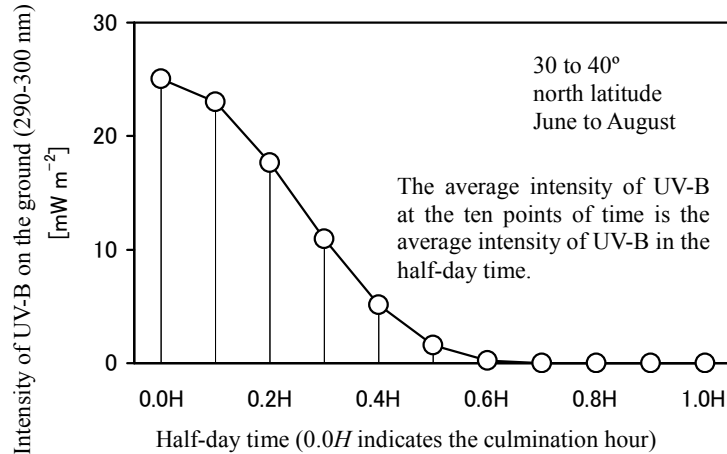


Figure 2.1-7: Exemplary calculation of the intensity of UV-B reaching the ground at each point of time during the half-day time

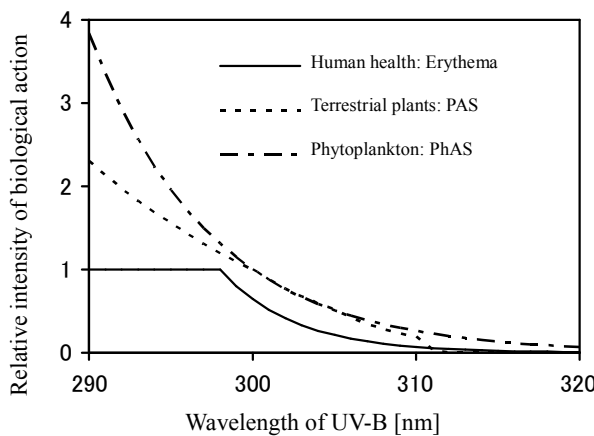


Figure 2.1-8: Wavelength dependence of the impact of UV-B on each endpoint

The resultant amount of UV-B is a physical amount. On the other hand, the intensity of the biological action of UV-B is said to have wavelength dependence, the degree of which varies among species. The wavelength dependence of the impact of UV-B on human health, terrestrial plants, and phytoplankton was calculated based on the International Commission on Illumination (CIE) (CIE 1987), Caldwell (1971), and Behrenfeld et al. (1993) respectively (Figure 2.1-8).

After that, we integrated the wavelength dependence made relative by assuming that the impact of 298 nm on human health and the impact of 300 nm in plants are 1, to derive the

conversion factor for wavelength dependence in each wavelength band. By multiplying the physical amount of UV-B in each wavelength band by the conversion factor, we derived the amounts of UV-B corrected by wavelength – that is, the corrected amount of UV-B impacting on human health (erythema), the corrected amount of UV-B impacting on terrestrial plants (PAS: plant action spectra), and the corrected amount of UV-B impacting on phytoplankton (PhAs: phytoplankton action spectra).

f Increase in the amount of UV-B due to new emission of ODS

By the use of the relations derived so far, it is possible to calculate the annual amount of UV-B corrected by wavelength in each latitude band after additional emission of an arbitrary amount of ODS. This amount of UV-B is the amount three years after emission. The difference from the annual amount of wavelength-corrected UV-B in 1998 indicates an increase in the amount due to additional emission of ODS. However, because calculation is needed for each arbitrary amount of emission, it cannot be treated as a factor suitable for LCA. We calculated an increase in the amount of wavelength-corrected UV-B if the amount of emission of ODS was 0, 100, 200, and 500 kt yr^{-1} , and checked the linearity. As a result, we gained good linearity concerning all types of ODS (example: Figure 2.1-9). Therefore, we regarded the inclination of each straight line as F_{UVBI} , the factor that indicates an increase in the amount of wavelength-corrected UV-B due to emission of a unit amount of X . F_{UVBI} can be calculated as a factor for each type of ODS in each latitude band for each biological division (human health, terrestrial plants, and phytoplankton).

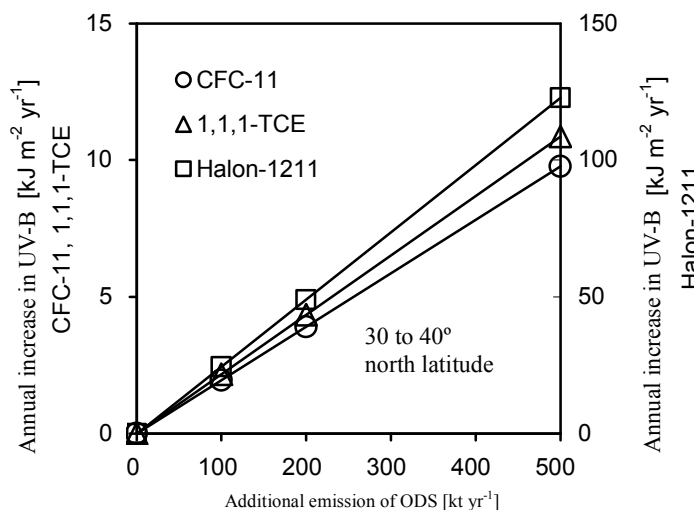


Figure 2.1-9: Relation between additional ODS emission and annual UV-B increase
Of the 13 types of ODSs whose damage functions were calculated directly, taking CFC-11, Halon-1211, and 1,1,1-TCE as examples, the figure shows results in the latitude band between 30 and 40 degrees north latitude.

g Correction by the atmospheric lifetime of ODS

We derived a correction factor by the atmospheric lifetime to estimate the entire impact of ODS that is emitted at a certain point of time and exists in the atmosphere for a certain period. This is based on the idea that, if the atmospheric density of the emitted substance at the time of emission is 1 and the density at the time of complete removal is 0, the impact at a certain point of time is in proportion to this standardized density. We expressed a decline in the standardized density by an exponential function, integrated the atmospheric lifetime of each

ODS (WMO 1999), and regarded the result as F_{LT} , an atmospheric lifetime correction factor that indicates the total amount of impact.

$$F_{LT} = \int_3^\infty C(t) dt = \int_3^\infty e^{-t/LT} dt \quad (2.1-13)$$

In this equation, C is standardized atmospheric density, and LT is atmospheric lifetime [yr]. The beginning of integration is 3 because it takes three years for the emitted ODS to reach the stratosphere.

The total amount of impact can be calculated by multiplying the initial amount of damage at the time when the impact of ODS emitted at a certain point of time begins to emerge (three years after the emission) by F_{LT} .

(4) Human health: damage functions for skin cancer

a Relation between the amount of UV-B and skin cancer morbidity

We extracted skin cancer morbidity in each country or region from statistics provided by the International Agency for Research on Cancer (IARC) (Ferlay et al. 1997) and classified it by skin color (Caucasian, Asian, and black races). Moreover, with regard to Caucasians, we considered using an epidemiological survey on skin cancer morbidity in Australia (Armstrong 1993). For each skin color or skin cancer type, we formulated a primary regression equation that uses skin cancer morbidity as the objective variable and the annual amount of erythema-corrected UV-B in 1998 calculated from the latitude of each country or region as the explanatory variable. After that, we regarded the inclination of the equation as FSCI, a factor that gives an increase in skin cancer morbidity due to an increase in the unit amount of annual erythema-corrected UV-B (Figure 2.1-10).

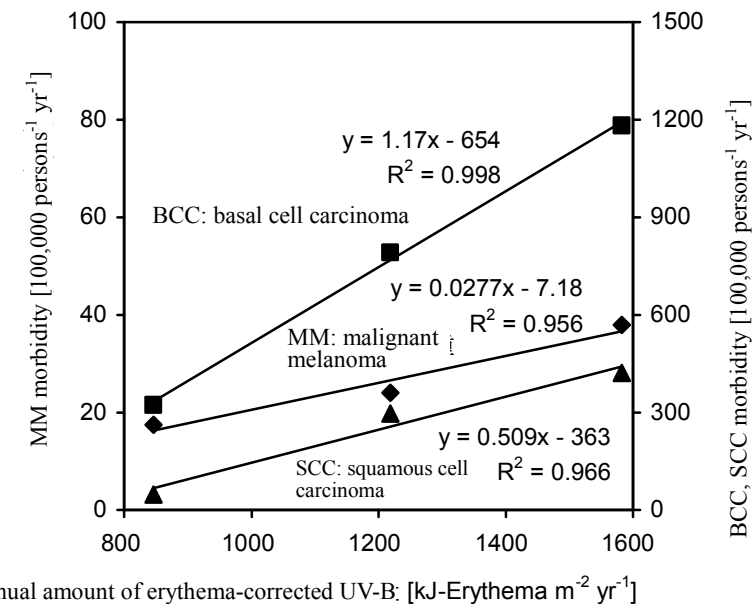


Figure 2.1-10: Relation of annual amount of erythema-corrected UV-B and cancer skin morbidity (Caucasians)

We related the annual amount of erythema-corrected UV-B calculated by a method developed under LIME to an epidemiological survey on skin cancer morbidity (Caucasians) in Australia (Caldwell 1971).

With regard to Caucasians, the FSCI gained from the epidemiological survey in Australia was dozens of times larger than that gained from IARC's statistics. We adopted the FSCI gained from the epidemiological survey in Australia for LIME in view of the following reasons: 1) It was thought that skin cancer morbidity in Australia, which is composed mainly of immigrants, is close to the response to a rapid increase in UV-B; 2) F_{SCI} showed a good correlation with the amount of wavelength-corrected UV-B; and 3) Factors could be obtained for each of malignant melanoma, basal cell carcinoma, and squamous cell carcinoma.

b Calculation of damage functions for skin cancer

We multiplied F_{UVBI} of human health in each latitude band by F_{SCI} to find an increase in skin cancer morbidity in each latitude band due to emission of 1 kg yr⁻¹ of ODS [100,000 persons⁻¹ yr⁻¹]. This value corresponds to the point of time when the impact of ODS emission begins to emerge.

Next, we estimated the population of each race (divided by skin color into Caucasian, Asian, and black races) in each latitude band based on population statistics and the location of each country. We summed up products of the population of each race and an increase in skin cancer morbidity in each latitude band to calculate an increase in the global number of skin cancer sufferers with additional emission of 1 kg yr⁻¹ of ODS. We regarded this as the initial value, multiplied it by F_{LT} , and regarded the result as SCI_{global} [person kg⁻¹], the total impact of the newly emitted ODS in the period when the ODS continues to exist.

$$SCI_{global}(X) = F_{LT}(X) \cdot \sum_i \sum_j F_{UVBI}(X, i, Erythema) \cdot F_{SCI}(j) \cdot Pop(i, j) \quad (2.1-14)$$

In this equation, i is a latitude band, and j is skin color.

Table 2.1-4: Damage functions for skin cancer (partial)

Latitude band	Damage function in each latitude band	CFC-11			Halon-1211			HCFC-22		
		MM	Other	Total	MM	Other	Total	MM	Other	Total
80-90° N lat.	0.00e+0	0.00e+0	0.00e+0	0.00e+0	0.00e+0	0.00e+0	0.00e+0	0.00e+0	0.00e+0	0.00e+0
70-80° N lat.	1.86e-9	6.49e-9	8.34e-9	4.69e-9	1.64e-8	2.11e-8	7.47e-11	2.61e-10	3.36e-10	
60-70° N lat.	1.20e-6	4.20e-6	5.40e-6	3.04e-6	1.06e-5	1.37e-5	4.84e-8	1.69e-7	2.17e-7	
50-60° N lat.	2.55e-5	8.90e-5	1.14e-4	6.44e-5	2.25e-4	2.89e-4	1.03e-6	3.58e-6	4.61e-6	
40-50° N lat.	5.42e-5	1.89e-4	2.43e-4	1.37e-4	4.77e-4	6.14e-4	2.18e-6	7.59e-6	9.78e-6	
30-40° N lat.	2.69e-5	9.16e-5	1.19e-4	6.76e-5	2.30e-4	2.98e-4	1.08e-6	3.69e-6	4.77e-6	
20-30° N lat.	3.28e-6	9.32e-6	1.26e-5	8.20e-6	2.33e-5	3.15e-5	1.32e-7	3.75e-7	5.07e-7	
10-20° N lat.	1.11e-6	2.43e-6	3.53e-6	2.76e-6	6.05e-6	8.81e-6	4.46e-8	9.77e-8	1.42e-7	
Equator to 10° N lat.	4.49e-7	1.25e-6	1.70e-6	1.12e-6	3.13e-6	4.25e-6	1.81e-8	5.04e-8	6.85e-8	
Equator to 10° S lat.	2.18e-6	7.15e-6	9.33e-6	5.44e-6	1.79e-5	2.33e-5	8.77e-8	2.88e-7	3.76e-7	
10-20° S lat.	4.37e-6	1.46e-5	1.90e-5	1.09e-5	3.65e-5	4.74e-5	1.76e-7	5.89e-7	7.65e-7	
20-30° S lat.	5.32e-6	1.82e-5	2.35e-5	1.33e-5	4.54e-5	5.87e-5	2.14e-7	7.32e-7	9.46e-7	
30-40° S lat.	6.78e-6	2.35e-5	3.03e-5	1.70e-5	5.90e-5	7.60e-5	2.73e-7	9.47e-7	1.22e-6	
40-50° S lat.	1.87e-6	6.53e-6	8.40e-6	4.71e-6	1.65e-5	2.12e-5	7.52e-8	2.63e-7	3.38e-7	
50-60° S lat.	3.15e-7	1.10e-6	1.42e-6	8.02e-7	2.80e-6	3.60e-6	1.27e-8	4.43e-8	5.70e-8	
60-70° S lat.	0.00e+0	0.00e+0	0.00e+0	0.00e+0	0.00e+0	0.00e+0	0.00e+0	0.00e+0	0.00e+0	0.00e+0
70-80° S lat.	0.00e+0	0.00e+0	0.00e+0	0.00e+0	0.00e+0	0.00e+0	0.00e+0	0.00e+0	0.00e+0	0.00e+0
80-90° S lat.	0.00e+0	0.00e+0	0.00e+0	0.00e+0	0.00e+0	0.00e+0	0.00e+0	0.00e+0	0.00e+0	0.00e+0
Global total		1.33e-4	4.58e-4	5.91e-4	3.36e-4	1.15e-3	1.49e-3	5.37e-6	1.84e-5	2.38e-5

- The unit of damage function is DALY kg⁻¹. That is, an increase in the number of potential skin cancer sufferers with addition emission of 1 kg of the ODS is converted into DALY.
- The total of damage functions in each latitude band is used as the global damage function for LIME.

We regarded SCIglobal converted into DALY as damage functions for skin cancer. As DALY, we used values calculated by reference to Goedkoop et al. (2000), 5.9 DALY person⁻¹ (malignant melanoma), and 0.34 DALY person⁻¹ (other types of skin cancer (basal cell carcinoma and squamous cell carcinoma). Table 2.1-4 shows some of the damage functions we obtained.

(5) Human health: damage functions for cataract

a Relation between the amount of UV-B and cataract morbidity

Because information on cataract morbidity was scarce, we estimated cataract morbidity by the use of a survey on the ratio of cataract sufferers (Sasaki et al. 1999). This survey was carried out in Singapore, which is near the equator, in Amami and Noto in Japan, which are in the middle latitude band, and Reykjavik in Iceland, which is in a high latitude band. We regarded the ratio of cataract sufferers in people in their 50s, 60s, and 70s as the ratio for the median age of each age group (for example, 54.5 years old in the case of people in their 50s) and drew a regression curve for each place. Because the ratio of cataract sufferers increases by age and the maximum ratio is 100%, a logistic curve with the maximum value of 100 was adopted as the form of each regression curve (Figure 2.1-11). The form of the curves showed the possibility that people in their 40s would suffer a cataract whose severity is Level II or higher. Moreover, assuming that 1) there is no difference in death rate between cataract sufferers and the others and 2) there is no difference in cataract morbidity between dead people and living people during a certain period, we regarded the inclination of each regression curve of the ratio of cataract sufferers as cataract morbidity. That is, by differentiating the regression curves, we obtained the equation for the calculation of cataract morbidity at the age of t . We formulated a regression equation, using morbidity at each place converted into an age-standard rate (ASR) (Ferlay et al. 1997) and using the annual amount of erythema-corrected UV-B at each place as the explanatory variable (Figure 2.1-12) and regarded the inclination as F_{CATI} , a factor that gives an increase in cataract morbidity due to an increase in the annual amount of erythema-corrected UV-B.

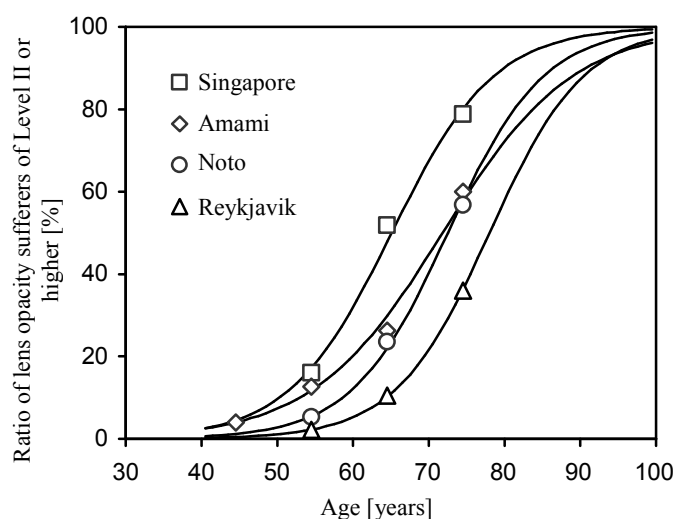


Figure 2.1-11: Relation of age and the ratio of lens opacity sufferers

We applied a logistic curve with the maximum value of 100% to the ratio of lens opacity sufferers by age group obtained by an epidemiological survey (Sasaki et al. 1999) and regarded the inclination of the curves as morbidity.

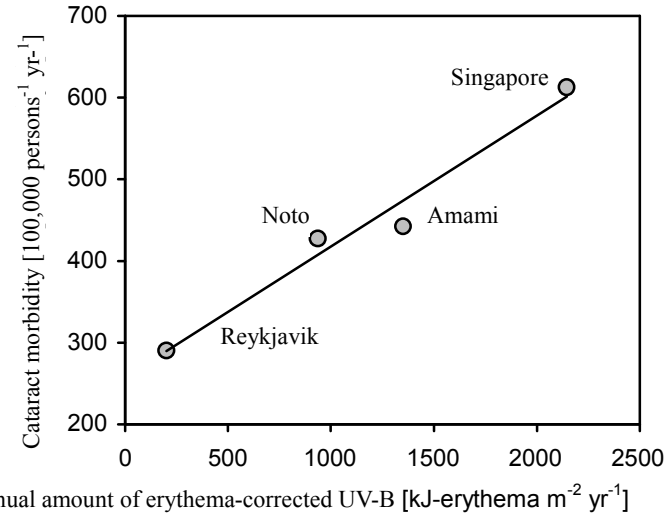


Figure 2.1-12: Relation between annual amount of erythema-corrected UV-B and cataract morbidity

Table 2.1-5: Damage functions for cataract (partial)

Damage function in each latitude band	CFC-11	CFC-12	Halon-1211	Halon-1301	CCl ₄	1,1,1-TCE	HCFC-22
80-90° N lat.	0.00e+0	0.00e+0	0.00e+0	0.00e+0	0.00e+0	0.00e+0	0.00e+0
70-80° N lat.	2.36e-9	2.47e-9	5.69e-9	3.47e-8	2.28e-9	1.60e-10	9.50e-11
60-70° N lat.	1.47e-6	1.54e-6	3.71e-6	2.16e-5	1.41e-6	9.96e-8	5.91e-8
50-60° N lat.	3.34e-5	3.49e-5	8.43e-5	4.90e-4	3.21e-5	2.26e-6	1.34e-6
40-50° N lat.	1.34e-4	1.40e-4	3.38e-4	1.97e-3	1.29e-4	9.09e-6	5.39e-6
30-40° N lat.	2.41e-4	2.52e-4	6.06e-4	3.53e-3	2.32e-4	1.64e-5	9.70e-6
20-30° N lat.	2.00e-4	2.09e-4	4.99e-4	2.91e-3	1.92e-4	1.36e-5	8.05e-6
10-20° N lat.	6.51e-5	6.81e-5	1.62e-4	9.46e-4	6.27e-5	4.42e-6	2.62e-6
Equator to 10° N lat.	7.75e-6	8.11e-6	1.94e-5	1.13e-4	7.46e-6	5.26e-7	3.12e-7
Equator to 10° S lat.	1.94e-5	2.03e-5	4.85e-5	2.83e-4	1.87e-5	1.32e-6	7.80e-7
10-20° S lat.	2.07e-5	2.17e-5	5.18e-5	3.02e-4	2.00e-5	1.41e-6	8.35e-7
20-30° S lat.	1.65e-5	1.73e-5	4.12e-5	2.40e-4	1.59e-5	1.12e-6	6.64e-7
30-40° S lat.	1.19e-5	1.25e-5	2.99e-5	1.74e-4	1.15e-5	8.09e-7	4.80e-7
40-50° S lat.	2.55e-6	2.67e-6	6.43e-6	3.74e-5	2.46e-6	1.73e-7	1.03e-7
50-60° S lat.	4.20e-7	4.39e-7	1.07e-6	6.20e-6	4.04e-7	2.85e-8	1.69e-8
60-70° S lat.	0.00e+0	0.00e+0	0.00e+0	0.00e+0	0.00e+0	0.00e+0	0.00e+0
70-80° S lat.	0.00e+0	0.00e+0	0.00e+0	0.00e+0	0.00e+0	0.00e+0	0.00e+0
80-90° S lat.	0.00e+0	0.00e+0	0.00e+0	0.00e+0	0.00e+0	0.00e+0	0.00e+0
Global total	7.54e-4	7.89e-4	1.89e-3	1.10e-2	7.26e-4	5.12e-5	3.03e-5

- The unit of damage function is DALY kg⁻¹. That is, an increase in the number of potential cataract sufferers with additional emission of 1 kg of the ODS is converted into DALY.
- The total of damage functions in each latitude band is used as the global damage function for LIME.

We related the annual amount of erythema-corrected UV-B calculated by a method developed under LIME to the cataract morbidity calculated under LIME based on an epidemiological survey (Sasaki et al. 1999).

b Calculation of damage functions for cataract

As in the case of skin cancer, we calculated an increase in cataract morbidity in each latitude band with emission of 1 kg yr⁻¹ of ODS [100,000 persons⁻¹ yr⁻¹]. However, we did not make classification by skin color.

We calculated the sum of products of population and an increase in cataract morbidity in each latitude band to obtain an increase in the global number of cataract sufferers with emission of 1 kg yr^{-1} of ODS. We regarded this value as the initial one, multiplied it by F_{LT} , and regarded the result as $CATI_{global}$ [person kg^{-1}], the total impact of the newly emitted ODS in the period when the ODS continues to exist.

$$CATI_{global}(X) = F_{LT}(X) \cdot \sum_i F_{UVBI}(X, i, Erythema) \cdot F_{CATI} \cdot Pop(i) \quad (2.1-15)$$

We used $CATI_{global}$ converted into DALY as a damage function for cataract. As DALY for cataract, we used 1.2 DALY person $^{-1}$, the value calculated by reference to Goedkoop et al. (2000). Table 2.1-5 shows some of the damage functions we obtained.

(6) Primary production: damage functions for the terrestrial ecosystem

a Relation between amount of UV-B and plant damage

The primary production of the terrestrial ecosystem is found mainly in forests. There are many case studies on the impact of UV-B on trees. However, quantitative information on the relation between the amount of exposure of UV-B and the growth of trees was limited to studies that used infant *Pinus taeda* (Sullivan et al. 1992; Naidu et al. 1993). Under LIME, we obtained the relation between an increase in the annual amount of PAS-corrected UV-B and a decrease in the growth rate on the dry basis, using data gained from the studies on *Pinus taeda*. We obtained the following information: 1) When the amount of ultraviolet rays that decreases stratospheric ozone by 25% was exposed for three years, biomass decreased by 15 to 20% in the research area (Sullivan et al. 1992); and 2) In a similar study, root, trunk, and leaf biomass decreased by 24%, 16%, and 18% respectively in the research area (Naidu et al. 1993). We estimated the median at a 17.5% decrease from 1) and the average at a 19.3% decrease from 2). Applying these experimental conditions to 30 to 40 degrees north latitude and using the method described in 2.1.3 (3), we calculated the annual amount of PAS-corrected UV-B in the base year and in the case of a 25% decrease in total ozone. With regard to each of 1) and 2), we calculated a decreasing rate of growth to the unit amount of annual PAS-corrected UV-B and regarded the average – $0.0193\% \text{ kJ-PAS}^{-1} \text{ m}^2 \text{ yr}$ as F_{PGDR} , the factor that determines a decreasing rate of growth as a result of the annual amount of PAS-corrected UV-B.

b Vegetation covered by the estimation of damage functions and its distribution

Pinus taeda is a conifer that mainly distributes on lowlands in the southeast part of the US. Generally, trees in highlands are resistant to UV-B, while trees in lowlands, such as *Pinus taeda*, are sensitive to UV-B (Environment Agency's Global Environmental Department 1995). Therefore, we calculated damage functions for the net primary productivity (NPP) in terrestrial areas, applying F_{PGDR} obtained from the studies on *Pinus taeda* to conifer forests in areas other than mountainous areas. An increase of UV-B due to ozone layer destruction is more conspicuous at high latitudes, and forests at high latitude bands are mainly coniferous. Therefore, we thought that damage functions for conifer forests could cover vegetation that seems to suffer the most from ozone layer destruction.

Under LIME, we estimated the area of conifer forests in each latitude band, extracting examples of areas mainly occupied by conifer trees from the global data on vegetation in a mesh of $1^\circ \times 1^\circ$ (Environment Agency's Global Environmental Department 1995). The total

is $35.5 \times 106 \text{ km}^2$, which is three times as large as $12.0 \times 106 \text{ km}^2$, the total area of northern conifer forests on the whole earth (Whittaker 1979). We interpreted that this was because other conifer forests were added to northern conifer forests. We uniformly regarded the NPP of conifer forests as $8000 \text{ kg ha}^{-1} \text{ yr}^{-1}$, the average for northern conifer forests (Whittaker 1979). We obtained $NPP(i)$, the total amount of NPP in the latitude band i , by multiplying the area of conifer forests in each latitude band by NPP per unit area.

c Calculation of damage functions for global terrestrial NPP (conifer forest NPP)

We calculated the amount of damage to NPP in each latitude band due to emission of 1 kg yr⁻¹ of ODS. We regarded this amount as the initial value, multiplied it by FLT, and regarded the result as the total impact of the newly emitted ODS on terrestrial NPP in the period when the ODS continues to exist – that is, damage functions for terrestrial NPP, $NPPD_{tr\ global}$ [kg kg⁻¹]. The table 2.1-6 shows some of the damage functions we obtained.

$$NPPD_{tr\ global}(X) = F_{LT}(X) \cdot \sum_i F_{UVBI}(X, i, PAS) \cdot F_{PGDR} \cdot NPP(i) \cdot 10^{-2} \quad (2.1-16)$$

Table 2.1-6: Damage functions for terrestrial NPP (partial)

	Latitude band	CFC-11	CFC-12	Halon-1211	Halon-1301	CCl ₄	1,1,1-TCE	HCFC-22
Damage function in each latitude band	80-90° N lat.	0.00e+0	0.00e+0	0.00e+0	0.00e+0	0.00e+0	0.00e+0	0.00e+0
	70-80° N lat.	5.96e-3	6.24e-3	1.51e-2	8.76e-2	5.74e-3	4.05e-4	2.40e-4
	60-70° N lat.	7.51e-1	7.86e-1	1.90e+0	1.11e+1	7.24e-1	5.10e-2	3.02e-2
	50-60° N lat.	1.75e+0	1.84e+0	4.44e+0	2.58e+1	1.69e+0	1.19e-1	7.06e-2
	40-50° N lat.	1.39e+0	1.45e+0	3.51e+0	2.04e+1	1.34e+0	9.44e-2	5.59e-2
	30-40° N lat.	5.02e-1	5.25e-1	1.26e+0	7.35e+0	4.83e-1	3.41e-2	2.02e-2
	20-30° N lat.	4.51e-3	4.72e-3	1.13e-2	6.57e-2	4.34e-3	3.06e-4	1.81e-4
	10-20° N lat.	0.00e+0	0.00e+0	0.00e+0	0.00e+0	0.00e+0	0.00e+0	0.00e+0
	Equator to 10° N lat.	0.00e+0	0.00e+0	0.00e+0	0.00e+0	0.00e+0	0.00e+0	0.00e+0
	Equator to 10° S lat.	0.00e+0	0.00e+0	0.00e+0	0.00e+0	0.00e+0	0.00e+0	0.00e+0
	10-20° S lat.	0.00e+0	0.00e+0	0.00e+0	0.00e+0	0.00e+0	0.00e+0	0.00e+0
	20-30° S lat.	0.00e+0	0.00e+0	0.00e+0	0.00e+0	0.00e+0	0.00e+0	0.00e+0
	30-40° S lat.	0.00e+0	0.00e+0	0.00e+0	0.00e+0	0.00e+0	0.00e+0	0.00e+0
	40-50° S lat.	0.00e+0	0.00e+0	0.00e+0	0.00e+0	0.00e+0	0.00e+0	0.00e+0
	50-60° S lat.	0.00e+0	0.00e+0	0.00e+0	0.00e+0	0.00e+0	0.00e+0	0.00e+0
	60-70° S lat.	0.00e+0	0.00e+0	0.00e+0	0.00e+0	0.00e+0	0.00e+0	0.00e+0
	70-80° S lat.	0.00e+0	0.00e+0	0.00e+0	0.00e+0	0.00e+0	0.00e+0	0.00e+0
	80-90° S lat.	0.00e+0	0.00e+0	0.00e+0	0.00e+0	0.00e+0	0.00e+0	0.00e+0
Global total		4.41e+0	4.61e+0	1.11e+1	6.48e+1	4.25e+0	2.99e-1	1.77e-1

- The unit of damage function is kg kg⁻¹. That is, an increase in the amount of potential damage to NPP with additional emission of 1 kg of the ODS is converted into the NPP amount on a dry basis.
- The total of damage functions in each latitude band (limited to conifer forests in areas other than mountainous areas) is used as the global damage function for LIME.

(7) Primary production: damage functions for the aquatic ecosystem

a Relation between amount of UV-B and damage to phytoplankton

The primary production of the aquatic ecosystem is mainly from phytoplankton. Although the amount of UV-B sharply decreases on the surface of water, UV-B is thought to have a harmful impact on phytoplankton. As a producer, phytoplankton distributes from the surface of water to the farthest depth that can receive the amount of sunlight necessary for

photosynthesis. Phytoplankton near the surface may receive the impact of UV-B exposure. Therefore, we introduced damage functions, taking into consideration a decline in UV-B with water depth.

The intensity of UV-B on the surface of water is expressed by the Lambert-Beer Law, and the UV-B dissipation factor depends on the density of chlorophyll (Saito et al. 1993). The dissipation factor has a dimension of [m-1] and we regarded the reciprocal as the farthest depth that can receive the impact of ultraviolet rays. On the other hand, the density of phytoplankton is indicated by chlorophyll-a, which indicates the amount of photosynthesis.

The NPP of phytoplankton can be calculated by equation 2.1-17.

$$NPP_{aq} = (1 - R) \cdot EC_C^{-1} \cdot C_{fix} \quad (2.1-17)$$

In this equation, NPP_{aq} is the NPP of phytoplankton [$\text{kg m}^{-2} \text{ yr}^{-1}$]; R is the ratio of carbon lost by respiration among the carbon assimilated by photosynthesis ($= 0.4$) (Aruga 1986); EC_C is the ratio of carbon to the dry weight of phytoplankton ($= 0.359$; the so-called Redfield ratio) (Redfield et al. 1963); and C_{fix} is the fixed amount of carbon [$\text{kgC m}^{-2} \text{ yr}^{-1}$]. C_{fix} can be calculated by equation 2.1-18.

$$C_{fix} = C_{fix}^u \cdot D \cdot Z_0 \cdot 10^{-6} \quad (2.1-18)$$

In this equation, C_{fix}^u is the amount of carbon fixed by 1 mg of chlorophyll in a year [$\text{mgC mg}^{-1} \text{ yr}^{-1}$]; D is the density of chlorophyll on the surface of water [mg m^{-3}]; and Z_0 is the farthest depth of water that can receive the impact of UV-B [m].

On the surface of water, irrespective of water depth, we fixed D and regarded Z_0 as the reciprocal of the dissipation factor k . In addition, we expressed k by $k = 0.7D$, an empirical equation at a wavelength of 305 nm (Saito et al. 1993). Therefore, the item $D \cdot Z_0$ in the equation 2.1-18 becomes a fixed value ($= 1.43$). Meanwhile, C_{fix}^u was calculated according to the empirical equation obtained from the relation between the amount of irradiated UV-B and the photosynthesis rate of phytoplankton in high latitude bands (Behrenfeld et al. 1993a). This yields the following equation:

$$C_{fix}^u = (1 - 0.000116 UVB_{PhAS}) \cdot C_{fix}^{u0} \quad (2.1-19)$$

In this equation, C_{fix}^{u0} is the amount of carbon fixed by 1 mg of chlorophyll per day [$\text{mgC mg}^{-1} \text{ day}^{-1}$] when there is no UV-B exposure (equation 2.1-20) (Behrenfeld et al. 1993b). UVB_{PhAS} is the daily amount of PhAS-corrected UV-B [$\text{J-PhAS m}^{-2} \text{ day}^{-1}$] (equation 2.1-21).

$$C_{fix}^{u0} = 2.87 \cdot h_{day} \quad (2.1-20)$$

$$UVB_{PhAS}(z) = UVB_{PhAS}(0) \cdot e^{-kz} \quad (2.1-21)$$

In these equations, h_{day} is the number of sunlight hours per day [hr], and z is an arbitrary depth of water [m]. We calculated Z' , the water depth that equally divides the cumulative total of UV-B amounts between the surface of water ($z = 0$) and the water depth Z_0 and regarded Z' as the water depth for equation 2.1-21. Z' can be calculated by equation 2.1-22.

$$Z' = \frac{1}{k} \ln\left(1 + \frac{1}{2e}\right) \quad (2.1-22)$$

If equation 2.1-22 is substituted into equation 2.1-21,

$$UVB_{PhAS}(z) = \frac{2e}{2e+1} \cdot UVB_{PhAS}(0) \quad (2.1-23)$$

We grasped the global distribution of water areas from a set of pixel data obtained in a satellite observation project (GSFC 2000). We calculated the amount of damage by pixel. We regarded the total pixel amount of damage in the water areas in each latitude band as the amount of damage in the whole latitude band. At the other endpoints, we estimated the amount of damage due to an increase in the annual amount of UV-B. However, because intervals for the estimation of damage amount should be shorter in light of the lifespan of phytoplankton, we estimated the amount of damage in each season. Because an experiment that introduced equation 2.1-19 (Behrenfeld et al. 1993a) dealt with marine plankton in a polar region, and the amount of irradiated UV-B corresponded to that in the polar region, the amounts of UV-B in middle to low latitude bands were beyond the scope of the regression equation. However, because an increase in the amount of UV-B due to ozone layer destruction is conspicuous at high latitudes, and damage to NPP in water areas is thought to occur at high latitudes, we thought that damage functions only for high latitudes (more than 50 degrees north latitude and more than 50 degrees south latitude) could cover most of the damage to aquatic NPP.

b Calculation of damage functions for global aquatic NPP (NPP of marine and terrestrial phytoplankton)

We calculated the amount of damage to aquatic NPP due to emission of 1 kg yr^{-1} in each of the latitude bands beyond 50 degrees north or south latitude, multiplied the amount by F_{LT} , and regarded the product as the damage function for aquatic NPP, $NPPD_{aq\ global} [\text{kg kg}^{-1}]$, which is the total impact on aquatic NPP during the time when the newly emitted ODS continues to exist in the atmosphere.

Table 2.1-7: Damage functions for NPP in water areas (partial)

	Latitude band	CFC-11	CFC-12	Halon-1211	Halon-1301	CCl ₄	1,1,1-TCE	HCFC-22
Damage function in each latitude band	80-90° N lat.	4.43E-2	4.59E-2	1.11E-1	6.48E-1	4.27E-2	3.00E+3	1.75E-3
	70-80° N lat.	2.33E+0	2.44E+0	5.87E+0	3.42E+1	2.25E+0	1.58E-1	9.35E-2
	60-70° N lat.	7.10E+0	7.43E+0	1.79E+1	1.04E+2	6.84E+0	4.82E-1	2.86E-1
	50-60° N lat.	2.72E+1	2.85E+1	6.86E+1	3.99E+2	2.62E+1	1.85E+0	1.10E+0
	Excluding 50° N lat. - 50° S lat.							
	50-60° S lat.	1.52E+2	1.59E+2	3.86E+2	2.24E+3	1.46E+2	1.03E+1	6.11E+0
	60-70° S lat.	8.64E+1	9.04E+1	2.24E+2	1.30E+3	8.33E+1	5.87E+0	3.47E+0
	70-80° S lat.	1.02E+1	1.07E+1	2.73E+1	1.57E+2	9.88E+0	6.95E+1	4.11E-1
	80-90° S lat.	0.00E+0	0.00E+0	0.00E+0	0.00E+0	0.00E+0	0.00E+0	0.00E+0
	Global total	2.85E+2	2.99E+2	7.29E+2	4.23E+3	2.75E+2	1.94E+1	1.15E+1

- The unit of damage function is kg kg^{-1} . That is, an increase in the amount of potential damage to NPP with additional emission of 1 kg of the ODS is converted into the NPP amount on the dry basis.
- The total of damage functions in each latitude band (more than 50 degrees north latitude and more than 50 degrees south latitude) is used as the global damage function for LIME.

$$NPPD_{aq}(X, i) = \sum_i \sum_s 3.683 \cdot A(i) \cdot Day(s) \cdot H(i, s) \cdot F_{UVBI}(X, i, s, PAS) \cdot 10^{-9} \quad (2.1-24)$$

In this equation, s is the season, A is the area [m^2] of the latitude band i , and $Days(s)$ is the number of days in the season (s).

Table 2.1-7 shows some of the damage functions we obtained.

(8) Social assets: damage functions for agricultural production

a Relation between amount of UV-B and damage to farm products

There were a great number of case studies on the impact of UV-B on farm products (Krupa et al. 1989). However, because many of them aimed for qualitative assessment, quantitative information was extremely limited. In this situation, the United Nations Environment Programme (UNEP) (UNEP 1998) showed information obtained from 49 existing experiment cases concerning relative changes in yield due to UV-B exposure. Soybean, rice, green pea, and mustard were used for the experiments. Although conditions differed from case to case, a 20% decrease in the amount of stratospheric ozone was generally assumed. An average change in the yield of each crop species was -3.7% for soybean (29 cases), -1.4% for rice (14 cases), -11.0% for green pea (4 cases), and -19.5% for mustard (2 cases).

Assuming that these experiments were carried out in the latitude bands between 30 and 40 degrees north latitude, we calculated the annual amount of PAS-corrected UV-B in the base year and in the case of a 20% decrease in the total ozone by the method mentioned in 2.1.3 (3). We calculated the rate of yield decrease with the unit amount of annual Pas-corrected UV-B and regarded the rate as F_{CYDR} , the factor for the calculation of the yield decrease rate as a result of an increase in the annual amount of PAS-corrected UV-B.

b Global yield of main farm products

We extracted the production of the crop species m in each country in 1998 from FAOSTAT (FAO 2000), the database of the UN Food and Agriculture Organization (FAO), and estimated the yield $CP(i, m)$ in the latitude band i . If a country extends over two or more latitude bands, we proportionally divided the yield according to area, excluding the polar regions.

c Calculation of global damage functions for farm products

We calculated damage to crop yield in each latitude band resulting from the emission of 1 kg yr⁻¹ of ODS. We multiplied this initial value by F_{LT} and regarded the result as CPD_{global} [kg kg⁻¹], the total impact on the crop species m during the time when the newly emitted ODS continues to exist.

$$CPD_{global}(m, X) = F_{LT}(X) \cdot \sum_i \sum_m F_{UVBI}(X, i, PAS) \cdot F_{CYDR}(m) \cdot CP(i, m) \quad (2.1-25)$$

Moreover, we converted CPD_{global} obtained as weight into a monetary value and used it as the damage function for agricultural production. We estimated the unit prices of soybean, rice, green pea, and mustard to be 240, 243, 550, and 30 yen kg⁻¹ respectively, referring to the

producer unit prices of soybean and rice in Japan (Ministry of Agriculture, Forestry and Fisheries 2002a) and the producer unit prices of green pea and mustard in Japan from FAOSTAT (FAO 2000). Table 2.1-8 shows some of the damage functions we obtained.

Table 2.1-8: Damage functions for agricultural production (partial)

	Latitude band	CFC-11					HCFC-22				
		Soybean	Rice	Green pea	Mustard	Total	Soybean	Rice	Green pea	Mustard	Total
Damage function in each latitude	80-90° N lat.	0.00e+0	0.00e+0	0.00e+0	0.00e+0	0.00e+0	0.00e+0	0.00e+0	0.00e+0	0.00e+0	0.00e+0
	70-80° N lat.	4.46e-7	2.33e-7	7.01e-6	6.76e-8	7.75e-6	1.79e-8	9.38e-9	2.82e-7	2.72e-9	3.12e-7
	60-70° N lat.	1.10e-3	7.06e-5	4.92e-3	2.74e-5	6.12e-3	4.42e-5	2.84e-6	1.98e-4	1.10e-6	2.46e-4
	50-60° N lat.	2.66e-2	1.57e-2	3.21e-1	1.66e-3	3.65e-1	1.07e-3	6.34e-4	1.29e-2	6.69e-5	1.47e-2
	40-50° N lat.	6.51e-1	4.13e-1	8.14e-1	1.37e-3	1.88e+0	2.62e-2	1.66e-2	3.27e-2	5.51e-5	7.56e-2
	30-40° N lat.	9.50e-1	1.03e+0	3.46e-1	3.22e-4	2.32e+0	3.82e-2	4.14e-2	1.39e-2	1.30e-5	9.35e-2
	20-30° N lat.	1.73e-1	1.13e+0	2.81e-1	1.29e-3	1.58e+0	6.96e-3	4.54e-2	1.13e-2	5.19e-5	6.38e-2
	10-20° N lat.	2.83e-2	3.66e-1	5.73e-2	2.20e-5	4.51e-1	1.14e-3	1.47e-2	2.31e-3	8.87e-7	1.82e-2
	Equator to 10° N lat.	6.12e-3	2.21e-2	1.97e-3	3.45e-7	3.02e-2	2.46e-4	8.92e-4	7.93e-5	1.39e-8	1.22e-3
	Equator to 10° S lat.	9.23e-2	1.04e-1	6.97e-3	0.00e+0	2.03e-1	3.72e-3	4.18e-3	2.81e-4	0.00e+0	8.18e-3
	10-20° S lat.	1.82e-1	3.39e-2	1.77e-2	4.45e-7	2.33e-1	7.32e-3	1.37e-3	7.12e-4	1.79e-8	9.40e-3
	20-30° S lat.	2.56e-1	2.43e-2	3.53e-2	1.42e-6	3.16e-1	1.03e-2	9.77e-4	1.42e-3	5.70e-8	1.27e-2
	30-40° S lat.	2.17e-1	1.63e-2	2.98e-2	7.85e-7	2.63e-1	8.74e-3	6.57e-4	1.20e-3	3.16e-8	1.06e-2
	40-50° S lat.	9.16e-2	2.22e-3	1.54e-2	3.26e-8	1.09e-1	3.69e-3	8.93e-5	6.22e-4	1.31e-9	4.40e-3
	50-60° S lat.	9.14e-3	2.67e-4	6.55e-4	0.00e+0	1.01e-2	3.68e-4	1.07e-5	2.63e-5	0.00e+0	4.05e-4
	60-70° S lat.	0.00e+0	0.00e+0	0.00e+0	0.00e+0	0.00e+0	0.00e+0	0.00e+0	0.00e+0	0.00e+0	0.00e+0
	70-80° S lat.	0.00e+0	0.00e+0	0.00e+0	0.00e+0	0.00e+0	0.00e+0	0.00e+0	0.00e+0	0.00e+0	0.00e+0
	80-90° S lat.	0.00e+0	0.00e+0	0.00e+0	0.00e+0	0.00e+0	0.00e+0	0.00e+0	0.00e+0	0.00e+0	0.00e+0
Global total		2.68e+0	3.15e+0	1.93e+0	4.70e-3	7.77e+0	1.08e-1	1.27e-1	7.78e-2	1.89e-4	3.13e-1

- The unit of damage function is yen kg⁻¹. That is, an increase in the potential damage to agricultural production as a result of addition emission of 1 kg of the ODS is converted into Japanese yen.
- The total of damage functions in each latitude band is used as the global damage function for LIME.

(9) Social assets: damage functions for wood production

Damage to terrestrial NPP as primary production simultaneously brings about damage to wood production as social assets. Because the target of the damage functions for terrestrial NPP is conifer forests, we assumed that all of them have direct impact on wood production. Based on 9,360 yen m⁻³, the average producer unit price of wood in Japan (Ministry of Agriculture, Forestry and Fisheries 2002b) (for sawing, wood chips, and pulp), we estimated the wood density to be 500 kg m⁻³ and gained a unit price of 18.7 yen kg⁻¹. We used the unit price for converting the damage functions for terrestrial NPP into a monetary value and regarded them as the damage functions for wood production. Table 2.1-9 shows some of the damage functions we obtained.

(10) Arrangement of damage functions of ozone layer destruction and damage factors

We added up endpoint damage functions for each area of protection (human health, social assets, and primary production) and regarded the result as the damage factor of ozone layer destruction. That is, the total of damage functions for skin cancer and cataract is used as the damage factor for human health, the total of damage functions for agricultural production and wood production is used as the damage factor for social assets, and the total of damage functions for terrestrial NPP and aquatic NPP is used as the damage factor for primary

production. The damage factors are shown in Appendix 2. For reference, Table 2.1-10 shows the damage functions and factors of ODSs whose damage functions could be calculated directly.

Table 2.1-9: Damage functions for wood production (partial)

	Latitude band	CFC-11	CFC-12	Halon-1211	Halon-1301	CCl ₄	1,1,1-TCE	HCFC-22
Damage function in each latitude	80-90° N lat.	0.00e+0	0.00e+0	0.00e+0	0.00e+0	0.00e+0	0.00e+0	0.00e+0
	70-80° N lat.	1.12e-1	1.17e-1	2.82e-1	1.64e+0	1.08e-1	7.58e-3	4.49e-3
	60-70° N lat.	1.41e+0	1.47e+1	3.56e+1	2.07e+2	1.36e+1	9.55e-1	5.66e-1
	50-60° N lat.	3.28e+1	3.44e+1	8.31e+1	4.83e+2	3.16e+1	2.23e+0	1.32e+0
	40-50° N lat.	2.60e+1	2.72e+1	6.58e+1	3.83e+2	2.51e+1	1.77e+0	1.05e+0
	30-40° N lat.	9.40e+0	9.87e+0	2.36e+1	1.38e+2	9.05e+0	6.38e-1	3.78e-1
	20-30° N lat.	8.44e-2	8.87e-2	2.11e-1	1.23e+0	8.13e-2	5.73e-3	3.40e-3
	10-20° N lat.	0.00e+0	0.00e+0	0.00e+0	0.00e+0	0.00e+0	0.00e+0	0.00e+0
	Equator to 10° N lat.	0.00e+0	0.00e+0	0.00e+0	0.00e+0	0.00e+0	0.00e+0	0.00e+0
	Equator to 10° S lat.	0.00e+0	0.00e+0	0.00e+0	0.00e+0	0.00e+0	0.00e+0	0.00e+0
	10-20° S lat.	0.00e+0	0.00e+0	0.00e+0	0.00e+0	0.00e+0	0.00e+0	0.00e+0
	20-30° S lat.	0.00e+0	0.00e+0	0.00e+0	0.00e+0	0.00e+0	0.00e+0	0.00e+0
	30-40° S lat.	0.00e+0	0.00e+0	0.00e+0	0.00e+0	0.00e+0	0.00e+0	0.00e+0
	40-50° S lat.	0.00e+0	0.00e+0	0.00e+0	0.00e+0	0.00e+0	0.00e+0	0.00e+0
	50-60° S lat.	0.00e+0	0.00e+0	0.00e+0	0.00e+0	0.00e+0	0.00e+0	0.00e+0
	60-70° S lat.	0.00e+0	0.00e+0	0.00e+0	0.00e+0	0.00e+0	0.00e+0	0.00e+0
	70-80° S lat.	0.00e+0	0.00e+0	0.00e+0	0.00e+0	0.00e+0	0.00e+0	0.00e+0
	80-90° S lat.	0.00e+0	0.00e+0	0.00e+0	0.00e+0	0.00e+0	0.00e+0	0.00e+0
Global total		8.25e+1	8.64e+1	2.09e+2	1.21e+3	7.95e+1	5.60e+0	3.32e+0

- The unit of damage function is yen kg⁻¹. That is, we regarded potential damage to terrestrial NPP due to additional emission of 1 kg of the ODS as damage to wood production and converted it into Japanese yen.
- The total of damage functions in each latitude band (limited to conifer forests in areas other than mountainous ones) is used as the global damage function for LIME.

Table 2.1-10: Damage functions and factors of ozone layer destruction (limited to ODSs for which direct calculation is possible)

ODS	Human health (DALY kg ⁻¹)			Social assets (Yen kg ⁻¹)			Primary production (kg kg ⁻¹)		
	Skin cancer	Cataract	Total	Agri. production	Forestry production	Total	Terrestrial	Aquatic	Total
CFC-11	5.91e-4	7.54e-4	1.34e-3	7.77e+0	8.25e+1	9.03e+1	4.41e+0	2.85e+2	2.90e+2
CFC-12	6.19e-4	7.89e-4	1.41e-3	8.14e+0	8.64e+1	9.45e+1	4.61e+0	2.99e+2	3.03e+2
CFC-113	6.33e-4	8.07e-4	1.44e-3	8.33e+0	8.84e+1	9.67e+1	4.72e+0	3.05e+2	3.10e+2
Halon-1211	1.49e-3	1.89e-3	3.38e-3	1.95e+1	2.09e+2	2.28e+2	1.11e+1	7.29e+2	7.41e+2
Halon-1301	8.67e-3	1.10e-2	1.97e-2	1.14e+2	1.21e+3	1.33e+3	6.48e+1	4.23e+3	4.30e+3
CCl ₄	5.70e-4	7.26e-4	1.30e-3	7.49e+0	7.95e+1	8.70e+1	4.25e+0	2.75e+2	2.79e+2
1,1,1-TCE	4.01e-5	5.12e-5	9.13e-5	5.28e-1	5.60e+0	6.13e+0	2.99e-1	1.94e+1	1.97e+1
HCFC-22	2.38e-5	3.03e-5	5.41e-5	3.13e-1	3.32e+0	3.63e+0	1.77e-1	1.15e+1	1.16e+1
HCFC-123	1.53e-6	1.95e-6	3.49e-6	2.01e-2	2.14e-1	2.34e-1	1.14e-2	7.39e-1	7.51e-1
HCFC-124	9.13e-6	1.16e-5	2.08e-5	1.20e-1	1.27e+0	1.39e+0	6.80e-2	4.40e+0	8.47e+0
HCFC-141b	5.25e-5	6.70e-5	1.20e-4	6.91e-1	7.34e+0	8.03e+0	3.92e-1	2.53e+1	2.57e+1
HCFC-142b	3.62e-5	4.62e-5	8.24e-5	4.76e-1	5.05e+0	5.53e+0	2.70e-1	1.74e+1	1.77e+1
CH ₃ Br	2.87e-6	3.66e-6	6.53e-6	3.78e-2	4.06e-1	4.44e-1	2.17e-2	1.43e+0	1.45e+0

- Under LIME, the total of damage functions for each area of protection is used as the damage factor.

2.1.4 Procedure for impact assessment of ozone layer destruction

Below, we will concretely describe procedures for characterization of ozone layer destruction and damage assessment. Those who carry out the procedures can select what is suitable for their purpose from among characterization, damage assessment, and integration, and use it for LCA or the like.

The characterization result CIOzone can be obtained from the inventory of the type X of ODS, Inv (X), and the characterization factor CFOzone(X). CIOzone can be regarded as the total ODS emissions converted into CFC-11, a typical ODS.

$$CI^{Ozone} = \sum_X (CF_{ozone}(X) \times Inv(X)) \quad (2.1-26)$$

There are several lists of the characterization factor CFOzone (X). Because priority is given to high scientific reliability and an international organization's authorization, we recommended the ODP ∞ presented in the WMO Scientific Assessment (WMO 1999) as the characterization factor.

In addition, the damage assessment result $DI(Safe)$ can be obtained from each ODS's $Inv(X)$ and the damage factor for each area of protection $DF^{Ozone}(Safe, X)$.

$$DI(Safe) = \sum_X DF^{Ozone}(Safe, X) \cdot Inv(X) \quad (2.1-27)$$

$DI(Safe)$ means the potential amount of damage to each area of protection $Safe$. This equation enables damage assessment concerning human health, social assets, and primary production. With regard to common areas of protection, comparison and integration with amounts of damage that occur through different impact categories are possible.

$IF^{Ozone}(X)$, the factor that integrates impacts on human health, social assets, and primary production, is used for integration. The single index SI can be obtained from each ODS's $Inv(X)$ and the integration factor $IF^{Ozone}(X)$. The obtained result can be directly compared and added with the assessment results of other impact categories.

$$SI = \sum_X (IF^{Ozone}(X) \times Inv(X)) \quad (2.1-28)$$

Appendices 1, 2, and 3 show the characterization factor $CF^{Ozone}(X)$, the damage factor $DF^{Ozone}(Safe, X)$, and the integration factor $IF^{Ozone}(X)$ respectively.

[References for Section 2.1]

Armstrong BK (1993): How much melanoma is caused by sun exposure?, *Melanoma Research*, 3 : 395 - 401

Behrenfeld BJ, Chapman JW, Hardy JT, Lee IIH (1993a): Is there a common response to ultraviolet — B radiation by marine phytoplankton?, *Marine Ecology Progress Series*, 102 : 59 – 68

Behrenfeld BJ, Hardy JT, Gucinski H, Hanneman A, Lee IIH, Wones A (1993b): Effect of Ultraviolet — Bon Primary Production along Transects in the South Ocean, *Marine Environmental Research*, 35 : 349 - 363

CIE (International Commission on Illumination) (1987): A reference action spectrum for ultraviolet-induced erythema in human skin, *CIE Research Note, CIE Journal*, 6: 17 - 22

CMDL (Climate Monitoring and Diagnostic Laboratory) (1998): Halocompounds Dataset, CMDL/NOAA

Caldwell MM (1971): Solar ultraviolet radiation and the growth and development of higher plants *Photobiology* 6, Academic Press, New York, p. 131 - 177

Daniel JS, Solomon S, Albritton DL (1995): On the Evaluation of Halocarbon Radiative Forcing and Global Warming Potentials. *J. Geophys. Res.*, 100, (D1): 1271 - 1285

FAO (Food and Agriculture Organization) (2000): FAOSTAT, FAO

Ferlay J, Black RJ, Whelan SL, Parkin DM (1997): CI5VII: Electronic Database of Cancer Incidence in Five Continents 7, IARC Cancer Base No. 2, IARC (International Agency for Research on Cancer)/WHO, CD —ROM with Booklet

GSFC (Goddard Space Flight Center) (2000): SeaWiFS Project, GSFC/NASA

Goedkoop M, Spriensma R (2000): The Eco — indicator 99, A Damage Oriented Method for Life Cycle Impact Assessment, Methodology Report 2nd edition

Hauschild M, Wenzel H (1998): Environmental assessment of products, Chapman & Hall, London

Hayashi K, Itsubo N, Inaba A (2000): Development of Damage Function for Stratospheric Ozone Layer Depletion —A Tool Towards the Improvement of the Quality of Life Cycle Impact Assessment —, *Int. J. LCA*, 5 :265 - 272

Hayashi K, Nakagawa A, Itsubo N, and Inaba A (2004): Expansion of Damage Function for Stratospheric Ozone Depletion to Cover Major Endpoints Regarding Life Cycle Impact Assessment, *Int. J. LCA*, Online First, DOI : <http://dx.doi.org/10.1065/lca2004.11.189>, p.12

Houghton JT (1986): The Physics of Atmospheres 2nd edition, Cambridge University Press

Kaye JA, Penkett SA, Ormond FM (eds.) (1994): Report on Concentrations, Lifetimes, and Trends of CFCs, Halons and Related Species, NASA Reference Publication, 1339, NASA

Krupa SV, Kickert RN (1989): The greenhouse effect; impacts of ultraviolet — B (UV — B), carbon dioxide (CO_2), and ozone (O_3) on vegetation. *Env. Poll.*, 61 : 263 - 293

Mac Peter R, Beach E (1996): TOMS Version 7 O_3 Gridded Data: 1978 — 1993, GSFC/NASA, CD —ROM

Matthews E (1983): Global vegetation and land use: new high resolution data bases for climate studies, *Journal of Climate and Applied Meteorology*, 22 : 474 - 487

Naganobu M, Kutsuwada K, Sasai Y, Taguchi S, Siegel V (1999): Relationships between Antarctic krill (*Euphausia superba*) variability and westerly fluctuations and ozone depletion in the Antarctic Peninsula area, *J. Geophys. Res.*, 104 : 20651 - 20665

Naidu SL, Sullivan JH, Teramura AH DeLucia EH (1993): The effects of ultraviolet — B radiation on photosynthesis of different aged needles in field — grown loblolly pine, *Tree Physiology*, 12 : 151 - 162

Nichols et al. (1996): In Towards a Methodology (Udo de Haes ed.), SETAC — Europe, Brussels

Ozone Research and Monitoring Project, Report No. 37

Redfield AC, Ketchum BH, Richards FA (1963): The Influence of Organisms on the Composition of Sea Water. In *The Sea* Vol. 2 (Hill ed.), Interscience, London, 26 - 77

Sasaki K, Sakamoto Y, Fujisawa K, Kojima M, Shibata T (1997): A New Grading System for Nuclear Cataracts —An Alternative to the Japanese Cooperative Cataract Epidemiology Study Group's Grading System, *Cataract Epidemiology, Developments in Ophthalmology*, 27, Karger, Basel, p. 42 - 49

Solomon S, Albritton DL (1992): Time — dependent ozone depletion potentials for short — and long — term forecasts. *Nature*, 357: 35 - 37

Steen B (1999): A Systematic Approach to Environmental Priority Strategies in Product Development (EPS)

Version 2000 — Models and Data of the Default Method, CPM Report 1999:5, Chalmers University of Technology, Goteborg

Sullivan JH, Teramura AH (1992): The effects of ultraviolet — B radiation on loblolly pine. 2. Growth of field —grown seedlings, *Trees Structure and Function*, 6: 115 - 120

UNEP (1998): Environmental Effect of Ozone depletion 1998 Assessment

UNEP (2000): The Ozone Secretariat (Montreal Protocol) — UNEP, <http://www.unep.ch/ozone/home.htm>.

WMO (1992): Scientific Assessment of Ozone Depletion

WMO (1995): Scientific Assessment of Ozone Depletion 1994, World Meteorological Organization Global

WMO (1999): Scientific Assessment of Ozone Depletion: 1998. WMO Global Ozone Research and Monitoring Project: Report No.44

Whittaker RH (1979): Communities and Ecosystems (trans. Hogetsu K), Baifukan

Aida M (1982): The Atmosphere and Radial Assumption – Investigation on Atmospheric Heat Sources and Radiation Budget, Tokyodo Publishing

Asakura T, Sekiguchi Y, Nitta T (ed.) (1995): New Meteorology Meteorological Handbook, Asakura Publishing, p. 17 - 22

Aruga Y (1986): Production Ecology of Marine Phytoplankton, Ecology of Algae (collectively written by Akiyama, Aruga, Sakamoto, Yokohama), Uchida Rokakuho Publishing, p. 81 - 121

Ichihashi M, Sasaki M (ed.) (2000): Photo-Developed Bioscience Series 4: Creatures' Photolesion and Protection Mechanism, Kyoritsu Publishing

Ogura Y (1999): General Meteorology, 2nd edition, University of Tokyo Press

Environment Agency's Global Environmental Department (supervised) (1995): Ozone Layer Destruction –

Impact of Ultraviolet Rays on Human Health and the Plant and Ecological Systems, Chuohoki Publishing, p. 12 - 15

Environment Agency (1998): FY1997 Annual Report on the Results of Observation of the Ozone Layer, Environment Agency

Meteorological Agency (1998): Annual Report on Monitoring the Ozone Layer Vol. 8, Meteorological Agency, CD-ROM

Saito H, Kasai H, Taguchi S (1993): Research on Assessment of Impact of an Increase in Ultraviolet Rays on Phytoplankton, FY1992 Report of Research Results under the Global Environment Research Fund A-5, Environment Agency, p. 163 - 174

Sasaki K, Kojima M, Sasaki H, Kato N, Ono M, Jonasson F, Cheng HM, Chew SJ, Shui YB, Taylor H, McCarty C, Robman L (1999): A-4, Research on the Impact of Ultraviolet Rays on Human Health from the Epidemiological Viewpoint, FY1998 Compilation of Reports of Research Results under the Global Environment Research Fund, Environment Agency, p. 31 - 42

Ministry of Agriculture, Forestry and Fisheries (2002a): 76th Statistical Yearbook of the Ministry of Agriculture, Forestry and Fisheries

Ministry of Agriculture, Forestry and Fisheries (2002b): 2000 Report on Supply and Demand of Lumber

Fuwa K, Morita M (written and edited) (2002): Global Environment Handbook 2nd Edition, Asakura Publishing, 26

2.2 Global warming

(Changes in LIME2)

- Uncertainty assessment of damage factors was carried out.
- Under LIME1, the degree of temperature rise in the future was estimated by use of the DICE model based on two types of emissions scenarios: the IS92a scenario and a scenario that fixes emissions at the amount in 1990. Under LIME2, the degree of temperature rise in the future was fixed by the use of the result of calculation by the simplified climate model MAGICC based on two types of emissions scenarios: the median of the SRES scenario used for the future climate prediction shown in the IPCC Third Assessment Report, and a scenario that fixes emissions at the amount in 2000. The fixed degree of temperature rise was applied to the damage function for human health and the damage function for social assets (energy consumption and farm products). In addition, the calculation formulas of these damage functions and some of the parameters were reviewed mutually.
- Consequently, the period for adding up differences in the amount of emissions and the amount of damage was changed from 1990-2063 (the year when carbon dioxide concentration will double) under LIME1 to the actual 2000-2063 under LIME2.
- The definitional identity of the damage function for social assets (land loss) due to a rise in the sea level was reviewed into a form more consistent with other endpoints, and the result of output (the amount of rise in sea level) by MAGICC was used in a similar way as in the case of the damage function for human health and the like.

2.2.1 What phenomenon is global warming?

Gases with a high capacity to absorb infrared rays exist in the atmosphere. Although most of the visible light that constitutes the main part of solar energy penetrates the atmosphere, some infrared rays radiated from the surface of the ground to outer space are absorbed in such gases, resulting in a rise in temperature. This is called the greenhouse effect, and gases that are involved in the greenhouse effect are called greenhouse gases (GHG). If there were no greenhouse effect, the average temperature on the surface of the ground is calculated to be about -18°C . Therefore, the greenhouse effect itself is beneficial for the existence of creatures.

However, as a result of an increase in the consumption of fossil fuels due to rapid development of economic industries in the modern era, the amount of artificial emission of carbon dioxide (CO_2), a typical GHG, has sharply increased. In addition, the amount of artificial emission of gases that have stronger greenhouse effect than CO_2 , such as methane (CH_4), nitrogen monoxide (N_2O), and halocarbons (such as CFCs), has been increasing. As a result, there is fear that the temperature may rise, and the rise in temperature may cause various effects. This phenomenon is called global warming.

(1) Cause of global warming

Figure 2.2.1 shows the causal relationship between GHG emissions leading to global warming and the occurrence of damage and also shows routes of damage. Although the routes exist theoretically, scientific verification of most of the routes has still not been completed through observation thus far (although many scientists have made efforts to solve the problem of global warming, “scientific verification” herein means verification by the Intergovernmental Panel on Climate Change (IPCC)). There are two viewpoints for verification: the viewpoint of whether the phenomenon has occurred in reality, and the viewpoint of whether the causal relationship can be proved.

According to IPCC, among the phenomena in Figure 2.2-1, those that have actually occurred include an increase in atmospheric GHG concentration, a decrease in glacial areas other than the polar areas, a melting or decrease in permanently frozen soil, and a rise in sea level. Causal relationships have been proved completely only concerning an increase in the artificial emission of GHG and an increase in atmospheric GHG concentration at the uppermost level of impact routes (IPCC 2001a). The other phenomena are 1) those about which observation results that can serve as evidence exist, but the verification of causal relationships is somewhat uncertain, and 2) impacts that have been theoretically predicted (through laboratorial observation or computer simulation), but still have not been observed. The causal relationships in the upper part of the figure, such as a rise in temperature, a change in rainfall, other weather phenomena, and disaster damage directly related to them, fall under 1), while the causal relationships shown in the lower part of figure, such as impact on agricultural production, have only undergone laboratorial impact assessment, which falls under 2).

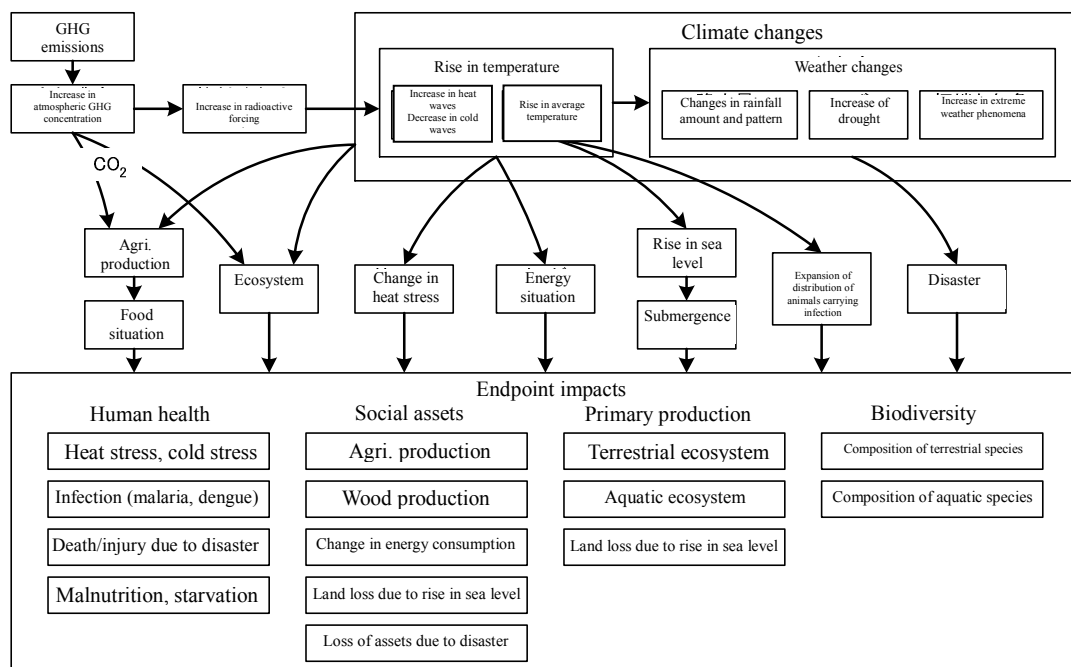


Figure 2.2-1: Causal Relationships of Global Warming

In this way, impact assessment of global warming is rarely confirmed as a fact. Therefore, attention should be paid to impact assessment often being the result of prediction about damage in the future. Such predictive research has been carried out by the use of many research resources, because there is the possibility that if damage occurs, serious damage may spread all over the world for a long time. Therefore, the “precautionary principle” has been applied to the prediction of impact of global warming to some extent.

IPCC’s WG1, which deals with scientific basics (mainly, weather knowledge), has classified the certainty of these causal relationships into seven probabilities, ranging from “almost certain” to “very unlikely” (IPCC 2001a). Its WG2 has classified the reliability of impact prediction into five ranks, ranging from “very likely” to “very unlikely” (IPCC 2001a).

With regard to the prediction of a rise in temperature, which belongs to causal relationships shown in the upper part of the figure, IPCC has classified a rise in maximum temperature, an increase in heat waves, a rise in the lowest temperature, and a decrease in cold waves as “very likely (probability of 90 to 99%),” while it has applied not probability assessment but prediction based on GHG emissions scenarios to a rise in the average temperature (IPCC 2001a). That is, although it is highly likely that the temperature will rise in the future (which will be typically reflected in rises in the maximum and minimum temperatures), the degrees of the rises depend on which scenario is chosen. It has been predicted that a rise in the intensity of rainfall will be “very likely (probability of 90 to 99%)” (IPCC 2001a). When selecting category endpoints, we will refer to IPCC’s probability assessment about the occurrence of damage as a criterion for screening (for the probability assessment mentioned below, see the IPCC’s third report “Synthesis Report”) (IPCC 2001a).

(2) Endpoints of global warming

Damage assessment in the area of global warming is greatly different from that in the other impact areas, in that the number of category endpoints is large because there are various types of impact and routes as shown in Figure 2.2-1 “Causal Relationships of Global Warming.” Under LIME, after preparing a list of category endpoints to be protected, we screened the endpoints by the following criteria to choose objects of assessment.

- 1) The probability of occurrence of damage should be more than about the middle.
- 2) Damage should be thought to be large according to existing research or public perception.
- 3) There should be quantitative information for assessment.

With regard to 1), we basically referred to IPCC’s second and third reports. With regard to 2), we mainly referred to the results of damage accumulation-type economic impact assessment (Fankhauser 1995, Tol 1995, ExternE 1999) and also examined what are addressed by other LCA impact assessment methods (Steen 1999, Goedkoop et al. 1999). With regard to 3), we examined global data availability. However, even if such criteria are used, because the existing research contains uncertainty, note that such screening also has uncertainty. Table 2.2-1 shows the objects of calculation of damage functions under LIME.

Table 2.2-1: Category Endpoints of Global Warming and the Objects of LIME

Area of protection	Category endpoint	Object of calculation of damage function	Screening		
			(1)	(2)	(3)
Human health	Heat stress	Increase in deaths due to increase in heat stress Decrease in deaths due to relaxation of cold stress	○	Heat stress, cold stress	○ ○ △
	Infection	Increase in infection suffered through animals	○	Malaria, dengue	○ ○ ○
			×	Yellow fever, schistosomiasis, etc.	△ × △
	Air pollution	Worsening of impact of tropospheric ozone	×	Poor quantitative information	△ △ ×
	Disaster damage	Weather disasters, such as flood and typhoon	○	Death damage	○ ○ △
Social asset	Malnutrition, Starvation	Change in the food situation due to change in agri. production	○	Aspect of malnutrition (excluding starvation)	△ ○ △
	Agri. production	Changes in quantity/quality of farm products	○	Value of agri. production (limited to 3 main grains)	○ ○ ○
	Wood production	Changes in growth speed/quality of forests	×	Value of wood production	△ ○ ×
	Fishery production	Impact on fish/aquaculture	×	Poor quantitative information	△ ○ ×
	Energy consumption	Increase in no. of days of cooling, decrease in no. of days of heating	○	Value of energy consumption	○ ○ ○
	Land loss	Land loss due to submersion caused by sea level rise	○	Value of lost land area	○ ○ △
	Water resources	Change in amount of available fresh water	×	Poor quantitative information (impact is partially reflected in agri. production)	○ △ △
	Immigration	Incurrence of immigration cost due to rise in sea level	×	Poor quantitative information	○ △ ×
	Assets loss	Loss of social assets due to weather disaster	×	Poor quantitative information	○ × ×
Primary production	Impact on insurance	Increase in insurance cost	×	Poor quantitative information	○ × ×
	Terrestrial ecosystem	Change in production capacity of terrestrial plants	×	Net primary production (NPP) of latent vegetation	○ ○ △
	Aquatic ecosystem	Change in production capacity of phytoplankton	×	Poor quantitative information	○ ○ ×

	Land loss	Land loss due to submersion caused by sea level rise	×	NPP corresponding to lost land area	○	○	△
Biodiversity	Terrestrial ecosystem	Change in composition of species due to climate change	×	Poor quantitative information	-	-	-
	Aquatic ecosystem	Change in composition of species due to climate chang	×	Poor quantitative information	-	-	-

(Note) Screening criteria

- 1) The probability of occurrence of damage should be more than about the middle.
- 2) Damage should be thought to be large according to existing research or public perception.
- 3) There should be quantitative information for assessment.

○: fulfilling the criteria; △: in the middle between fulfillment and non-fulfillment; ×: not fulfilling the criteria

a Impact on human health

The impact of global warming on human health can be divided into direct damage and indirect damage, according to the route of the impact of an aspect of climate change.

The direct damage that is the easiest to imagine and highly interests researchers is the impact of temperature rise on human health. A temperature rise during summer gives heat stress to human bodies and mainly causes metabolic diseases. A typical example is heat stroke. However, the most common cause of death is sharp worsening of existing diseases (Honda et al. 1998). On the other hand, global warming decreases cold stress in winter, which reduces the incidence of cerebral disease. IPCC has predicted as follows: “If the frequency and intensity of heat waves increase, impact on death and disease will be the largest in urban areas, and elderly persons, sick persons, and people who cannot use air conditioners in particular will be influenced (high reliability)”; “Warmer winter and less cold waves will decrease the number of deaths caused by coldness in many countries located in the temperate zone (high reliability).” Although health damage by heat stress and cold stress fulfills the screening criteria 1) and 2), it is difficult to assess globally whether it fulfills criterion 3), because there are only limited data in advanced countries about the current situation of damage. However, under LIME, we assess health damage by heat stress and cold stress, placing importance on the probability of occurrence of damage and taking into consideration that there is a precedent (ExternE 1999).

The other direct damage is disaster damage caused by flood and other extreme weather due to global warming and an increase in the water cycle on the surface of the ground. According to IPCC, the criterion for rainfall is “more intense rainfall (highly likely; in all regions),” and the impact is “an increase in the number of floods, landslides, avalanches or mudslides (high reliability).” The screening criterion 1) was passed. Regarding 2), although this is the smallest area among the areas covered by economic assessment of global warming damage, it has been an object of assessment before. As for 3), irrespective of whether the impact of global warming is included or not, it is possible to grasp the current situation of damage statistically.

Indirect damage includes an increase in damage from infectious diseases, malaria and dengue. This is because the ranges of the animals that carry infectious diseases, such as mosquitoes, expand due to global warming. IPCC has made the following assessments: “In the regions

with limited or poor public health, a rise in temperature extends the malaria-stricken areas into higher areas (high-middle reliability) and higher latitude areas (middle-low reliability)" and "With regard to other diseases carried by animals, climate change has impact on the borders of the current infectious areas (including both beneficial and adverse impacts) (middle-high reliability)." With regard to malaria, although IPCC made these assessments, there are studies that indicate no relation between global warming and an increase in damage from malaria (Reiter 2000, Hey et al. 2002). So long as importance is placed on IPCC's assessments, damage from malaria fulfills all the screening criteria.

The other indirect damage is what is called "socially contingent damages," which occurs in relation to the local social and economic situation in the future. This includes the occurrence of starvation in developing countries due to continuation of a disaster, such as a drought. With regard to weather disasters, IPCC has assessed that "These natural disasters not only directly cause death or injury but also cause an increase in infectious diseases (including diarrhea and respiratory diseases) and damage to public health infrastructures through housing loss, movement of population, pollution of feed water, and lack of food production (very high reliability)." In relation to changes in agricultural production, IPCC has assessed that "Climate change increases the number of undernourished people (middle reliability)." Although the occurrence of socially contingent damage is highly probable as shown above, the degree of damage is highly uncertain because it depends on social conditions. With regard to the screening criteria, fulfillment of 2) is problematic, while the other criteria are fulfilled.

In conclusion, with regard to human health, we assess heat and cold stress, malaria and other infectious diseases, disaster damage, and malnutrition as endpoints.

b Impact on the ecosystem

Because the ecosystem is keeping balanced with the current temperature and other weather conditions, it can be thought that a rise in temperature and other changes in weather conditions disturb the balance of the ecosystem and have some impact on the ecosystem. In terms of biodiversity, it is thought that this appears as changes in the composition of terrestrial and aquatic species. However, because the ecosystem involves highly complicated phenomena that depend on the interdependence among the activities of animals and plants and on the local environmental characteristics (climate, soil, etc.) and consists of various sub-ecosystems, it is difficult to find endpoints where the impact of changes in weather conditions can be observed directly. At present, most research only predicts the impact in specific regions or under specific conditions. Under LIME, therefore, we do not assess biodiversity in the category of global warming.

On the other hand, with regard to plant productivity, a basis for biological activity, there are three main impacts of global warming on plant productivity. This first is the impact of photosynthesis on net primary production. For example, a rise in temperature increases plant respiration and restrains transpiration on the surface of leaves. The second impact is plants' moving to more suitable regions due to a change in temperature, which causes changes in productivity in each region and a resultant change in global productivity. The third impact is not directly related to global warming. A rise in CO₂ concentration, the main cause of global warming, activates photosynthesis and increases plant productivity (fertilizer effect). However, because we could not obtain sufficient findings to assess them, we exclude plant productivity from the objects of assessment.

c Impact on social assets

Global warming causes not only a rise in temperature but also changes in weather conditions, such as cloudiness and precipitation. Such weather conditions influence the ecosystem through impact on photosynthesis and finally influence the production of the primary industries, which include agricultural, forestry, and fisheries industries necessary for human life.

In addition, it is thought that a rise in temperature is accompanied by changes in human life. The plainest example is an increasing in cooling and a decrease in heating, which lead to changes in the consumption of energy, such as electricity and gas. With regard to changes in energy consumption, IPCC has specified “a decrease in demand for heating energy (high reliability)” and “an increase in demand for cooling energy (high reliability),” which fulfills the screening criterion 1). Criterion 2) is also fulfilled, as suggested by other studies (Fankhauser 1995, ExternE 1999). With regard to criterion 3), we decided to use existing research on the relation between the number of days of cooling and heating and the temperature.

In the primary industries, assessment of agricultural damage due to impact on vegetation has been frequently carried out. It is thought that the yield of farm products, such as rice and wheat, changes according to changes in the net primary productivity of vegetation due to climate changes. It is difficult to assess impact on farm production, because impact may cause damage or benefits, depending on the region, kind, and remedies, and because it is predicted that the degree of impact differs. With regard to impact on farm products, IPCC made the following predictions: “Although CO₂ concentration increases the production of grain, it is uncertain that this benefit exceeds the decrease in production due to heat and drought (middle reliability),” “Although a rise in the lowest temperature is beneficial to some farm products (especially in the temperate zone), it gives damage to other products (especially in the low latitude zone) (high reliability),” “A rise in the highest temperature gives harm to many products (high reliability),” “In the middle latitude zone, if agricultural technical measures are taken, a rise in the temperature by less than 2 to 3°C increases the production of grain, but decreases the production of other products (low to middle reliability),” and “In the tropics, no matter how much the temperature rises, the production of grain decreases (middle reliability).” Impact on farm products fulfills screening criteria 1) and 2) because of IPCC’s description, and criterion 3) also is fulfilled because of many assessments in Japan and overseas.

In the field of forestry, like farm products, the growth of raw lumber is influenced by a change in net primary productivity. With regard to terrestrial vegetation, IPCC has suggested that “the impact of climate changes may greatly destroy the ecosystem (high reliability)” and has described that “Although a rise in CO₂ concentration increases net primary production, a rise in temperature has both beneficial and adverse impacts (high reliability).” In addition, with regard to the value of forests, IPCC has mentioned not only the net primary productivity but also the values of biodiversity, wood, fuels, non-wood products, and recreation. However, because, like data on the ecosystem, data on these aspects are insufficient for assessment, the value of forests is not addressed under LIME.

It is thought that social adaptation measures are taken, such as irrigation and breed improvement, to prevent decreases in farm products and wood production that would otherwise occur due to global warming. In the field of agriculture, since IPCC’s second

report, research on adaptation to global warming has been carried out. Under LIME, however, we examined the net impact of global warming without taking into consideration the impact of possible social adaptation on the production of farm products and wood. In addition, although the risk of impact of an increase in weeds on farm products has been predicted, it is not addressed under LIME because there is no result of quantitative assessment.

Moreover, not only farm products but also livestock and fisheries may receive the impact of global warming. IPCC has made the following predictions: “The temperature will more frequently rise due to El Niño (caused by global warming), which will have adverse impact on fishes (high reliability)” and “With regard to aquaculture, because climate changes have adverse impact on the amount of cultured fishes’ feed, such as herring and anchovy, the production of cultured fishes also receives adverse impact.” However, because global warming is still under study, and quantitative assessment is difficult, it is impossible to fulfill screening criterion 3). Therefore, livestock and fisheries are not addressed under LIME. In addition, there is the feedback effect whereby, if there is a change in energy consumption or the ecosystem, CO₂ emissions also are changed accordingly. However, because it is unclear how to assess this feedback effect, the effect is not addressed under LIME, but will be discussed in the future.

2.2.2 Characterization of global warming

(1) Characterization factors for global warming

The characterization of global warming is carried out by adding up the products of the inventory of each GHG and the characterization factor for each GHG. For the purpose of LCA, global warming potential (GWP) (IPCC 1990) is often used as the characterization factor for global warming. GWP is an index widely used under IPCC and the United Nations Framework Convention on Climate Change (UNFCCC). GWP can be calculated by dividing the time integral value of radiation forcing caused by emission of the unit amount of the type *i* of GHG by that of CO₂.

$$GWP_{T,i} = \left(\int_0^T a_i \cdot C_i(t) dt \right) / \left(\int_0^T a_{CO_2} \cdot C_{CO_2}(t) dt \right) \quad (2.2-1)$$

In this equation, *a*, *C* (*t*) and *T* are infrared absorption capacity [Wm⁻² kg⁻¹], atmospheric concentration [kg m⁻³] at time *t*, and the integration period [yr] respectively.

One of the important issues is the fixing of an integration period for GWP. Because atmospheric lifetime differs among GHGs, GWP changes greatly, depending on the integration period. IPCC’s third report (IPCC 2001b) specifies GWPs with integration periods of 20 years, 100 years, and 500 years. The report (IPCC 2001b) states that the selection of an integration period depends on users’ concerns. That is, the report recommends that a short-term GWP should be used for short-term impact, such as impact on clouds, while a long-term GWP should be used for long-term impact, such as a rise in sea level. In the field of LCA, 100-year GWP has been used frequently. This seems because 100 years is appropriate for considering changes in the quality and scale of human activities. Leiden University’s Institute of Environmental Sciences (CML) (2000) in Holland has temporarily recommended the use of the 100-year GWP, taking a moderate stand between the

following ways of thinking: 1) from the viewpoint of uncertainty, it is desirable to use a highly-reliable short-term GWP; and 2) from the viewpoint of completeness of environmental impacts, it is desirable to use a long-term GWP.

(2) Characterization factors for global warming under LIME

Under LIME1, we discussed a list of recommendable GWPs based on existing research. We mainly examined the following three points: 1) Which GWP to select from among those published at various points of time; 2) How many years the integration period should be; and 3) Whether only direct effects should be included or indirect effects should also be included.

a Timing of publication

Depending on the timing of publication, the value of GWP differs due to changes in the storage of atmospheric GHG and the circulation velocity and improvement in the methodology used for calculation. Under LIME1, for the purpose of use for LCA, we recommended the selection of the latest list as of 2001 contained in IPCC's third report (IPCC 2001b), which shows the value of GWP recalculated based on GHG concentration at that time.

b Integration period

The published list shows three types of GWP with integration periods of 20 years, 100 years, and 500 years.

In the case of the GWP with an integration period of 20 years (GWP_{20}), the GWP of a GHG whose atmospheric lifetime is comparatively short, such as CH_4 , appears relatively large. GWP_{20} is suitable for assessing the contribution to the progress rate of global warming.

In the case of the GWP with an integration period of 100 years (GWP_{100}), the number of years is mainly fixed as the period for environmental improvement goals. GWP_{100} has often been used for LCA. GWP_{100} has characteristics somewhere between those of GWP_{20} and GWP_{500} .

In the case of the GWP with an integration period of 500 years (GWP_{500}), the GWP of a GHG whose atmospheric lifetime is extremely long, such as perfluorocarbon, appears relatively large. GWP_{500} is suitable for assessing long-term impact, such as a rise in sea level. In addition, because GWP with an infinite integration period (which covers all the impacts of atmospheric emissions) has not been published, GWP_{500} is the most suitable for considering all the impacts of emissions at present. Moreover, GWP_{500} is the most suitable at present, because international organizations only published values with an infinite integration period concerning the ozone depletion potential (ODP) used for assessment of emission of substances that cause ozone layer destruction.

For the purpose of impact assessment of global warming, the year when CO_2 concentration becomes double (according to a prediction based on the scenario adopted for LIME, 2063) is often used as the benchmark. In addition, the impacts of global warming vary drastically, and both short-term and long-term impacts are important. Therefore, under LIME, the 100-year integration period was recommended.

c Direct effects and indirect effects

A gas has two types of greenhouse effects: direct effects that accompany the radiation forcing of the gas, and indirect effects caused by the transformation of the gas or the gas's chemical reaction with another gas. IPCC (2001b) treats indirect effects differently according to type of GHG as follows:

- 1) CH₄: presentation of GWP as a net effect resulting from the inclusion of indirect effects into the numerical table of direct effects
- 2) Carbon monoxide (CO): presentation of literature data only irrespective of its indirect contribution to greenhouse effects as a precursor substance
- 3) Ozone depletion substance (ODS): presentation of not representative values of indirect effects but their estimated range
- 4) Nitrogen oxide and non-methane hydrocarbon: presentation of not concrete figures but qualitative expressions

Under LIME1, we recommended a net value of the indirect effects of CH₄, because the indirect effects have already been included in the existing GWP and it is unnecessary to separate them from the direct effects. With regard to CO, because IPCC did not discuss a recommendation value, it did not decide a recommendation value, although it presented literature data. With regard to the indirect effects of ODS, because uncertainty was so high that representative values could not be obtained, we only recommended the GWP of the direct effects. In addition, although GWP values of nitrogen oxide and non-methane hydrocarbon may be presented in the future, there are no values suitable for LCIA at present. Therefore, we did not address them.

Recent research recommended that GWP should include indirect effects as a characterization factor for LCA (Brakkee 2007).

d Recommended characterization factor for global warming under LIME

Under LIME2, based on the above-described discussions, we recommended that the 100-year GWP presented in IPCC's fourth report (IPCC 2007), which presents the latest GWPs, should be used as the characterization factor for global warming. The characterization factor is as shown in Appendix A1.

2.2.3 Damage assessment of global warming

Under LIME2, we evaluated environmental impact caused by the additional emission of CO₂. By applying GWP to the result of CO₂, we calculated damage factors for all the GHGs about which characterization factors were recommended. However, the fertilizer effect of agricultural impact depends on CO₂ concentration. Therefore, we calculated damage factors both for the case of inclusion of fertilizer effect and for the case of exclusion of fertilizer effect. After that, we applied GWP to the result of CO₂ in the case of the exclusion to obtain the damage function for the other GHGs.

(1) Basic policy for calculation of damage factors

a Flow until calculation of damage factors

Under LCA, a midpoint approach that used GWP as the characterization factor was the main impact assessment method for global warming. However, because the midpoint approach cannot calculate concrete damage, damage assessment requires an endpoint approach. Under LIME, we developed a method of assessing global warming by an endpoint approach.

Under LIME, what quantitatively expresses the relation between inventory and impact on each category endpoint is defined as the damage function, and the damage function for each area of protection is defined as the damage factor. The category endpoints for global warming and the objects of calculation of damage function are as shown in Table 2.2-1, which includes almost all the important category endpoints described in Section 2.2.1.

Figure 2.2-2 shows a flowchart of calculation of damage functions and factors. The damage function for global warming indicates how much the amount of latent damage increases with the emission of a unit amount of the type X of GHG – for example, how many people latently suffer malaria with the emission of 1 kg of CO₂.

We assumed that quantitative information, such as atmospheric lifetime, could be obtained concerning the GHGs about which the damage function for global warming would be calculated. The procedure for the calculation can be summarized as follows: 1) estimation of changes in climate elements (such as average temperature and precipitation) according to the two scenarios (a fixed amount of emissions and an increasing amount of emissions) until CO₂ concentration becomes double; 2) calculation of changes in the amount of damage according to changes in climate elements at each category endpoint (such as malaria and dengue); 3) calculation of the amount of damage per unit amount of CO₂ by dividing the difference between the amounts of damage in the two scenarios by the difference between the amounts of CO₂ emissions in the scenarios; and 4) calculation of damage factors for other GHGs by applying GWP.

b Method to calculate the amount of damage per unit amount of emissions

The method of calculating marginal damage is useful for assessment of impact of environmentally damaging substances. This method calculates the amount of damage from additional emissions in a certain situation. In the field of economic assessment of damage, there are research cases where marginal damage from CO₂ emissions is calculated as a marginal cost (Fankhauser 1995, Tol 1995, ExternE 1999). Under LIME also, such research cases are used for screening. However, some problems exist concerning the calculation of marginal damage from GHG emissions.

Global warming is a long-term phenomenon. Because damage from temporary emissions also lasts for a long time, the calculation of marginal damage requires the integration of the amount of damage for a period between the time of emissions and a highly uncertain distant future. Because this period greatly differs from scenario to scenario, and the degree of damage differs according to CO₂ concentration at that time and the amount of emissions in the future, they greatly influence the result of assessment of the amount of damage. In the case of monetary assessment, such a problem is addressed by introducing a discount rate. In this case, there arises another problem – the total amount of damage greatly differs according to

the size of the discount rate. Because of such reasons, under LIME, we did not select the marginal assessment method that calculates an increase in the integral quantity of damage with an increase in the annual amount of emissions.

Under LIME, we added up single-year amounts of damage by the use of two types of CO₂ emissions scenarios: 1) a fixed baseline amount of emissions (LIME1: 1990; LIME2: 2000) (in this case also, atmospheric CO₂ concentration is increasing and global warming is progressing); and 2) a scenario of an increasing amount of emissions (LIME 1: IS92a scenario; LIME 2: the median of each scenario of SRES) (see Column 2.2-1). However, under LIME2, common actual amounts of emissions between 1990 and 2000 were input to both the scenario of a fixed amount of emissions and the scenario of an increasing amount of emissions (Figure 2.2-3). We decided that the calculation period should last until CO₂ concentration becomes double (2063). The result of division of the difference between the amounts of damage in the two scenarios (Figures 2.2-4 and 2.2-5) by the difference between the total amounts of CO₂ emissions (Figure 2.2-3) was regarded as the damage function for a unit amount of CO₂ emissions. Time-series (annual) global average values of atmospheric CO₂ concentration and temperature was calculated by the DICE model (Fankhauser 1995) under LIME1 and by the MAGICC model (Wigley 2003) under LIME2. The regional temperature and precipitation used for damage assessment for malaria and agriculture were obtained from several existing general circulation models (GCM) concerning the time when CO₂ concentration becomes double according to the scenario of an increasing amount of emissions. Under LIME, based on impact assessment at the time when CO₂ concentration becomes double, we calculated single-year amounts of impact under the two scenarios by interpolation from time-series temperature data. The following equation was used for construction of the damage function:

[Amount of damage to human health]

$$D(CO_2) = \frac{\int_{1990}^t D(t)dt - \int_{1990}^t D_0(t)dt}{\int_{1990}^t E(t)dt - \int_{1990}^t E_0(t)dt} \quad (2.2-2)$$

- $D(CO_2)$: damage function (amount of change (damage) per unit amount of CO₂ emissions)
- t : covered years (each of the years between 1990 to the year when CO₂ concentration becomes double)
- $D(t)$: amount of damage in covered years (in the case of the increasing emissions scenario)
- $D_0(t)$: amount of damage in covered years (in the case of the fixed emissions scenario)
- $P(t)$: production volume in covered years (in the case of the increasing emissions scenario)
- $P_0(t)$: production volume in covered years (in the case of the fixed emissions scenario)
- $E(t)$: CO₂ emissions in covered years (in the case of the increasing emissions scenario)
- $E_0(t)$: CO₂ emissions in covered years (in the case of the fixed emissions scenario)

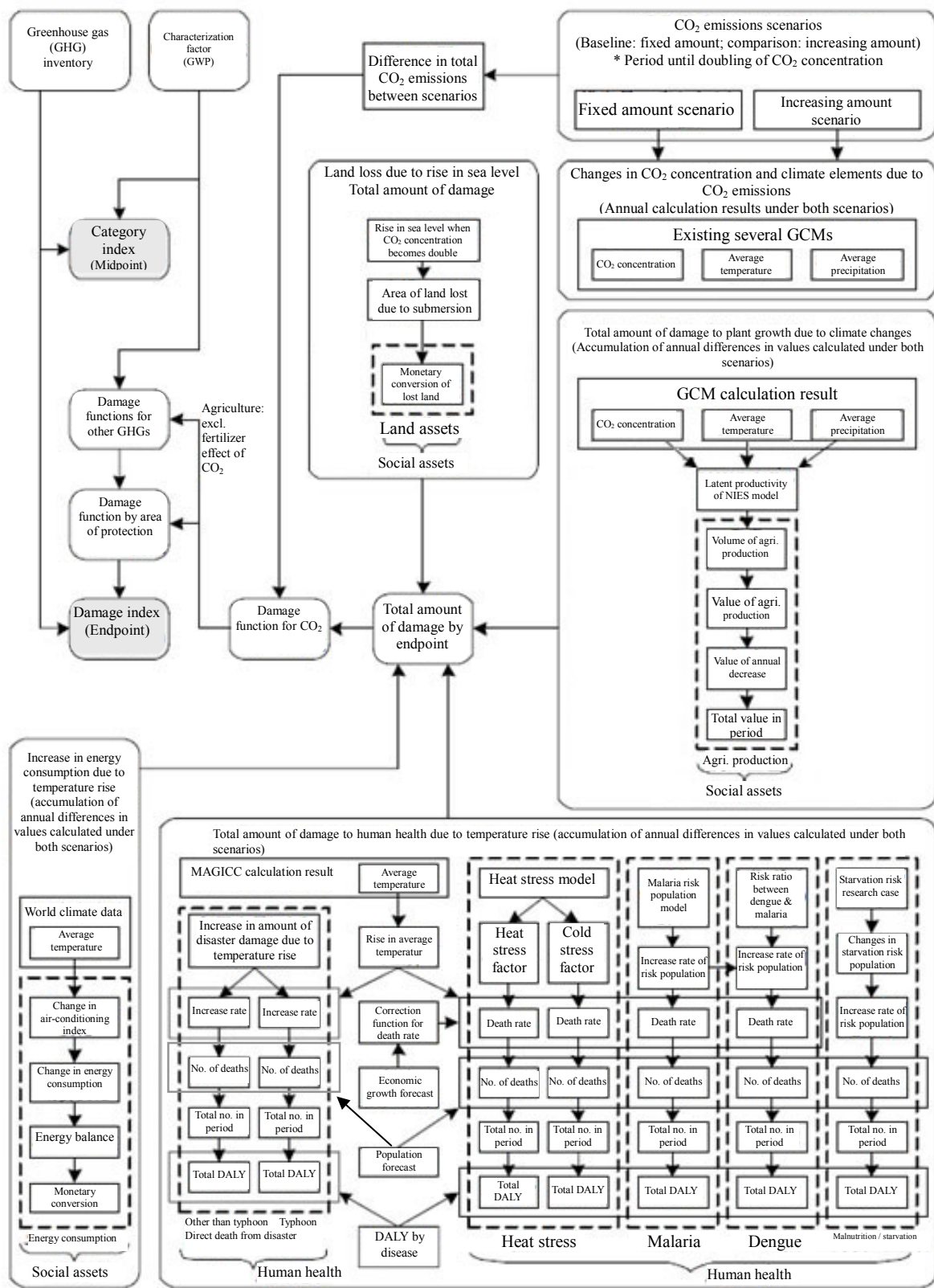


Figure 2.2-2: Flowchart of Estimation of Damage Functions for Global Warming

[In the case of damage to the volume of agriculture and other production]

$$D(CO_2) = \frac{\int_{1990}^t P_0(t)dt - \int_{1990}^t P(t)dt}{\int_{1990}^t E(t)dt - \int_{1990}^t E_0(t)dt} \quad (2.2-3)$$

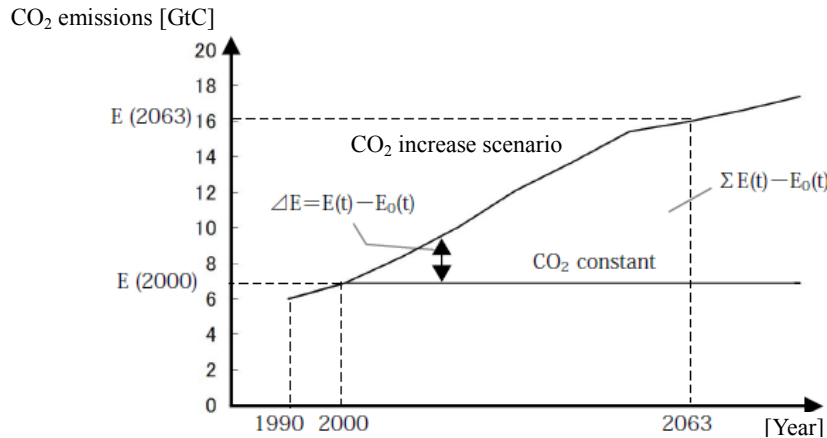


Figure 2.2-3: Interannual Changes in CO₂ Emissions and the Method of Calculating Difference between Scenarios

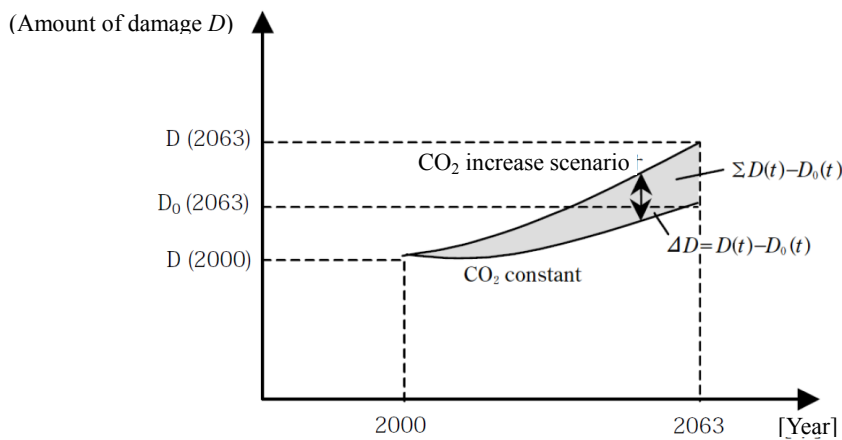


Figure 2.2-4: Interannual Changes in the Amount of Damage to Human Health, etc. and the Method of Calculating Difference between Scenarios

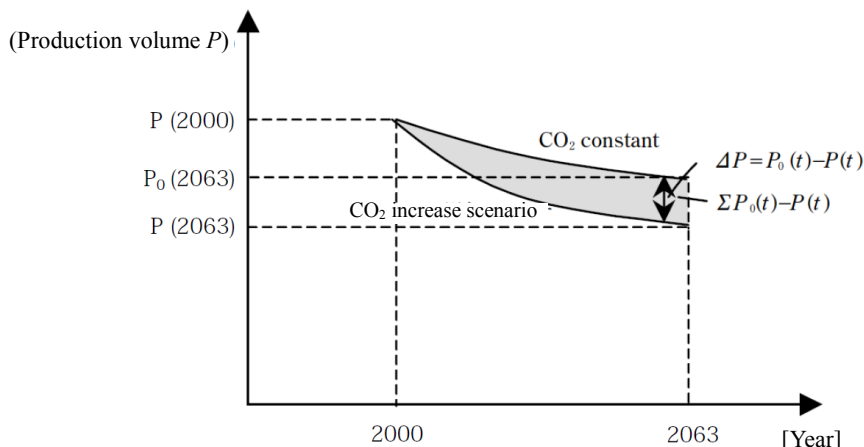


Figure 2.2-5: Interannual Changes in Production Volume and the Method of Calculating Difference between Scenarios

With regard to the GHGs other than CO₂, the above-mentioned amount of CO₂ damage and the 100-year GWP should be used. Because, in the case of CO₂, the fertilizer effect is included in the production volume of farm products, the relation between CO₂ emissions and the amount of damage should be calculated, excluding the fertilizer effect, and multiplied by GWP.

$$D(GHG) = D(CO_2) \cdot GWP(GHG) \quad (2.2-4)$$

D (GHG): amount of damage per unit amount of GHG emissions (1990 to the year when CO₂ concentration becomes double)

D (CO₂): amount of damage per unit amount of CO₂ emissions (1990 to the year when CO₂ concentration becomes double; no fertilizer effect)

GWP (GHG): GWP of the GHG in question

c Benchmark assessment at the time of doubling of CO₂ concentration

Damage assessment has so far focused on the damage at the time when CO₂ concentration becomes double, because the time has been used as the benchmark point of time and because it has been used as the base point of time for time-series prediction. Such prediction is carried out by interpolating or extrapolating damage in another period from benchmark assessment.

Column 2.2-1

Greenhouse Gas Emissions Scenarios

To address criticism of IS92, IPCC organized a special project team in 1996 and published the “Special Report on Emissions Scenarios” (2000) (“SRES Scenarios”).

SRES describes six scenarios corresponding to four storylines. Table 2.2-A summarizes the characteristics of the storylines and the scenarios.

Table 2.2-A: SRES's six scenarios corresponding to four storylines

Storyline	Scenario
A1: continuation of high economic growth	Three scenarios toward technological innovation A1FI “scenario of high growth society that depends on fossil fuel” A1T “scenario of high growth society toward advanced technology” A1B “scenario of well-balanced high growth”
A2: blocked areas in the world	A2: “scenario of heterogeneous society”
B1: simultaneous realization of environmental conservation and economic growth under international cooperation	B1 “scenario of recycling-oriented society”
B2: emphasis on local problems and fairness	B2 “scenario of regional coexistence society”

To predict the future climate based on these scenarios, six integrated assessment modeling groups presented 35 types of emissions estimates.

With regard to the climate response to emissions, we extracted seven GCMs from among 18 GCMs, picked out characteristics as intensification parameters, such as climate sensitivity (1.7 to 4.2°C; 2.8°C on average), ocean thermohaline circulation, and the difference in thermal response between land and sea, and matched the seven GCMs with the 35 emissions estimates, resulting in 245 cases (7×35). Figure 2.2-A shows the results of evaluation of climate changes in the 245 cases (summarized and extracted from Matsuoka (2005)).

Mid-range scenarios for the 245 cases are used for the assessment of the increase scenarios under LIME2.

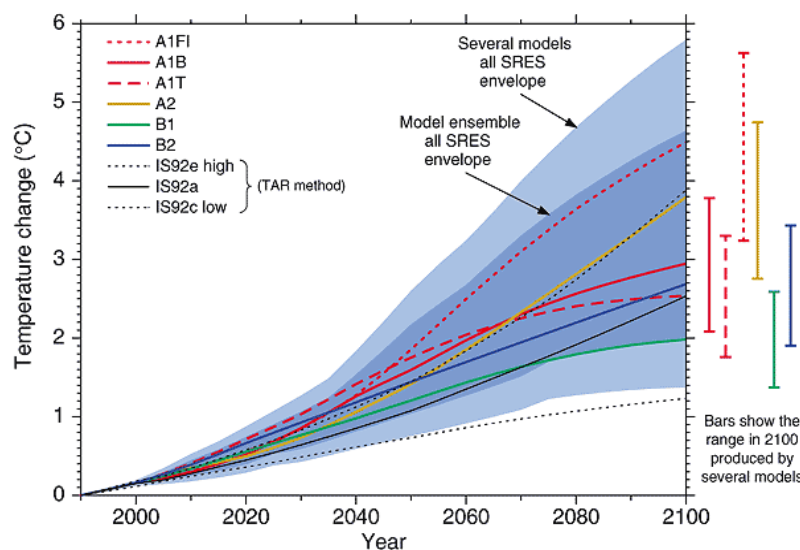


Figure 2.2-A: Result of Future Estimation of a Range of Temperature under TAR

- The light parts indicate the minimum and maximum values of the 245 cases. They correspond to the uncertainty and unclarity, into which both the diversity of future society and the unclarity of the climate system are combined.
- The thick parts are the minimum and maximum of the 35 tracks as average results corresponding to GMC parameters, which differ among the 35 estimated emissions. They roughly correspond to the diversity of future society.
- The line graphs on the left are typical emissions scenarios among the 35 tracks (marker scenarios).
- The bars on the right are ranges of increase in 2100 when the 245 calculated values are grouped into six emissions scenarios. They correspond to the unclarity for the climate system.

(Interpretation by Matsuoka (2005) was extracted and referred to.)
 (Source) http://www.grida.no/climate/ipcc_tar/wg1/fig9-14.htm

d Policy for assessment of damage to human health

Under LIME, damage functions are basically prepared based on changes in the relative risk per temperature rise. The relative risk (RR) is expressed as the mortality ratio by cause of damage at the time of temperature rise and is applied to the current baseline risk by region. That is, because the death rate by cause (absolute risk) differs from region to region, the impact of global warming is expressed as the ratio to the baseline risk. The relative risk should be treated as a variation of the original ratio. Under LIME, however, to simplify calculation, we assume that the relation between temperature rise and damage is linear and that the relative risk per temperature rise minus 1 (RR-1) is the increase rate of mortality by cause per temperature rise [%]. We multiply the baseline risk [the current number of deaths] in each region by the increase rate and then by the temperature rise at a certain point of time [year] to calculate the increased number of deaths by cause due to global warming in that year. Equation 2.2-5 calculates damage by cause, using the relative risk at the time of temperature rise.

$$D_{\text{nonadjusted}}(c, r, t) = BL(c, r) \cdot (RR(c) - 1) \cdot \Delta C(t) \quad (2.2-5)$$

In this equation, $D_{\text{nonadjusted}}(c, r, t)$ is the amount of damage by cause c in region r at time t . $BL(c, r)$ is the amount of damage that occurred by the current cause c in region r . $RR(c)$ is the damage ratio (relative risk) due to cause c at the time when the temperature rises by 1°C. $\Delta C(t)$ is the global average temperature rise from the base year (1990).

As the index of health damage, LIME has adopted DALY, which integrates death damage and injury damage. In the field of global warming, the value of DALY for damage is calculated by estimating the number of deaths and multiplying it by the ratio of deaths to DALY (DALY per death).¹ Basically, the data on the number of deaths by cause and DALY in "The World Health Report (2000)" published by the World Health Organization (WHO) are used for the calculation of the ratio of deaths to DALY. Therefore, because the baseline risk is a current statistical value, the increase rate [%] of death damage by cause per temperature rise based on the relative risk directly influences the magnitude of the damage function as the increase rate of DALY by cause.

Human health and energy consumption receive impact from regional population changes and economic growth. With regard to population, we assumed that the amount of impact is in simple proportion to increase in population. As for impact on human health, we applied the function below to the impact calculated for each region and age in every field to reflect an increase in regional population and impact on regional economy (Equation 2.2-6). However, because malnutrition and starvation described in 2.2.3 (6) reflect the future population for impact assessment in the literature used for BL and RR , Equation 2.2-6 itself is not incorporated in the damage function, and an increase in regional population and impact on regional economy are used only for setting a rate of variability of parameters for uncertainty assessment.

$$D(c, r, t) = D_{\text{nonadjusted}}(c, r, t) \cdot \Delta \% POP(r, t) \cdot Y(r, t)^{-0.417} \cdot Y(r; 1990)^{0.417} \quad (2.2-6)$$

In this equation, $D(c, r, t)$ is the amount of damage by cause c in region r at time t . $D_{\text{nonadjusted}}(c, r, t)$ is the amount of damage by cause c in region r . $\Delta \% POP(r, t)$ is the

¹ If the number of deaths is small and DALY is large (disease that causes many infant deaths and relatively long periods of disorder), DALY per case may become longer than average life expectancy.

increase rate of population from base year (1990) in region r at time t . And $Y(r, t)$ is GDP per capita at purchasing power parity in region r at time t . The second half of this equation was derived based on the result of regression analysis of the logarithms of the death rate by all causes in each country (World Bank 2001) and GDP per capita at purchasing power parity (World Bank 2001) (Figure 2.2-6). With regard to the predicted regional GDP per capita, we used the results of the long-term prediction of IIASA/WEC “Global Energy Perspective” (IIASA/WEC 1988). We also used its classification of regions as it was. We calculated the population increase rate based on the medium-variant prediction of the UN’s “World Population Prospects the 2002 Revision” (United Nations 2003) (for the result of calculation of human health damage by region and by cause, see Table 2.2-3).

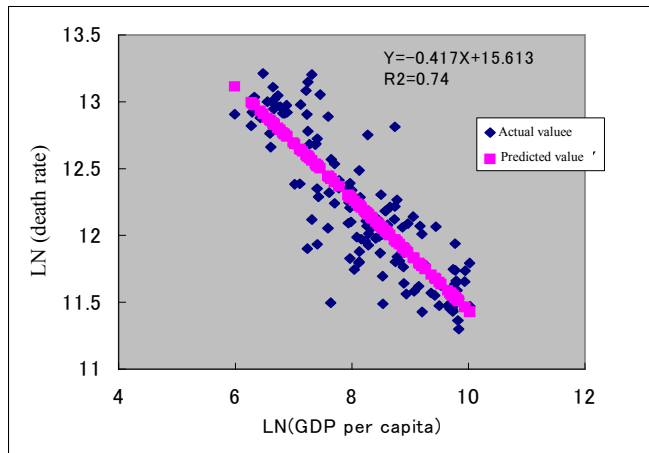


Figure 2.2-6: Relation of the Death Rate and GDP per Capita by Country

(Note) The death rate is the number of deaths per million population.

(Source) World Bank (2001): World Development Indicators for GDP per capita and the death rate; values are as of 1990.

e Basic policy for uncertainty assessment

In 2.2.3 (10), referring to Itsuno and Inaba (2005), we arranged uncertainties and issues concerning the damage function. Table 2.2-2 shows the uncertainties incorporated into the quantitative uncertainty assessment under LIME2.

Table 2.2-2: Basic policy for uncertainty assessment of the damage function for global warming

Process	Covered element	Parameter for probability distribution	Assessment policy
(2)Changes in climate elements	Temperature rise Sea level rise	1) Climate sensitivity (MAGICC model)	Referring to Wigley et al. (2001), set a lognormal distribution with a 90% confidence interval between 1.5 to 4.5°C and a median of 2.6°C. Calculate temperature rise and sea level rise according to climate sensitivity, using a regression curve of outputs calculated for different degrees of climate sensitivity under MAGICC (objective variable: the ratio of a temperature rise or a sea level rise at the climate sensitivity in question to that at a climate sensitivity of 2.6°C; explanatory variable: climate sensitivity) (determine parameters of the regression curve every decade for each emissions scenario).

(3) to (6) Changes in the amount of damage (Human health)	Socioeconom ic scenario	2) Population by region (Prediction for 2050)	Set a normal distribution, using the median of the UN population forecast (2003) as the mean value and regarding one-tenth of the median as the standard deviation.
		3) GDPppp/cap by region (Prediction for 2050)	Based on values for each scenario in IIASA/WEC (1998), set a triangular distribution with a mode value M as the representative value, with a minimum value of $M \times 95\%$ and a maximum value of $M \times 130\%$.
		4) Change in population by starvation risk without global warming	Set a normal distribution, assuming 20% of the decrease rate of 0.47% per year set based on Parry et al. (1999) to be the standard deviation.
Dose-respons e relation (Relative risk of -1 per temperature rise of 1°C)	5) Malaria sufferer risk	Set a gamma distribution by approximating the dispersion and mean values of results of several GCMs shown in Matsuoka et al. (1994).	
	6) Dengue sufferer risk	Use results concerning malaria.	
	7) Prediction of impact increase by heat stress at the time of doubling of CO ₂ concentration	As a multiplier, apply a lognormal distribution with a geometric standard deviation of 2 to the prediction result of the number of victims (heat stress) or beneficiaries (cold stress) by region. (Assuming order-level dispersion)	
	8) Prediction of impact decrease by cold stress at the time of doubling of CO ₂ concentration		
	9) Disaster damage risk	Set a gamma distribution with positive values approximate to a lognormal distribution.	
	10) Disaster (typhoon) damage risk	Set a beta distribution so that low probabilities will become higher.	
	11) Starvation risk (%/ Δ °C) ²	Set a normal distribution, using as the standard deviation the standard error for the regression analysis that used results shown in Parry et al. (1999).	
	Death rate decrease effect by economic growth	12) Regression coefficients for GDP/cap and death rate	Set a normal distribution, using the standard error for regression analysis as the standard deviation.
DALY per death	13) Malaria	Set a normal distribution, using 10% of the mean value as the standard deviation: MEA: $N(84.9,$ $8.49)$; AFR: $N(88.4, 5.83)$; other regions: N (79.2, 7.92).	
	14) Dengue	Set a normal distribution, using 10% of the mean value as the standard deviation: $N(70.8, 7.08)$.	
	15) Heat stress	Set a lognormal distribution with a mean value of 2.0 and another one with a standard deviation of 1.8 (assuming order-level dispersion).	
	16) Cold stress		

		17) Disaster	Set a normal distribution, using 10% of the mean value as the standard deviation: $N(45.1, 4.5)$.
		18) Disaster (typhoon)	
		19) Malnutrition	Set a normal distribution, using 10% of the mean value as the standard deviation: $N(106.1, 10.6)$.
Changes in the amount of damage (Social assets)	(9) Rise in sea level (land)	20) Degree of sea level rise	See (1) above (assessment of difference according to climate sensitivity).
		21) Area of submergence when the seal level rises by 50 cm	As the multiplier, apply a lognormal distribution with a geometrical average of 1 and a geometrical standard deviation of 1.7 (assuming order-level dispersion).
		22) Land price	As the multiplier, apply a uniform distribution between 0 and 2 by reference to difference between documents (Fankhauser (1995), Tol (2002)).
	(7) Agricultural impact	Global total change in latent productivity (per degree of temperature rise) ($\Delta P/^\circ C$)	23) Set a normal distribution, using as the standard deviation the standard error for $\Delta P/^\circ C$ based on the result of regression analysis of the results of calculation of two conditions about GCM output and the result calculated by use of NIES's model about latent productivity in the base year.
			24) Select $\Delta P/^\circ C$ based on five different GCM outputs with equal probability.
		25) Fertilizer effect factor	Set a normal distribution where the representative value of the parameters shown in Cure et al. (1986) and a 95% confidence interval are used as the mean value and the standard deviation $\times 1.96$, respectively.
		26) Farm product price	Set a distribution based on existing research on price changes in the future.
	(8) Energy consumption	27) Socioeconomic scenario	Same as for human health.
		28) Heating index / cooling index	Apply a lognormal distribution with a geometrical standard deviation of 1.5 as the multiplier, assuming order-level dispersion.
		29) Prediction equation of energy consumption per capita for heating (household, business) and cooling (household, business)	Set a normal distribution where the standard error of the regression factor based on the result of regression analysis of GDP/cap is used as the standard deviation.
Calculation of damage factors for other GHGs	GWP	30) GWP	Set a normal deviation where a 90% confidence interval (5% to 95%) is $\pm 35\%$ (IPCC AR4 WG1, p. 214).

(2) Calculation of temperature change due to GHG emissions

Under LIME1, we carried out temporal-spatial assessment by the use of the DICE model. Under LIME2, we calculated a temperature change every year from 1990 (actually 2000) to 2100, using MAGICC (see Column 2.2-2).

Column 2.2-2

Classification of climate models and MAGICC model

The climate model used for researching global warming differs according to purpose and is divided into several levels according to degree of detail (Randall et al. 2007, Meehl et al. 2007). The most complicated model is AOGCM (Atmosphere-Ocean General Circulation Model). A famous global simulator has been carrying out calculation by the use of several types of AOGCM. One of them is K-1 Coupled GCM (MIROC) 3.2 (high resolution version), which has the highest spatial resolution among the types of AOGCM included in the list in IPCC's Fourth Assessment Report (Randall et al. 2007) (Koike 2006). The operation of AOGCM requires many computer resources.

On the other hand, the so-called SCM (Simple Climate Model) is a simple model expressed by a combination of global boxes. This model uses climate sensitivity and other parameters given beforehand (based on calculation results under AOGCM) to calculate GHG concentration and radiation forcing in the atmosphere and predict temperature and sea level rise on global average. Because calculation requires only a short time, it is easy to repeat calculation many times according to different emissions scenarios and parameters.

There is a model between the two: EMIC (Earth System Model of Intermediate Complexity). This model is used for research on interaction among the elements of the climate system, etc.

A typical SCM is MAGICC (Model for the Assessment of Greenhouse-Gas Induced Climate Change), which has been widely used – for example, IPCC Assessment Reports issued so far have used it. MAGICC is a model developed by Wigley et al. A version of the program that runs on a personal computer has been available together with SCENGEN (a program that produces a spatial climate change scenario by the use of the results of MAGICC). Under LIME2, for the purpose of damage assessment, we calculated the degrees of temperature rise and sea level rise in the future by the use of MAGICC 4.1 (Wigley 2003), the version that IPCC tuned according to each AOGCM and used for predicting global rises in temperature and sea level in the future for its Third Assessment Report (TAR).

Under LIME2, we conducted analysis by the use of the fixed emissions scenario in 2000 (hereinafter referred to as the “Fixed Emissions Scenario”) and the emissions scenario by the median (P50) of the SRES scenario presented in MAGICC (“Increasing Emissions Scenario”). In addition, we conducted uncertainty assessment based on the result of each prediction where a probability distribution was set for climate sensitivity. Figure 2.2-3 and Figure 2.2-7 show changes in CO₂ emissions according to the Fixed Emissions Scenario and the Increasing Emissions Scenario, and differences between the two scenarios. Figures 2.2-8 and 2.2-9 show changes in temperature rise according to the two scenarios and differences between the two.

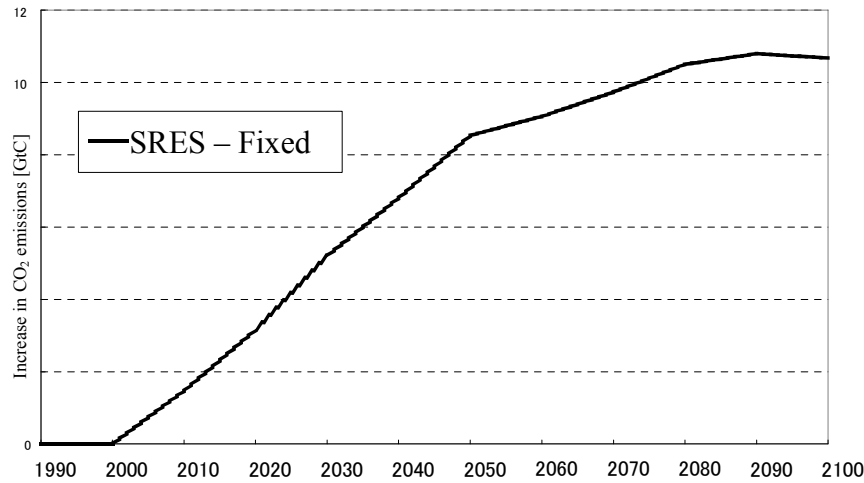


Figure 2.2-7: Changes in the Difference in CO₂ Emissions between the Fixed Emissions Scenario (2000) and the Increasing Emissions Scenario (P50)

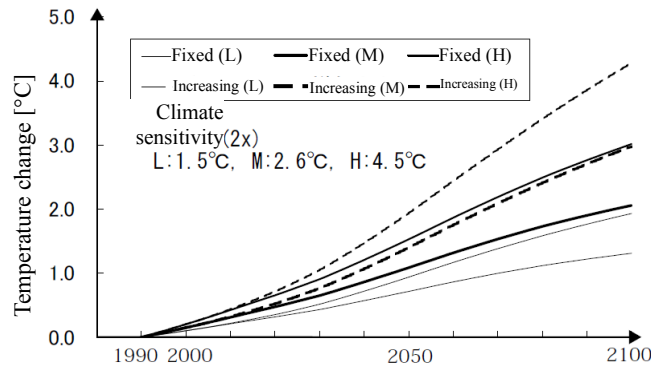


Figure 2.2-8: Changes in the degree of temperature rise according to the Fixed Emissions Scenario (2000) and the Increasing Emissions Scenario (P50) (L, M, H stand for low-level, mid-level, and high-level estimation, respectively)

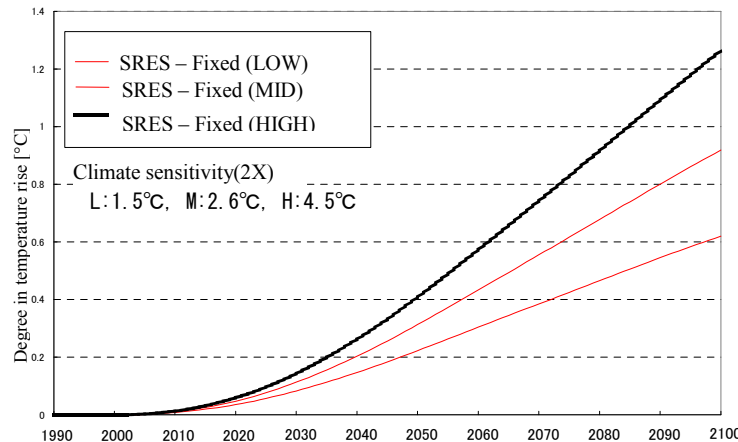


Figure 2.2-9: Changes in the difference in temperature rise between the Fixed Emissions Scenario (2000) and the Increasing Emissions Scenario (P50) (L, M, H stand for low-level, mid-level, and high-level estimation, respectively)

We compared the result of the assessment to the figure that shows the prediction results presented in TAR (Figure 2.2-A). Although Case M of the P50 scenario will change below the mean value of GCM in each marker scenario in the first half of the 21st century, it will become almost the same as A1B in 2100. As a result, the range between L and H is almost the same as the range in thick envelope.

Initially, Case M of the Fixed Emissions Scenario will change as in the case of IS92a (TAR method) and become almost the same as B1 in 2100. As a result, Case H is similar to Case M of the P50 scenario. Case L was found to be smaller than the result of prediction by each GCM in each SRES scenario.

(3) Human health: damage function for heat stress

It is thought that the impact of heat stress can be divided into acute damage and chronic damage. Under LIME, we assessed acute fatal damage rather than restriction of available information. With regard to the dose-response coefficient of heat stress (D-R coefficient), we adopted the hypothesis formulated by Honda et al. (1998), which was based on surveys in various regions in Japan. According to this hypothesis, if the daily maximum temperature is higher or lower than the optimum value (which varies according to regional annual average temperature), the death risk for the elderly increases by $2 \times 10^{-6} \text{ }^{\circ}\text{C}^{-1} \text{ day}^{-1}$. To apply this coefficient to regions other than Japan, we used Equation 2.2-6 for adjusting the D-R coefficient of heat stress (Equation 2.2-7).

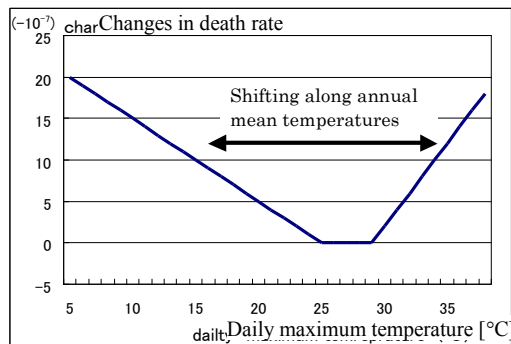
$$DR(n) = 0.000131 Y(n)^{-0.417} \quad (2.2-7)$$

In this equation, $DR(n)$ is the D-R coefficient of heat stress by country, and $Y(n)$ is GDP per capita based on the purchasing power parity in country n . Because, according to the above-described hypothesis, Japan's $DR(n)$ is $2 \times 10^{-6} \text{ }^{\circ}\text{C}^{-1} \text{ day}^{-1}$, and GDP per capita based on the purchasing power parity in Japan is US\$18,700, we obtained a coefficient of 0.000131 by the use of both. Under LIME, we assumed the range of 5°C centering on the optimum value as the optimum range and thought that if the daily maximum temperature is higher or lower than the optimum range, damage occurs (Figure 2.2-10). The optimum value V of the annual average daily maximum temperature was obtained from the following equation. The range of $\pm 2.5^{\circ}\text{C}$ is the optimum range.

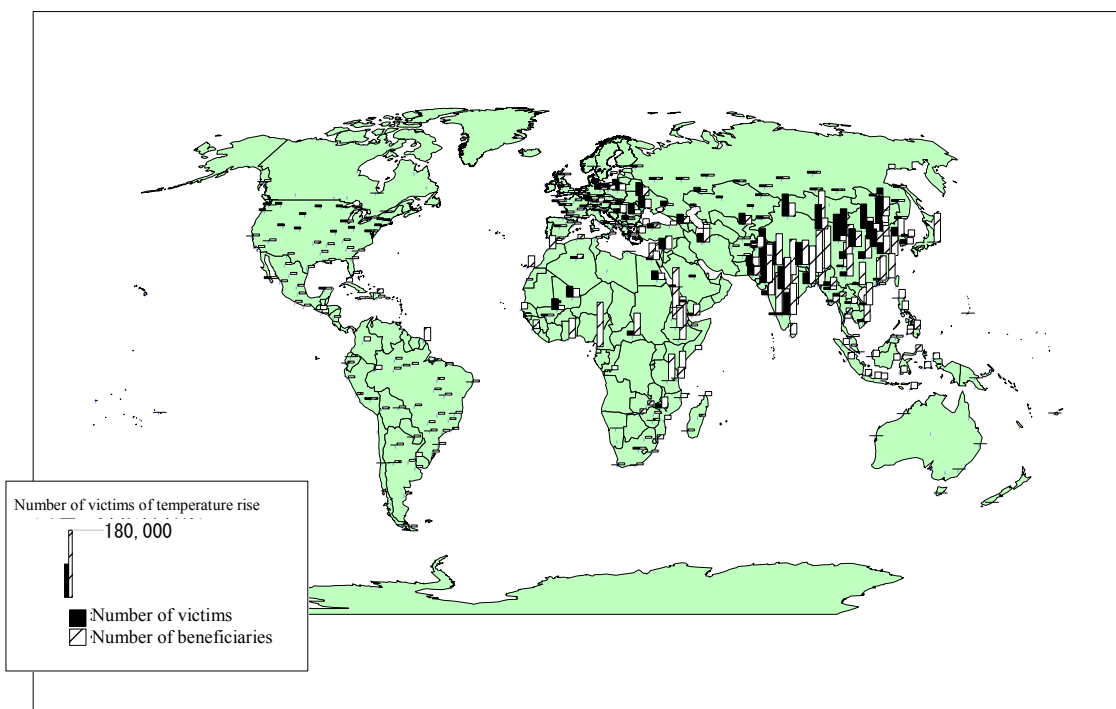
$$V = 2.5 T_{nor} - 7 \quad (2.2-8)$$

In this equation, T_{nor} is the annual average temperature by region on condition that the upper limit of the maximum value is 34°C . This upper limit was calculated by reference to precious research by Kalkstein (1993) about health damage from heat stress in developing countries, which found that the threshold of a rise in the death risk in the two cities of Shanghai and Gaungzhou was 34°C .

In addition, because it can be thought that the D-R coefficient on the side of lower temperature includes not only the impact of cold stress but also the impact of an increase in respiratory disease (such as influenza), under LIME, we referred to Kunst et al. (1993) and estimated the D-R coefficient of cold stress to be half of heat stress.

**Figure 2.2-10: Relation between Daily Maximum Temperature and Death Rate**

(Note) The bottom of the V shape is the range of optimum temperatures where the death rate does not increase. If the daily maximum temperature exceeds or falls below the range, the death rate increases. The inclination of the straight line is the D-R coefficient. Under LIME, it is assumed that the range of optimum temperatures moves along the regional average temperature.

**Figure 2.2-11: Number of Health Victims of Heat Stress due to Global Warming when CO₂ Concentration Becomes Double (by temperature observation point)**

The Japan Meteorological Agency's World Weather Data (1982 to 1998) contains data collected at 353 observation points before 1995. Based on the data, we calculated the period average of daily maximum temperature day by day and the period average of annual average temperature. Next, we calculated the optimum range of daily maximum temperature at each point by the use of Equation 2.2-8 and counted the number of days when the daily maximum temperature exceeded or fell below the range as days when damage from heat or cold stress might occur. We also counted the number of days when the daily maximum temperature rose uniformly by 1.5°C (when CO₂ concentration became double).

We dealt with the population aged 65 and over and multiplied each country's population in 1994 by 14% (the average ratio of population aged 65 and over according to the Organization

for Economic Cooperation and Development (OECD)). If the number of observation points used for adding up the number of days when damage might occur was one in a country, the country's whole population was allocated to the point. If there were two or more points in a country, the whole population was equally allocated among the points. If there was no observation point, we chose the most similar observation point in terms of climate from among the observation points in the neighboring countries and allocated the country's entire population to the observation point.

With regard to each observation point, each day when the temperature exceeded or fell below the optimum range, we calculated the number of victims from the temperature beyond the range, the D-R coefficient, and the population (Figure 2.2-11). We added up numbers to obtain the annual total. With regard to DALY in the case of heat stress and cold stress, although other research cases (Goedkoop, Spriensma 1999) adopted less than one year per death, because Honda et al. (1998) suggested a value for two or more years, we assumed 2.0 years per case and multiplied it by the total number of victims to obtain the total DALY. We obtained the damage function for heat stress by dividing the total of differences between an increase in DALY according to the CO₂ emissions increase scenario and the baseline increase in DALY by the difference in the total amount of CO₂ emissions between the scenarios.

Equation 2.2-9 calculates the number of health victims of heat stress, while Equation 2.2-10 calculates the number of health victims of cold stress.

$$D_{heat}(n, t) = POP_{elderly}(n, t) \cdot DR_{heat}(n, t) \cdot \Delta HD(n, t) \quad (2.2-9)$$

$$D_{cold}(n, t) = POP_{elderly}(n, t) \cdot DR_{cold}(n, t) \cdot \Delta CD(n, t) \quad (2.2-10)$$

In these equations, $D_{heat}(n, t)$ is the number of health victims of heat stress in country n at time t ; $POP_{elderly}(n, t)$ is the elderly population in country n at time t ; $DR_{heat}(n, t)$ is the D-R coefficient of heat stress in country n at time t ; $\Delta HD(n, t)$ is the number of days of the maximum temperature's excess of the threshold on the side of high temperature in country n at time t by point; $D_{cold}(n, t)$ is the number of health victims of cold stress in country n at time t ; and $DR_{cold}(n, t)$ is the D-R coefficient of cold stress in country n at time t , and $\Delta CD(n, t)$ is the number of days of the maximum temperature's excess of the threshold on the side of low temperature in country n at time t by point.

Based on the results, we obtained $BL_{(heat \text{ or } cold, r)} \cdot (RR_{(heat \text{ or } cold)} - 1)$ and substituted it into Equation 2.2-5.

(4) Human health: damage function for infection

a Malaria

Malaria has caused large death damage mainly in developing countries. The population in infected regions is 2.1 billion, the number of infected persons is 2.7 million every year (WHO 1998), and the number of deaths from infection is 1.1 million every year (WHO 2001). Malaria is a disease that continues to spread through anopheles' carrying malaria parasites and by the cycle of anopheles to human beings to anopheles. That is, the living cycle of malaria parasites requires two stages: living in human bodies and living in the bodies of anopheles. When they live in human bodies, they are not directly exposed to the climatic environment and therefore receive no effect of climate changes. However, it is predicted that the

existence of parasites in anopheles' bodies and anopheles will be influenced by climate changes, such as a rise in temperature.

We calculated the increase rate of deaths from malaria per temperature rise (relative risk), paying attention to the spread of anopheles over wider areas. Under LIME, however, we assume that anopheles spread over areas, including developing countries where malaria damage has occurred at present, but they do not spread in advanced countries where no malaria damage has occurred at present because of high-level public health infrastructures.

First, based on existing research (Matsuoka et al. 1994), we calculated the increase rate of population in regions infected with malaria due to temperature rise. The research prepared climate indices based on temperature, precipitation, and other outputs from six GCMs and predicted changes in the population in malaria-infected regions, focusing on the climate adaptability of anopheles. Because the GCMs used for the research are considerably old-fashioned, each of them assumed the degree of temperature rise at the time of doubling of CO₂ concentration to be 2.85 to 5.29°C. Therefore, we divided the increase rate of population in malaria-infected regions predicted based on each GCM by the degree of temperature rise at the time of doubling of CO₂ concentration, obtained an increase rate of 4.63% per rise of 1°C, and set $RR_{(malaria)}$ in Equation 2.2-5. Under LIME, we calculated the number of deaths by multiplying $BL_{(malaria, r)}$, the number of deaths in 1990 in regions infected with malaria at present, by the increase rate of population in malaria-infected regions (Equation 2.2-5).

We calculated DALY for malaria based on WHO (2001). Because WHO's DALY reflects a discount by the number of years of DALY per case, we calculated the ratio of the discounted DALY to the undiscounted DALY from literature (Murray et al. 1996) and converted WHO's DALY into an undiscounted value. As a result, we found that DALY per death was 88.3.

b Dengue

Dengue can be classified into standard dengue and dengue hemorrhagic fever, a serious type accompanied by a bleeding tendency. Dengue virus, regardless of type, is carried by garden striped mosquitoes or Asian Tiger mosquitoes. According to WHO, every year, about 20 million people contract dengue fever or dengue hemorrhagic fever (WHO 1998) and about 13,000 people die (WHO 2001). The amount of damage from dengue is about 1% that from Malaria. Therefore, the amount of damage from dengue, the current baseline for predicting the impact of global warming, is far less than that from malaria. Consequently, during damage estimation, attention is given to relative risk (the increase rate of health damage per temperature rise) in the impact of global warming. With regard to this, we referred to a study on prediction of changes in epidemic potential (EP) due to global warming (Martens et al. 1997). EP is only an index of potential risk of infection, which is not used for predicting the occurrence of damage. A rise in EP indicates that it becomes easier for infection to spread. In this study, based on three GCM outputs, the increase rate of EP due to global warming in regions infected steadily with malaria or dengue was calculated concerning each of the two diseases. The increase rate is 12 to 27% for malaria, while it is 31 to 47% for dengue. The ratio between the two indicates that EP for dengue will increase 2.2 times as much as EP for malaria. Under LIME, assuming that the increase rate of EP is reflected in the increase rate of health damage as it is, we estimated the relative risk of dengue per temperature rise ($RR_{(dengue)}$ in Equation 2.2-5) to be 9.26%, twice as much as 4.63%, the relative risk of malaria. Given that the types of carrier mosquitoes differ between the two

diseases, this estimation is rather rough. However, this is a result that reflects a shortage of existing studies on the impact of global warming on dengue and a low baseline. By the same method as applied to malaria, we calculated DALY for dengue based on WHO (2001) and obtained a value of 70.8.

Table 2.2-3: Increase in the amount of DALYS by region and by cause at the time of doubling of CO₂ concentration

Region	Malaria	Dengue	Heat stress	Cold stress	Disaster (excl. typhoon)	Disaster (typhoon)	Malnutrition	Total
AFR	2,433,066	0	27,936	-90,077	623	487	255,672	2,627,707
CPA	18,790	0	33,518	-32,392	792	1,310	17,864	39,883
EEU	0	0	2,727	-2,268	8	65	6,408	6,940
FSU	0	0	6,928	-6,773	129	33	84	401
LAM	4,696	0	9,404	-15,060	776	651	186,468	186,936
MEA	2,023,595	0	16,586	-21,532	667	34	346,579	2,365,929
NAM	0	0	5,982	-5,404	80	330	17,656	18,644
PAO	0	0	306	-2,631	14	52	4,840	2,582
PAS	19,868	0	13,148	-11,034	465	3,303	30,857	56,607
SAS	146,087	53,126	96,155	-47,117	4,191	43,671	325,291	621,404
WEU	0	0	4,090	-7,740	57	71	12,342	8,821
Total	4,646,102	53,126	216,780	-242,028	7,804	50,007	1,204,063	5,935,853

(Note) Regions are abbreviated as follows: NAM: North America, LAM: Latin America and the Caribbean, AFR: Sub-Saharan Africa, MEA: Middle East and North Africa, WEU: Western Europe, EEU: Central and Eastern Europe, FSU: Newly independent states of the former Soviet Union, CPA: Centrally planned Asia and China, SAS: South Asia, PAS: Other Pacific Asia, PAO: Pacific OECD

(5) Human health: damage function for disaster damage

Global warming is thought to increase typhoon, flooding, and other disasters through activation of water circulation. The current situation of disaster occurrence, which serves as the baseline for the estimation of damage from global warming, was grasped from the disaster database of the Louvain Catholic University's Center for Research on the Epidemiology of Disasters (EM-DAT). According to this, an average of 24,000 people have died every year due to types of disasters expected to receive the impact of global warming (flooding, landslide, tidal waves, and typhoon).

Under LIME, we assumed that the relative risk of disaster damage per rise of 1°C (the increase rate of damage per temperature rate) increases by 4% for a disaster other than typhoon and by 10% for typhoon. This is the conversion into the rate per rise of 1°C of the predicted increase rate of damage adopted for an existing study (in a study under ExternE, To1 adopted the prediction that the intensity of precipitation (winter precipitation; extratropical storm) would increase by 10% and the hurricane activity would increase by 25% (ExternE 1999)). By the same method as applied to malaria, we calculated DALY for disaster death based on WHO (2001) and obtained a value of 45.1.

(6) Human health: damage function for malnutrition/starvation

Malnutrition and starvation are directly caused by drought and other disasters or indirectly

caused through a change in the production of farm products due to progress in global warming.

We could not find quantitative information on an increase in starvation due to global warming and drought and other disasters. In addition, we could not find any significant interrelation between the number of deaths by country due to droughts that occurred in developing countries between 1960 and 2000 (EM-DAT) and the production of grain by country (UN Food and Agriculture Organization (FAO)). Meanwhile, in 2000, the number of deaths from starvation that accompanied disasters was 370 according to EM-DAT, and the number of deaths from protein-energy malnutrition was 272,000 according to WHO (WHO 2001). Because the number of deaths from malnutrition is obviously large, attention should be paid to the indirect impact of malnutrition when considering malnutrition and starvation.

When assessing the impact of global warming on malnutrition, we based our study on Parry et al. (1999) concerning the relation between global warming and the population at risk of starvation. The research estimated changes in the production of grain by the use of the output of GCM, modeled the economic effect into the world's food distribution, and estimated changes in the population at risk of starvation due to global warming. Therefore, it estimated the population at risk of starvation not due to disasters but due to malnutrition. The population at risk of starvation means the population that have the risk, not the number of deaths or the number of persons who suffer disease due to starvation. The scenario that made a comparison with global warming assumed that no climate change would occur until 2080 and, on this assumption, calculated an increase in the population at risk of starvation.

Because Parry et al. (1999) did not estimate an increase in the population at risk of starvation for the 2060s when CO₂ concentration will become double, we calculated an increase in the population at risk of starvation, using estimates for other years and the estimated degree of temperature rise for the 2060s from the output of GCM.

$$RR(t) - 1 = 0.041846\Delta C(t)^2 \quad (2.2-11)$$

In this equation, $RR(t)$ is the relative risk of the population at risk of starvation at time t . $\Delta C(t)$ is the increase in the global average temperature [°C] due to global warming at time t . 0.041846 is the regression coefficient in the case of regression of the increase in starvation risk calculated by Parry et al. (Parry et al. 1999) based on the increase in global average temperature. Therefore, $RR(t) - 1$ is the increase rate of population at risk of starvation at time t .

Assuming that the population at risk of starvation has a proportional relation to the number of deaths, we converted the increase in the population at risk of starvation into an increase in the number of deaths from malnutrition.

For this damage function, we used the following equation instead of Equation 2.2-5.

$$D_{\text{nonadjusted}}(c,r,t) = BL_{(c,r,t)} \cdot (RR(t) - 1) = BL_{(c,r,t)} \cdot (0.041846\Delta C(t)^2) \quad (2.2-12)$$

However,

$$BL_{(c,r,t)} = BL_{(c,r,1990)} \cdot (1+r) \cdot (t - 1990) \quad (2.2-13)$$

r is the increase rate of population at risk of starvation in the case of no impact of global warming, which was calculated based on Parry et al (1999). We calculated the undiscounted value as in the case of malaria, based on the quotient of the total DALY for protein-energy malnutrition as a cause of death and the number of deaths. Based on the result, we estimated the undiscounted value to be 106.1 by the same method as in the case of malaria.

(7) Social assets: damage function for agricultural production

The impact of global warming on agricultural production can be divided into the impact of a rise in temperature and accompanying climate changes (such as changes in precipitation) and the beneficial impact (fertilizer effect) of a rise in the concentration of CO₂, a typical GHG, on farm products. During the development of LIME, we considered both impacts to be impacts of global warming.

a Estimation of changes in agricultural production due to climate changes under a model for calculating potential production

The impacts of climate change on agricultural production include a rise in temperature, a change in precipitation, a shortage of water, a change in soil, and moving of land suitable for cultivation of farm products. Because, in this way, agricultural production is greatly influenced by not only temperature but also the values concerning precipitation and other climate conditions, the quality of soil, and other factors, it is impossible to express the impacts simply by a D-R coefficient with temperature.

Under LIME2, to estimate changes in agricultural production due to changes in temperature and precipitation, we used the model for calculating agricultural potential productivity that was developed by the National Institute for Environmental Studies and Kyoto University (Takahashi et al. 1997) and estimated production in 1990 and production at the time of doubling of CO₂ concentration.

Of the information given to the models, the predicted values of temperature and precipitation are based on GCM output. Because predicted values based on GCM greatly fluctuate from year to year and their uncertainty is high, if they are used as they are, it is impossible to obtain temperature and precipitation in a future year. Because of this, in this model, we corrected data by adding the average values in the decade after the future year to the values in 1990 as shown in Equation 2.2-14.

$$X(t) = \frac{1}{10} \sum_{t=9}^t \{x_1(t) - x_0(t)\} + X(1990) \quad (2.2-14)$$

In this equation, $X(t)$ is temperature or precipitation in year t ; $x_1(t)$ is GCM output on temperature or precipitation in year t under the CO₂ Increasing Emissions Scenario; $x_0(t)$ is GCM output on temperature or precipitation in year t under the fixed CO₂ concentration scenario; and $X(1990)$ is temperature or precipitation in 1990.

With regard to GCM, the model and the output differ among research groups. Because there is no definite difference in validity among models, selecting a model is difficult. Because of this, among studies conducted on the impact assessment of global warming, some studies also use the results of calculation that used some GCMs. Under LIME2, for each calculation trial,

we selected one of the results of calculation that used five GCM outputs, and had it reflected in the uncertainty assessment. In addition, we selected rice, wheat, and corn, which occupy almost 90% of total grain production in the world. Figures 2.2-12 and 2.2-13 show the potential production of rice in 1990 and at the time of doubling of CO₂ concentration, which was calculated in the model.

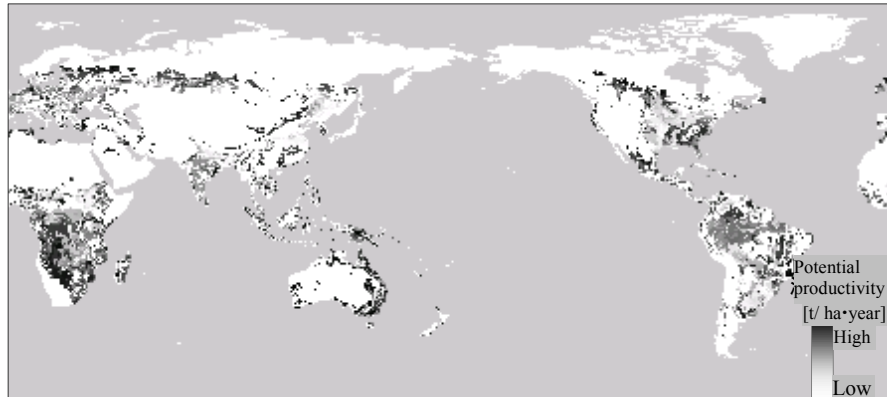


Figure 2.2-12: Potential productivity of rice (1990)

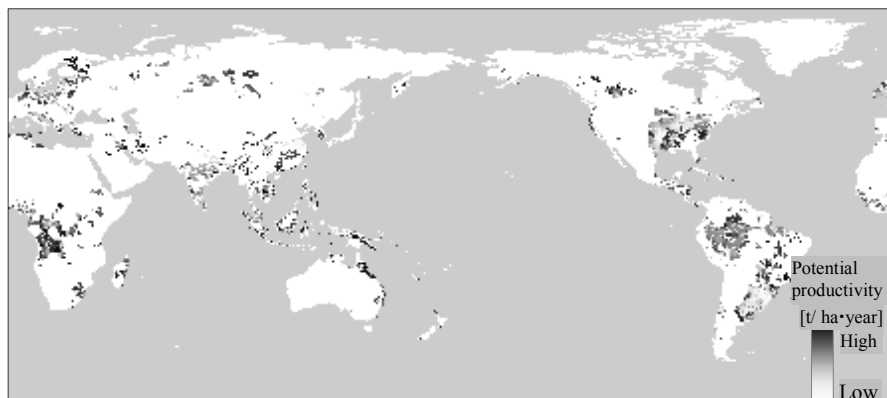


Figure 2.2-13: Potential productivity of rice (when CO₂ concentration becomes double; no consideration of fertilizer effect; use of output of CCCma)

The model calculates potential production (Takahashi et al. 1997). Because the calculation is carried out in each 5' × 5' mesh under the model, we obtained average potential productivity, $AP(n, t)$ [t – farm product/ha·year], by country/region by the use of Equation 2.2-15 (a is the number of meshes in each country/region; $AP(i, t)$ is the potential productivity of mesh i ; n is country; and t is year).

$$AP(n, t) = \frac{1}{a} \sum_{i=1}^a AP(i, t) \quad (2.2-15)$$

We calculated annual production by multiplying $Y(n, 1990)$, agricultural production in each country/region in 1990 (FAO 2000) by the ratio of AP , average potential productivity, in each country/region in each year to that in 1990, and totaled the annual production to obtain global production ($Y_{nofertilizereffect}$ is estimated production of farm products [t – farm products/year], excluding fertilizer effect).

$$Y_{\text{nofertilizereffect}}(t) = \sum_n \left[\frac{AP(n,t)}{AP(n,1990)} \times Y(n,1990) \right] \quad (2.2-16)$$

Under LIME2, we estimated annual $Y_{\text{nofertilizereffect}}(t)$ by calculating $\Delta Y_{\text{nofertilizereffect}}/\text{°C}$ for each GCM output and for each farm product through regression analysis on the degree of temperature rise based on the results of calculation of $Y_{\text{nofertilizereffect}}$ (2063) according to the CO₂ Increasing Emissions Scenario and the CO₂ Fixed Emissions Scenario, each using Equation 2.2-16 and the current $Y(1990)$ (Equation 2.2-17).

$$Y_{\text{nofertilizereffect}}(t) = Y(1990) + \Delta Y_{\text{nofertilizereffect}} \times \Delta C(t) \quad (2.2-17)$$

b Estimation of the fertilizer effect of CO₂

We considered the fertilizer effect of CO₂ on main grains – rice, wheat, and corn. Based on existing research (Cure 1986), we considered the fertilizer effect to be as shown in equations 2.2-18a and 2.2-18b, if within the range between 340 and 680 ppm.

[Rice, corn]

$$Y_{\text{fertilizereffect}}(t) = Y_{\text{nofertilizereffect}}(t) \cdot \left\{ 1 + \frac{f_{680}}{100} \cdot \left(\frac{C(t)}{340} - 1 \right) \right\} \quad (2.2-18a)$$

[Wheat]

$$Y_{\text{fertilizereffect}}(t) = Y_{\text{nofertilizereffect}}(t) \cdot \left\{ 1 + \frac{f_{680}}{100} \cdot \left(\frac{C(t)}{340} - 1 \right)^2 \right\} \quad (2.2-18b)$$

In this equation, $Y_{\text{nofertilizereffect}}(t)$ is production in year t , including the fertilizer effect; $Y_{\text{nofertilizereffect}}(t)$ is production in year t , excluding the fertilizer effect; f_{680} is the change rate of potential productivity at the time of doubling of CO₂ concentration (680 ppm) (Cure et al. 1986) (rice: + 15%; wheat: + 35%; corn: + 29%); and $C(t)$ is CO₂ concentration [ppm] in year t .

c Adding up of amounts of damage to farm production and calculation of damage function

We converted $Y(t)$, production on a weight basis, into money by multiplying the production of each species by the unit price (see the notes to Table 2.2-6) in order to apply the resultant production $P(t)$ to the damage function (Equation 2.2-3).

We calculated $Y(t)$ according to the Increasing Emissions Scenario and $Y_0(t)$ according to the Fixed Emissions Scenario, both in the case of consideration for the fertilizer effect (Equation 2.2-18) and in the case of no consideration for the fertilizer effect (Equation 2.2-17). After that, we multiplied them by unit price, expressed the results as $P(t)$ and $P_0(t)$, and applied Equation 2.2-3. We regarded the result of the application in the case of consideration for the fertilizer effect as the damage function for CO₂ and calculated the damage function for the GHG in question (other than CO₂) by multiplying the result of the application in the case of no consideration by GWP (Equation 2.2-4).

Column 2.2-3

NIES's model for calculation of potential productivity of farm products

This model was developed by the National Institute for Environmental Studies (NIES) and Kyoto University. The model uses a geographical information system and calculates potential productivity for each $5' \times 5'$ mesh in the world. "Potential productivity" herein means the maximum amount of harvestable farm products per unit area under some conditions. The model can calculate potential productivity for 12 types of products, including rice and wheat. The effect of irrigation is not taken into consideration.

Figure 2.2-B shows the structure of the model. First, the number of days suitable for cultivation of products during a year (growth period) is calculated based on climate data. After that, the maximum weights of harvestable farm products are calculated through simulation of growth of products during the growth period according to the parameter (growth characteristic parameter) for each species. The maximum weights are multiplied by the harvest coefficient (the ratio of the weight of harvestable and edible products to the total weight of cultivated products) to calculate the weight of actually harvestable products.

The calculation of productivity requires the input of climate data, a soil characteristics parameter, a parameter for the growth characteristics of products, the ratio of harvested products to produced products, and other numerical values. Under LIME, although we predict the impact of global warming in the future, we use current values for the soil parameter, the growth characteristic parameter, and the harvest coefficient. With regard to climate data, while we use the current value for the amount of clouds, we use the future values predicted by GCM output for temperature and precipitation.

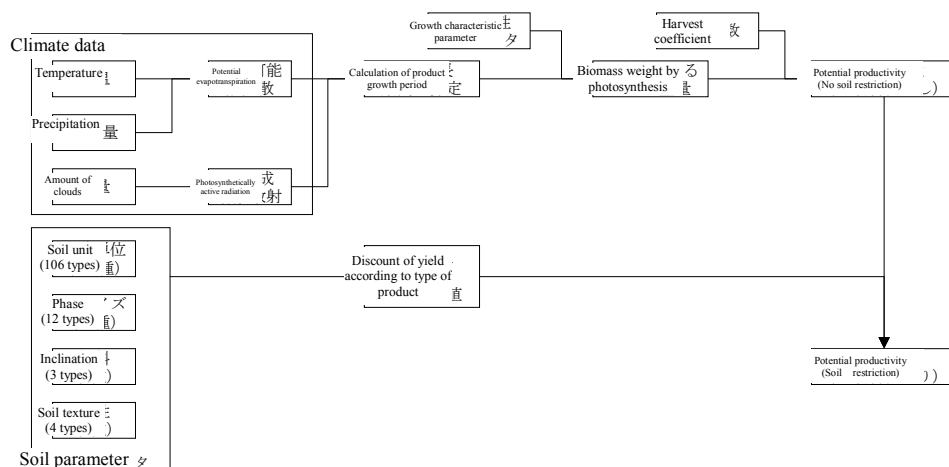


Figure 2.2-B: Flowchart of calculation of potential

(8) Social assets: damage function for energy consumption

Based on the Japan Meteorological Agency's World Weather Data (1982 to 1998), we estimated the numbers of heating and cooling indices at present and in the future in each country. The cooling index (cooling degree days) or the heating index (heating degree days) is the annual total of differences between standard temperature and the actual temperature on the days when the temperature exceeds or falls below the standard temperature. The indices

are used also for the design of cooling and heating systems (ExternE 1999). The standard temperature is 22°C in the case of cooling and 14°C in the case of heating. We set these values by reference to values adopted for general energy statistics (Institute of Energy Economics 2002). With regard to the cooling and heating indices, assuming that a rise in annual average temperature due to global warming is added directly to the regional daily average temperature, we calculated cooling and heating indices at each observation point in 2050 (on the assumption that the temperature rises by 1.5°C). After that, we divided the result by the value in 1990 and subtracted 1 from the divided result to calculate the increase rate of the cooling and heating indices.

$$\Delta CDD(r, 2050, 1.5) = \left(\frac{CDD(r, 2050, 1.5)}{CDD(r, 1990, 0)} \right) - 1 \quad (2.2-19a)$$

$$\Delta HDD(r, 2050, 1.5) = \left(\frac{HDD(r, 2050, 1.5)}{HDD(r, 1990, 0)} \right) - 1 \quad (2.2-19b)$$

In these equations, $\Delta CDD(r, t, \Delta C)$ is the increase rate of the cooling index from the base year (1990) in region r at time t with global average temperature rise ΔC ; $CDD(r, t, \Delta C)$ is the cooling index in region r at time t with global average temperature rise ΔC ; $\Delta HDD(r, t, \Delta C)$ is the increase rate of the heating index under the same conditions; and $HDD(r, t, \Delta C)$ is the heating index under the same conditions. An increase in cooling energy consumption and an increase in heating energy consumption in 2050 (on the assumption that the temperature rises by 1.5°C) can be expressed by the following equations (actual minus values showed a decrease in energy consumption):

$$D_{coolingenergy}(r, 2050, 1.5) = CE(r, 2050) \cdot \Delta CDD(r, 2050, 1.5) \quad (2.2-20a)$$

$$D_{heatingenergy}(r, 2050, 1.5) = HE(r, 2050) \cdot \Delta HDD(r, 2050, 1.5) \quad (2.2-20b)$$

In these equations, $D_{coolingenergy}(r, t, \Delta C)$ is an increase in cooling energy in region r at time t with global average temperature rise ΔC [Mtoe]; $CE(r, t)$ is cooling energy consumption in region r at time t [Mtoe]; $D_{heatingenergy}(r, t)$ is an increase in heating energy under the same conditions [Mtoe]; and $HE(r, t)$ is heating energy consumption under the same conditions [Mtoe].

Based on regional gross product, population, and the current cooling and heating indices, we estimated the ratio of cooling and heating energy consumption to the total business and household energy consumption in each region. We confirmed the result by the ratio of cooling and heating energy consumption to the total business and household energy consumption in each of the countries whose energy consumption statistics are available. We estimated the growth rate of energy consumption in the future by extrapolating an assumed regional growth rate that reflects the regional economic level, based on analysis of economic growth and cooling and heating energy demand in Japan in the past (Institute of Energy Economics 2002) (Figures 2.2-14 to 2.2-17). Based on this, we calculated the total annual increase in energy consumption. We used IIASA/WEC (1998) for regional economic growth (GDP per capita) necessary for extrapolation as in the case of health damage and used the UN's document (United Nations 2003) for population forecast. Table 2.2-4 shows the amount of increase in energy consumption by region in 2050 (on the assumption that the temperature rises by 1.5°C).

We added up the regional results by Equation 2.2-20 to obtain the global total, and calculated an increase in energy consumption in each year by the following equations:

$$D_{coolingenergy}(\text{world}, t, \Delta C(t)) = D_{coolingenergy}(\text{world}, 2050, 1.5) \div 1.5 \times \Delta C(t) \quad (2.2-21\text{a})$$

$$D_{heatingenergy}(\text{world}, t, \Delta C(t)) = D_{heatingenergy}(\text{world}, 2050, 1.5) \div 1.5 \times \Delta C(t) \quad (2.2-21\text{b})$$

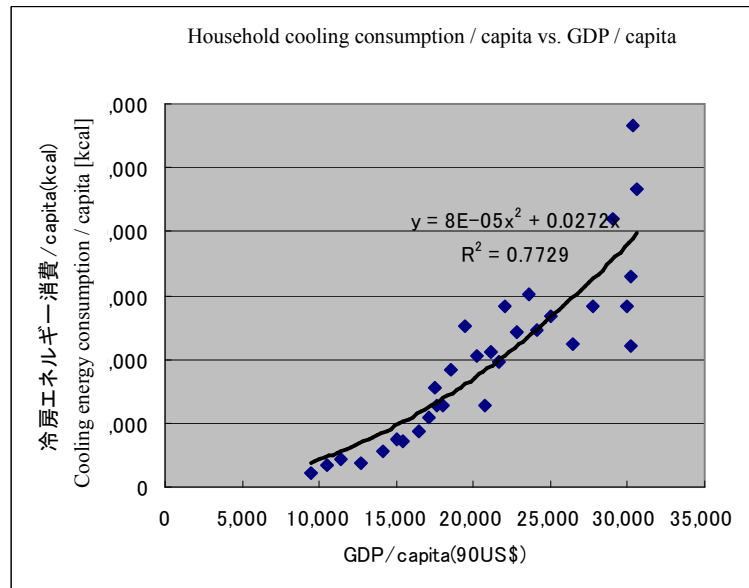


Figure 2.2-14: Relation between household cooling consumption per capita and GDP per capita (prepared based on data in Japan)

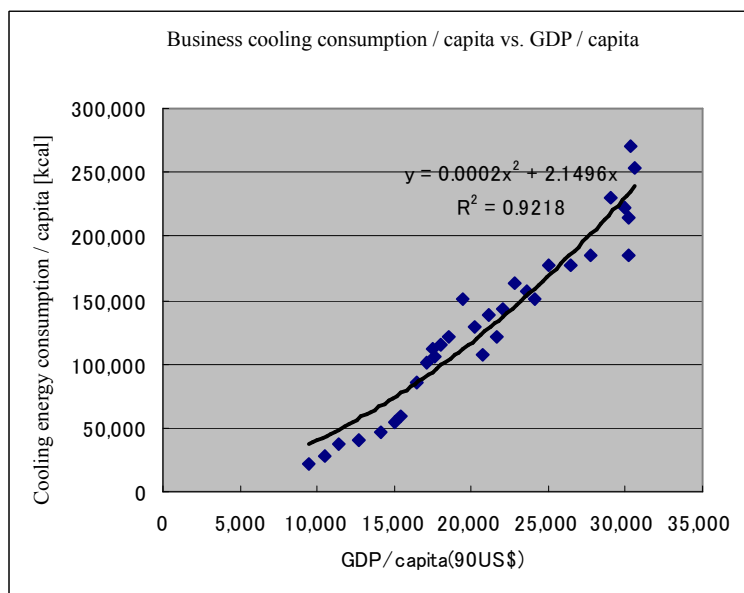


Figure 2.2-15: Relation between business cooling consumption and GDP per capita (prepared based on data in Japan)

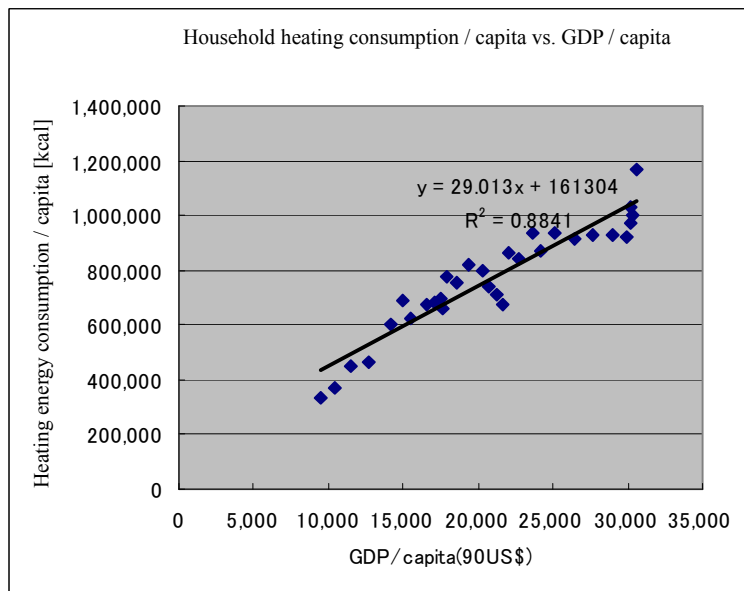


Figure 2.2-16: Relation between household heating consumption per capita and GDP per capita (prepared based on data in Japan)

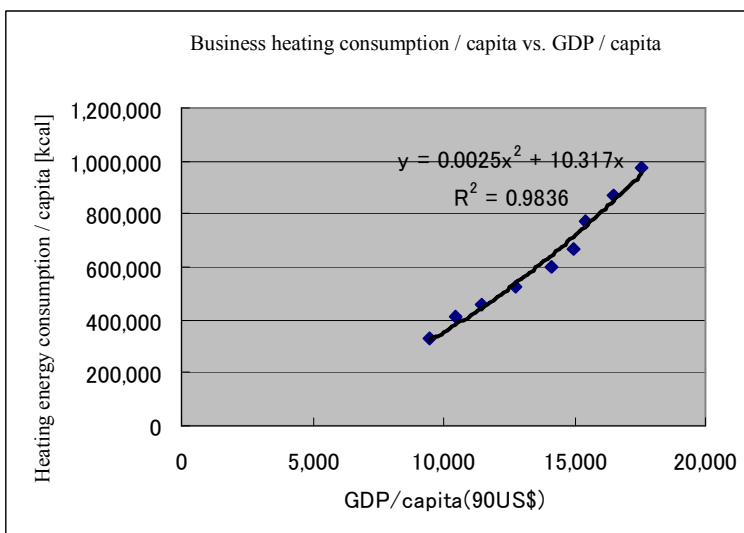


Figure 2.2-17: Relation between business heating consumption and GDP per capita (prepared based on data in Japan)

Moreover, we converted the amount of increase in energy consumption into an amount of money based on energy prices in Japan – the wholesale price of kerosene for heating and the total unit price of electricity for cooling.

We calculated the damage function by subtracting the total energy consumption calculated according to the CO₂ Fixed Emissions Scenario from the total energy consumption calculated according to the CO₂ Increasing Emissions Scenario and dividing the result by the difference in total CO₂ emissions between the two scenarios (Equation 2.2-2).

**Table 2.2-4: Increase in cooling and heating energy consumption by region in 2050
(assuming a 1.5°C rise) (unit: Mtoe)**

Region	Heating			Cooling			Total
	Household	Business	Subtotal	Household	Business	Subtotal	
AFR	-2,099	-487	-2,586	325	5,374	5,699	3,113
CPA	-20,109	-7,791	-27,900	953	6,440	7,393	-20,507
EEU	-2,774	-1,758	-4,532	41	182	223	-4,309
FSU	-10,642	-6,125	-16,766	163	730	893	-15,874
LAM	-3,538	-2,318	-5,855	1,703	8,700	10,403	4,548
MEA	-5,608	-1,630	-7,239	559	4,720	5,279	-1,960
NAM	-7,481	-7,098	-14,579	4,201	12,170	16,371	1,793
PAO	-1,123	-1,081	-2,204	1,162	3,249	4,411	2,207
PAS	-645	-426	-1,071	3,429	15,691	19,120	18,049
SAS	-1,935	-263	-2,199	756	10,773	11,530	9,331
WEU	-6,429	-6,396	-12,825	1,493	3,830	5,324	-7,502
Total	-62,384	-35,372	-97,756	14,785	71,860	86,645	-11,111

(Note) For the classification of regions, see Table 2.2-3.

(9) Social assets: damage function for land loss

There is a time lag between global warming and a rise in the sea level, because of thermal inertia. With regard to a rise in the surface of sea water, damage assessment concerning a rise in sea level in 2100 serves as the benchmark assessment at the time of doubling of CO₂ concentration. We assessed the degree of sea level rise until 2100 by the use of MAGICC. Figure 2.2-18 shows the result of calculation of sea level rise by the use of the Fixed Emissions Scenario and the Increasing Emissions Scenario (P50) in 2000. The figure also shows the range of assessment result according to climate sensibility.

Case M (mid-level) of the P50 scenario changes along almost the center of the thick range of the result predicted based on SRES in TAR and corresponds to the range between L and H.

With regard to land loss due to a sea level rise, as described in IPCC's report, damage is usually calculated with consideration for measures for damage prevention. In OECD countries, it has been predicted that most of the land will be saved from flooding because of expansion of breakwaters. However, how long coast can be protected differs among countries and regions. Under LIME, we assumed that at least coasts near residential areas would be protected. With regard to land loss, there is the possibility that damage may have been underestimated, because the cost of protecting coasts near residential areas was not taken into account.

First, we selected regions whose altitude is 0.5 m or lower, using ETOPO-5 (GRID-Tsukuba), an altitude data set of the National Geophysical Data Center (NGDC) of the US, together with the geographic information system (GIS). Based on the data set, whose graphic mode is 5 minutes latitude and longitude, we predicted that the meshes whose altitude is between -0.5 m and 0.5 m will be submerged when the sea level rises by 0.5 m (Figure 2.2-20). However,

we assumed that highly populated regions are not submerged, because of anti-flooding measures. That is, we used UNEP-GRID's world city population database and assumed that no submerge occurs within the meshes (whose graphic mode is 30 minutes latitude and longitude) where a city with a population of 100,000 or more exists. Table 2.2-5 shows the area of land that will be submerged when the sea level rises by 0.5 m on average, classifying by region and by type of land.

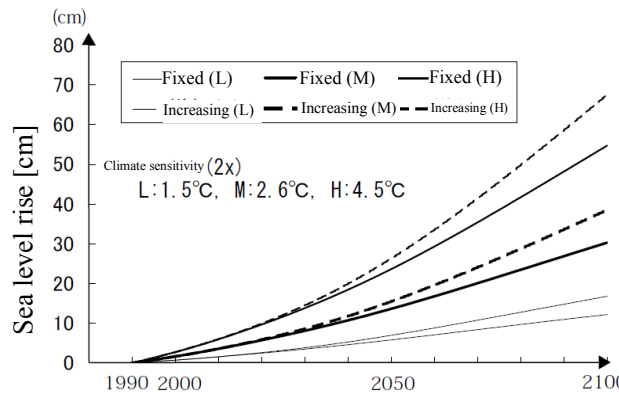


Figure 2.2-18: Assessment result of sea level change based on the Increasing Emissions Scenario(P50) and the Fixed Scenario by the use of MAGICC in 2000 (H, M, and L stand for high-level, mid-level, and low-level, respectively)

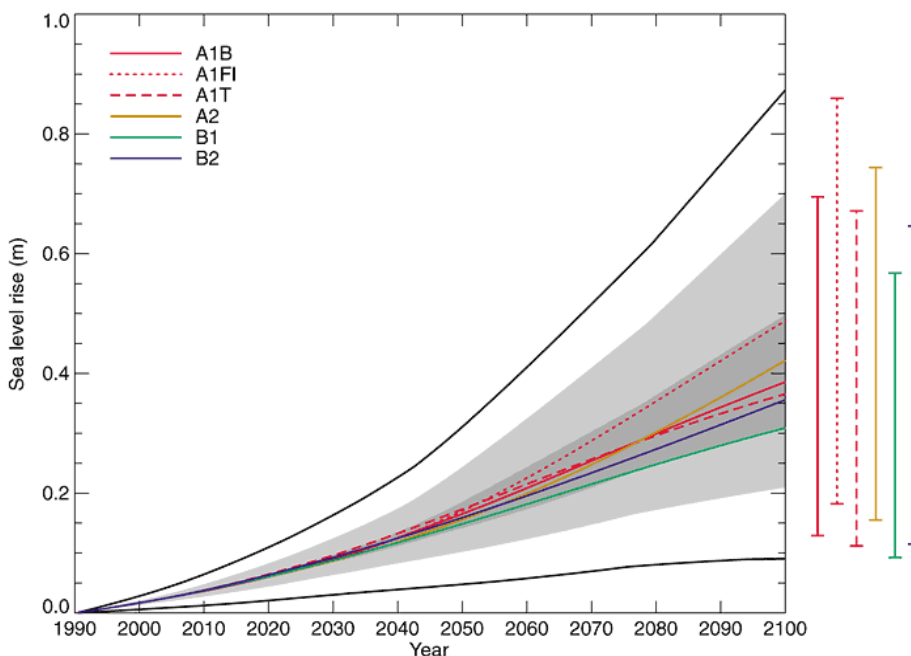


Figure 2.2-19: Predicted changes in the degree of sea level rise according to TAR (IPCC 2001b)

Although any prediction is considerably uncertain, the figure shows that a scenario with lower CO₂ emissions predicted a lower rise in the sea level.

Based on the result, we calculated the area of submergence in 2100 by the following equation:

$$D_{Land}(r, l, 2100) = PL(r, l) \div 0.5Ds(2100) \quad (2.2-22)$$

In this equation, $D_{Land}(r, l, t)$ is the area of land lost from lot l in region r in year t (Table 2.2-5); PL is the area of land lost when the sea level rises by 0.5 m (land with an altitude of

0.5 m or lower, excluding urban districts); and $D_s(t)$ is a rise in the sea level in year t calculated by MAGICC (Figure 2.2-18). Table 2.2-5 shows the area of land that will be submerged when the sea level rises by 0.5 m on average in 2100, classifying by region and by type of land.

We assumed that urban districts are not submerged by a rise in sea level. Although it may be possible to calculate the prices of lots used for some industries, such as agricultural land and forests, it is very difficult to calculate the prices of coastal lots not used for any industry – especially in developing countries. Moreover, it is more difficult to calculate the prices of dumping grounds, because they are rarely addressed. Studies in the past mainly adopted a method whereby land is divided into dry land and wet land before calculation of land prices. Under LIME, referring to an existing study that adopted such a method (Fankhauser 1995), we set the price of dry land in OECD countries at US\$2M/km², the price of wet land therein at US\$2.5M/km², the price of dry land in other countries at US\$1M/km², the price of wet land therein at US\$1.25M/km², and the price of a tundra or desert at \$0.

After that, we calculated the amount of damage for the scenarios by multiplying the result of Equation 2.2-22 by the land price (Equation 2.2-23).

$$D(2100) = \sum_{r,l} DF_{land}(r,l,2100) \cdot A(r,l) \quad (2.2-23)$$

$A(r, l)$ is the price of lot l in region r . We calculated the price according to the CO₂ Increasing Emissions Scenario and the CO₂ Fixed Emissions Scenario (expressed as $D(2100)$ and $D_0(2100)$ respectively in the following equation) and divided the price by the total amount of CO₂ emissions under both scenarios during the assessment period as in the case of Equation 2.2-2 to obtain the damage function for social assets concerning land loss due to sea level rise (Equation 2.2-24).

$$D(E_{CO_2}) = \frac{D(2100) - D_0(2100)}{\int_{1990}^t E(t) dt - \int_{1990}^t E_0(t) dt} \quad (2.2-24)$$

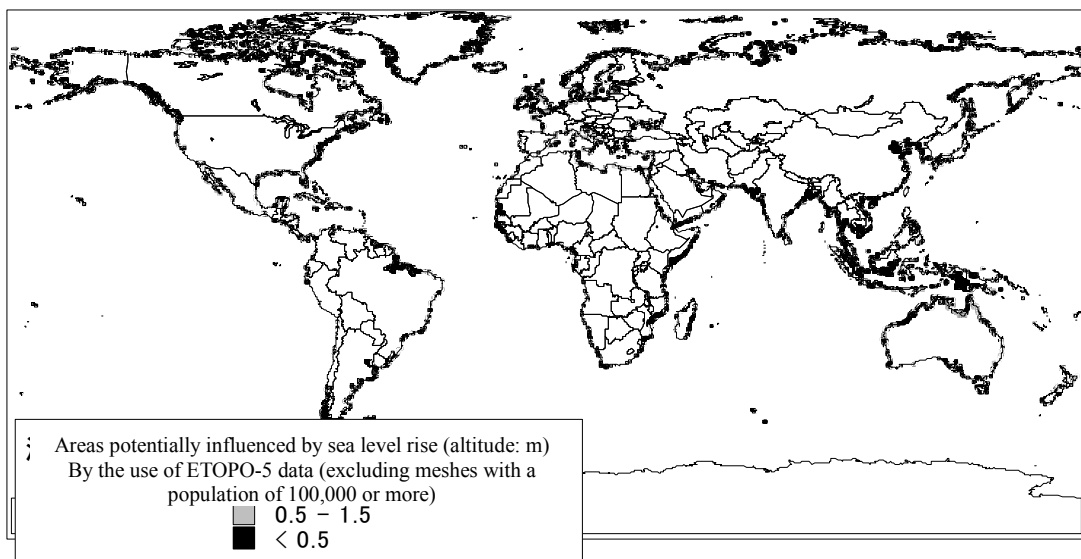


Figure 2.2-20: Areas potentially influenced by sea level rise

Table 2.2-5: Area of land to be lost until 2100 due to a 50 cm rise in sea level [km²]

Region	Dry land	Tundra & desert	Wet land	Total
AFR	61,464	14,676	43,882	120,022
CPA	56,188	711	29,461	86,360
EEU	1,648	0	2,484	4,132
FSU	17,033	52,433	41,921	111,387
LAM	178,219	11,953	71,832	262,004
MEA	11,599	11,525	14,462	37,586
NAM	45,262	76,284	79,451	200,997
PAO	51,894	711	37,676	90,281
PAS	151,818	510	195,699	348,027
SAS	60,878	0	14,928	75,806
WEU	30,460	7,469	33,470	71,399
Greenland	0	20,185	5,134	25,319
Total	666,463	196,457	570,400	1,433,320

(Note) For the classification of regions, see Table 2.2-3.

(10) Regionality in the damage function for global warming

Tables 2.2-3 to 2.2-5 show damage from global warming by region (when CO₂ concentration becomes double). First, with regard to health damage, Table 2.2-3 shows that AFR and MEA suffer most of the malaria damage, the largest damage. Although MEA includes the Middle East and North Africa, North Africa suffers most of the malaria damage according to WHO's statistics. Therefore, it can be said that most of health damage from global warming is caused by an increase in malaria damage on the African continent.

The second largest damage is malnutrition. Because the damage is in proportion to the current damage level, large damage has been predicted in AFR, MEA, and SAS, regions with low incomes. With regard to heat stress, which also causes large damage, most of the damage has occurred in SAS, which includes India, and CPA, which includes China. On the other hand, with regard to cold stress, which has been assessed to be beneficial (minus damage), health damage has greatly decreased in AFR. The region that receives the most damage from an increase in heat stress due to temperature rise is not the tropical zone, where the temperature is the highest in the world, but regions a little higher in latitude. The region that receives the largest benefit from temperature rise is not the far north region but the tropical zone. Although these facts are strange from a common sense standpoint, we have reached these prediction results because the model has a structure where the far north region is suitable for cold stress, while the tropical zone is suitable for heat stress, and because the size of regional population has been reflected in the impact. With regard to total damage by region, AFR and MEA account for most of it due to the size of malaria damage.

With regard to changes in cooling and heating energy consumption (Table 2.2-4), cooling energy consumption has greatly increased in PAS and other basically warm regions, while heating energy consumption has greatly decreased in FSU and other cold regions.

With regard to land loss due to sea level rise (Table 2.2-5), we estimated that land will be

greatly lost in NAM, LAM, and PAS, regions with long coastlines. In PAS especially, the amount of land loss will be large, and the monetary value of the land to be lost also will be large because tundra areas and deserts, whose land prices are zero, are hardly included in the land.

(11) Arrangement of the damage functions for global warming

To obtain a damage factor for global warming, we added up damage functions (damage factor per GHG emissions) at endpoints by type of substance and by area of protection (human health, social assets). Table 2.2-6 shows damage functions and factors of CO₂ by category endpoint.

With regard to the factors of the damage function, malaria is the largest in the field of health damage, and the size of the damage factors for health damage due to global warming is almost determined by the damage assessment of malaria. This is because the number of malaria sufferers has remained high mainly in Africa, where malaria is one of the main causes of death, and a rise in the relative risk due to temperature rise directly contributes to an increase in the number of sufferers. Moreover, because death damage is caused mainly at the stage of youth (at infancy), DALY per death is high. The second largest factor is malnutrition, but the size of the factor greatly depends on social conditions. Although heat stress and cold stress also are large factors in terms of absolute value, the damage (an increase in heat stress) is offset by the benefit (a decrease in cold stress).

In the field of social assets, the largest factor is agricultural impact. Among farm products, the production of wheat receives the largest damage. This is because the decrease rate of potential productivity per 1°C was estimated large. The second largest factor is land loss. This is because land loss reflects land productivity, and coastal lots, which are valued relatively high, will be lost globally. With regard to the impact on cooling and heating energy consumption, although the absolute sizes of the cooling and heating energy consumption are each near that of land loss, the damage (an increase in cooling) is offset by the benefit (a decrease in heating), like the case of heat and cold stress.

Figure 2.2-21 and Table 2.2-7 show the uncertainty analysis results and statistical amounts of the damage factors of CO₂ and CH₄ as examples, and Figure 2.2-22 shows the results of sensitivity analysis (rank correlation among parameters).

The rank correlation of damage factors for the health impact of CO₂ (Figure 2.2-22 (1) a) reflects the above-described details of damage functions and has extracted many malaria-related parameters as uncertainty factors. In addition, the impact of climate sensibility is large. The rank correlation of damage factors for the health impact of CH₄ (Figure 2.2-22 (2) a) extracted the GWP of CH₄ because of its large impact. The other results are the same as those for CO₂. In terms of median (Table 2.2-7), the ratio of the damage factor of CO₂ to that of CH₄ is 25 times, which is equal to the GWP of CH₄ (the 100-year GWP presented in IPCC Fourth Assessment Report (IPCC 2007)).

With regard to the damage factors for social assets, the rank correlation of CO₂ (Figure 2.2-22 (1) b) indicates that the main uncertainty factors are differences in the GCM output used for the prediction of potential productivity of each farm product and, like health impact, climate sensibility. On the other hand, the rank correlation of CH₄ (Figure 2.2-22 (2) b) indicates that the amount of damage under the Increasing Emissions Scenario has not been offset by the

fertilizer effect, because the effect is not included in the assessment. Because of this, there are differences from CO₂, such as large damage to rice production and extraction of price fluctuation as a large uncertainty factor due to the high unit price. As a result, in terms of median (Table 2.2-7), the ratio of the damage factor of CO₂ to that of CH₄ is 35 times, which is larger than 25, the GWP of CH₄.

Generally, the variation coefficient of each damage function is about 0.6, which seems lower than expected as uncertainty in assessment of global warming damage. This is because of the following reasons: only a single Increasing Emissions Scenario was addressed; the amount of damage was assessed for a short period until 2063, when CO₂ concentration becomes double; and the calculated amount of impact of temperature rise reflects the uncertainty of parameters based on the impact assessment research cited under LIME1, but cannot reflect differences in prediction results among various impact assessment studies.

Table 2.2-6: List of damage functions for global warming (CO₂)

	Sub-impact category	Category endpoint	Index	Damage/kg CO ₂	Damage factor
Social assets	Sea level rise	• Submergence damage	Land price	Dry land: 0.00011 US\$ [†] Wet land: 0.00012 US\$ [†]	3.0×10^{-1} yen/kg
	Impact on agriculture	• Decrease in potential production	Farm production [g]	Rice 0.27g (0.065 yen)*** Corn 0.61g (0.0082 yen)**** Wheat 1.50g (0.262 yen)*****	
	Energy consumption	• Change in energy consumption due to cooling increase and heating decrease	Secondary energy consumption [kcal]	Heating increase 5.1 kcal (−0.019 yen) * Cooling increase 1.3 kcal (0.0018 kWh) ** (0.031 yen)	
Health impact	[Direct] • Heat stress, cold stress • Disaster damage	• Change in death damage due to heat stress increase and cold stress decrease • Death damage due to increase in floods and typhoons	Loss of life expectancy (DALY)	Heat stress 3.9×10^{-9} DALY Cold stress -4.3×10^{-9} DALY Disaster (excl. typhoon) 1.4×10^{-10} DALY Typhoon 8.8×10^{-10} DALY	9.7×10^{-8} DALY/kg
	[Indirect] • Death damage due to increase in animal vector-borne infection • Malnutrition	Malaria death damage Dengue death damage • Death damage due to malnutrition	Loss of life expectancy (DALY)	Malaria 7.7×10^{-8} DALY Dengue 9.3×10^{-10} DALY 1.8×10^{-8} DALY	

- Because these are results of calculation of damage functions through substitution of representative values (point estimates) in parameters, they are not the same as representative values (median values) of uncertainty analysis results.

* Using the wholesale kerosene price of 3.67 yen/1,000 kcal (2000); source: Institute of Economy Economics, Japan “Handbook of Energy & Economic Statistics in Japan,” 2002

** Using the total unit price of electricity of 17.76 yen/kWh (2000); source: Institute of Economy Economics,

Japan "Handbook of Energy & Economic Statistics in Japan," 2002

*** Using farmer's selling price of rice of 243.42 yen/kg (government-selling/free distribution, 2000); source: Ministry of Agriculture, Forestry and Fisheries "Farm Price Statistics," 2000

**** Using the unit import price of 12.62 yen/kg (amount and volume of import) (2000); source: Ministry of Agriculture, Forestry and Fisheries "76th Statistical Yearbook," 2000

***** Using farmer's selling price of class-1 wheat of 164.28 yen/kg (government-selling, 2000); source: Ministry of Agriculture, Forestry and Fisheries "Farm Price Statistics," 2000

¶ Land prices were calculated at the rate of 1US\$=111 yen.

Table 2.2-7: Examples of results (statistical amounts) of uncertainty analysis of damage factors (CO_2 , CH_4)

	Damage factor (CO_2)		Damage factor (CH_4)	
	Health impact	Social assets	Health impact	Social assets
Statistical amount	DALY/kg CO_2	Yen/kg CO_2	DALY/kg CH_4	Yen/kg CH_4
No. of trials	50000	50000	50000	50000
Average value	1.63E-07	3.86E-01	4.07E-06	1.37E+01
Median	1.31E-07	3.23E-01	3.27E-06	1.21E+01
Standard deviation	1.02E-07	2.62E-01	2.73E-06	7.34E+00
Dispersion	1.04E-14	6.89E-02	7.46E-12	5.39E+01
Degree of skew	2.49	1.39	2.63	1.44
Kurtosis	12.7	6.15	14.5	6.42
Variation coefficient	0.624	0.680	0.671	0.535
10% value	8.00E-08	1.24E-01	1.80E-06	6.29E+00
90% value	2.87E-07	7.50E-01	7.30E-06	2.35E+01
Average standard error	4.55E-10	1.17E-03	1.22E-08	3.28E-02

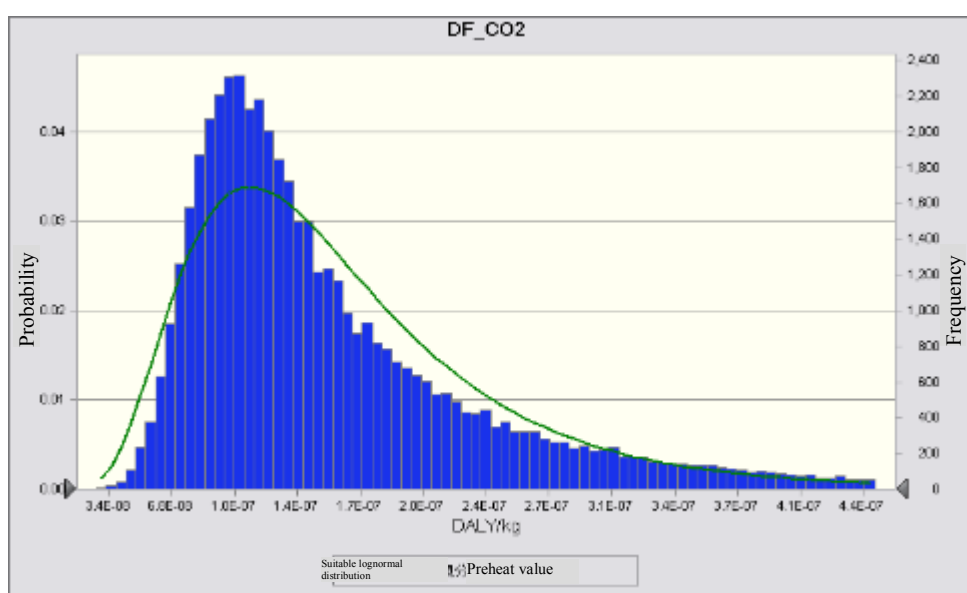


Figure 2.2-21a: Frequency distribution of prediction results of damage factors (health impact)

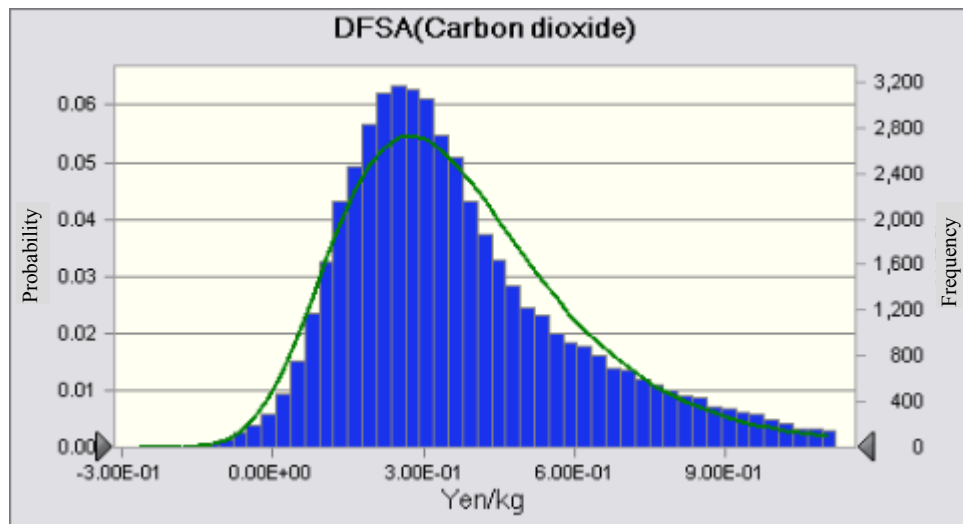


Figure 2.2-21b: Frequency distribution of prediction results of damage factors (social assets)

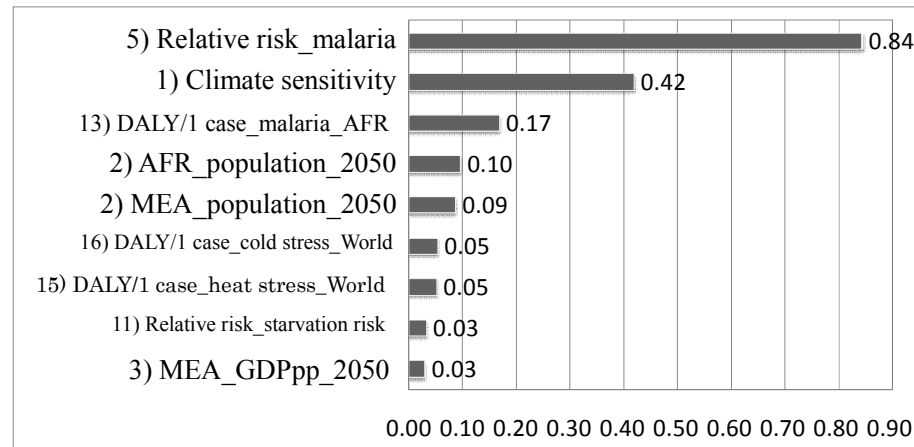


Figure 2.2-22 (1) a: Rank correlation among damage factors (health impact) (CO₂)

- Parameters of 0.03 and more were extracted.
- Numbers correspond to parameters shown in Table 2.2-2.

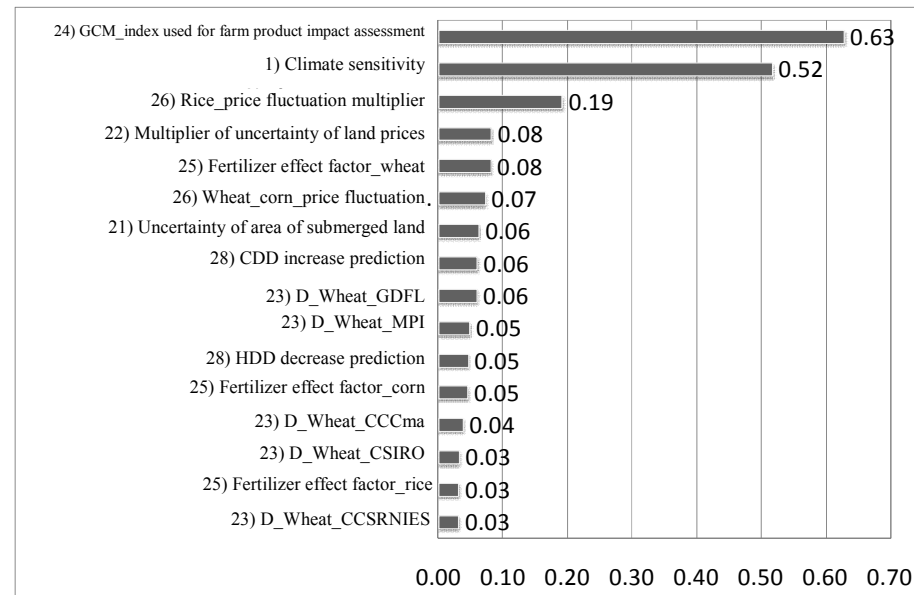
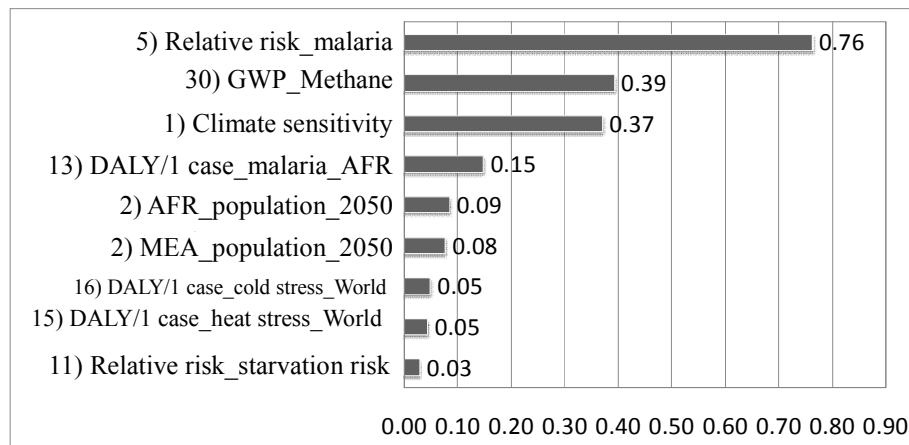


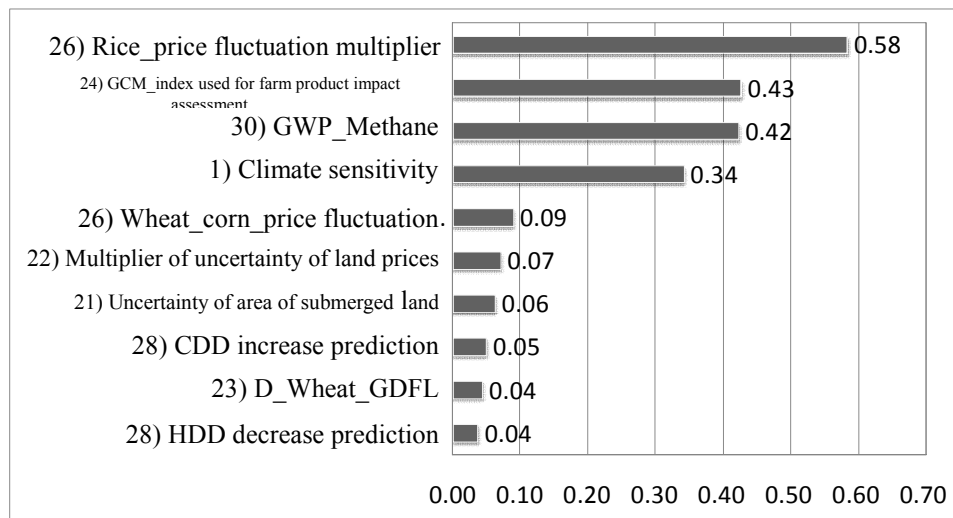
Figure 2.2-22 (1) b: Rank correlation among damage factors (social assets) (CO₂)

- Parameters of 0.03 and more were extracted.
- Numbers correspond to parameters shown in Table 2.2-2.

**Figure 2.2-22 (2) a: Rank correlation among damage factors (health impact) (CH₄)**

- Parameters of 0.03 and more were extracted.

- Numbers correspond to parameters shown in Table 2.2-2.

**Figure 2.2-22 (2) b: Rank correlation among damage factors (social assets) (CH₄)**

- Parameters of 0.03 and more were extracted.

- Numbers correspond to parameters shown in Table 2.2-2.

2.2.4 Procedure for impact assessment of global warming

In this section, we describe the procedure for impact assessment of global warming by the use of LIME. Those who carry out the procedure can select what is suitable for their purpose from among characterization, damage assessment, and weighting and use it for LCA, etc.

For the purpose of characterization, an index for midpoint approach – that is, a category indicator $CI^{Global\ warming}$ – can be obtained from the inventory of GHG $X\ Inv(X)$ and the characterization factor $CF^{Global\ warming}(X)$ (Equation 2.2-25). Although there are two or more $CI^{Global\ warming}(X)$, GWP₁₀₀ has been recommended under LIME. $CI^{Global\ warming}$ can be expressed as an amount of CO₂ emissions, the referential substance.

$$CI^{Global\ warming} = \sum_X \{ CF^{Global\ warming}(X) \times Inv(X) \} \quad (2.2-25)$$

The damage factor $DF^{Global\ warming} (Safe, X)$ is used for damage assessment. In the case of global warming, damage factors have been provided for human health, for which DALY is used as the index, and for social assets, for which monetary value [yen] is used as the index. Moreover, the damage index $DI (Safe)$ can be obtained from each GHG's $Inv (X)$ and the damage factor $DF^{Global\ warming} (Safe, X)$. This index means the amount of potential damage to each area of protection due to GHG emissions (Equation 2.2-26). It is possible to compare the index directly with results of damage assessment in other impact categories or add it to them on condition that the area of protection is the same.

$$DI (Safe) = \sum_X \{ DF^{Global\ warming} (Safe, X) \times Inv (X) \} \quad (2.2-26)$$

$IF^{Global\ warming}$, the factor that weights impact on human health and social assets, is used for weighting. The weighting index SI can be obtained from each GHG's $Inv (X)$ and the weighting factor $IF^{Global\ warming}$. The index can be compared directly with results of damage assessment in other impact categories or add it to them (Equation 2.2-27).

$$SI = \sum_X (IF^{Global\ warming} (X) \times Inv(X)) \quad (2.2-27)$$

The characterization factor $CF^{Global\ warming} (X)$, the damage factor $DF^{Global\ warming} (Safe, X)$, and the weighting factor $IF^{Global\ warming} (X)$ are attached hereto as Appendix 1, Appendix 2, and Appendix 3 respectively.

Many of the ozone depleting substances (ODS) mentioned in Section 2.1 are also GHGs. However, Sections 2.1 and 2.2 do not necessarily address the same substances. Because of this, note that, if any of the substances (ODS) included in the list of factors in Section 2.1 is not included in the list of factors in Section 2.2, it does not necessarily mean that the substance is not a GHG (and vice versa).

Acknowledgement

With regard to various aspects of the development of an LCIA method for global warming, we received advice from the committee members and the experts who reviewed our methodology. In addition, with regard to agricultural impact, Mr. Kiyoshi Takahashi, a researcher of the National Institute for Environmental Studies, provided us with a model for calculation of the potential productivity of farm products. We would like to express our deep gratitude to all of them. The responsibility for the contents of this chapter entirely belongs to the authors.

Column 2.2-4

Climate sensibility

For the purpose of discussions about the global warming problem, (equilibrium) climate sensibility generally means “a long-term equilibrium change in global mean near-surface air temperature that results from doubling of the atmospheric (equivalent) CO₂ concentration” (IPCC 1996). Because climate sensibility indicates how much the temperature finally rises when GHG concentration rises, it is a very important figure and an element whose uncertainty has great impact on the result of impact assessment in the upper part of the influence path between GHG emissions and occurrence of damage.

In the past, IPCC set climate sensibility at 1.5 to 4.5°C, which was not changed during the period between its first report in 1990 and the third report in 2001 (IPCC 2001b). This was estimated by experts mainly based on results of prediction under (two or more) GCMs. Differences in climate sensibility among GCMs are mainly due to the feedback component of clouds.

After the third report, many studies were carried out to estimate climate sensibility and improve quantitative probability assessment, including a likelihood value. Because climate sensibility cannot be measured directly, the relation between observable quantity and climate sensibility was established and new methods were used for estimating the range or probability density distribution of climate sensibility consistent with observation. Concretely, two new methods were used: a method that uses restrictions obtainable from past climate changes and a method that uses an extent of climate sensibility results of model ensemble experiments (Meehl 2007: IPCC AR4 WG1 Report Box 10.2).

In the fourth report, IPCC states that the level of scientific understanding and reliability concerning quantitative assessment of equilibrium climate sensibility has greatly improved since the third report and drew the following conclusions from the results mentioned in Figure 2.2-C (assuming that there is no official method established to obtain a single probability density distribution from different studies): equilibrium climate sensibility is likely to be between 2 to 4.5°C; the best estimate is about 3°C; and it is highly unlikely to be less than 1.5°C. Although it might be rather higher than 4.5°C, such a case is generally thought to be inconsistent with observation results (Meehl 2007).

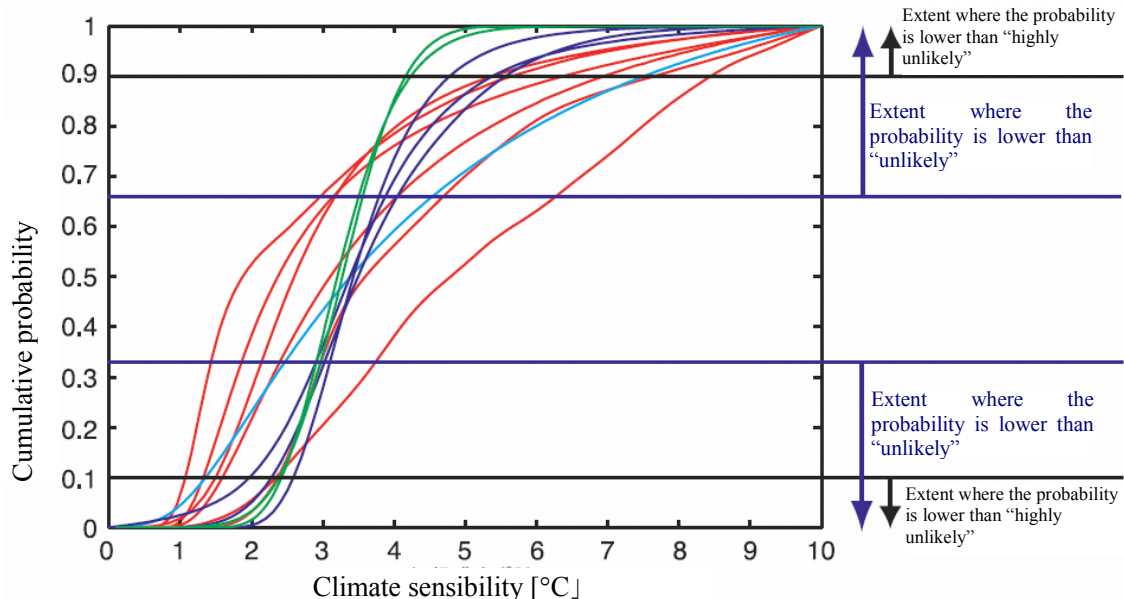


Figure 2-2-C: Cumulative distribution of climate sensibility by various methods

- Cumulative distribution of the climate sensibility calculated from observed temperature rise of the 20th-century (-----), model climatology (—), and alternative evidence (—) and the cumulative distribution of climate sensibility of AOGCM (.....). Horizontal lines and arrows are estimated probabilities defined in IPCC Fourth Assessment Uncertainty Guidance.

Source: Japan Meteorological Agency “IPCC Fourth Assessment Report, Working Group 1 Report, Technical Summary”

(http://www.data.kishou.go.jp/climate/cpdinfo/ipcc/ar4/ipcc_ar4_wg1_ts_Jpn.pdf)

Under LIME2, the version of simplified climate model MAGICC used for the third report (see Column 2.2-2) was used for prediction of the degree of temperature rise, etc. and the lognormal probability density distribution described in Wigley & Raper (2001) was used as climate sensibility (Figure 2.2-D).

As defined above, climate sensibility is a long-term equilibrium change. Because the temperature is not in equilibrium at the time of doubling of CO₂ concentration in 2063, a rise in the temperature at that time is predicted to be lower than climate sensibility (under LIME2, 1.85°C if climate sensibility is 2.6°C under the Increasing Emissions Scenario).

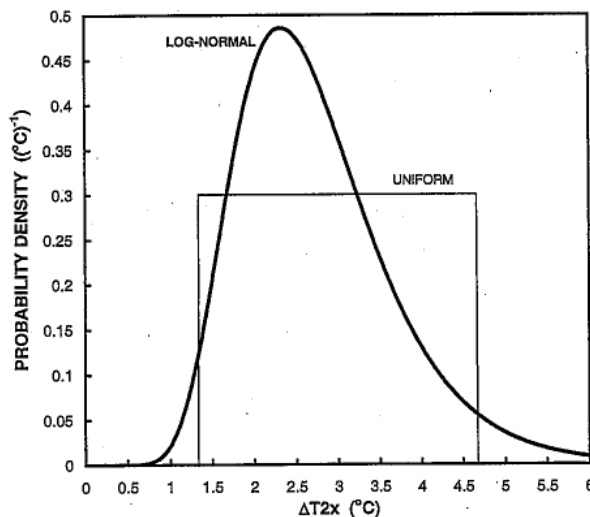


Figure 2.2-D: Probability density distribution of climate sensitivity established under LIME2

- 90% reliability section between 1.5°C and 4.5°C in either case
- Under LIME 2, a lognormal distribution case was used for the probability density distribution of climate sensibility.

Source: Wigley & Raper (2001)

[References for Section 2.2]

Brakkee KW ; Huijbregts MAJ ; Eickhout B ; Hendriks AJ ; Meent D van de, 2008, Int J LCA 2008; 13 (3):191-201

CML (2000)

Cure, Acock (1986): Agriculture and Forest Meteorology, 38: 127-14

ExternE (1999): Externality of Energy: Global Warming Damages

Fankhauser (1995): Valuing Climate Change; The Economics of the Greenhouse, Earthscan Publication Ltd., London

FAO (2000): FAOSTAT (FAO Statistical Database)

Goedkoop, Spriensma (1999): The Eco-indicator 99; A damage oriented method for Life Cycle Impact Assessment; Pethodology Report, PRe Consultants

GRID—Tsukuba, <http://www-cger.nies.go.jp/grid-j/gridtxt/grid1.html>

Hay, et al (2002): Climate change and the resurgence of malaria in the East African Highlands. *Nature* 415: 905-909

Honda, et al (1998): *J. Risk Res.*, 1:209-220

IIASA/WEC (1998): Global Energy Perspective

IPCC (1990): *Climate Change 1990*, Cambridge University Press, Cambridge and New York

IPCC (1995): *Climate Change 1995, The Science of Climate Change*. Cambridge University Press, Cambridge and New York

IPCC (2001a): *Climate Change 2001: The Synthesis Report*. Cambridge University Press, Cambridge and New York

IPCC (2001b): *Climate Change 2001: The Scientific Basis*. Cambridge University Press, Cambridge and New York

IPCC (2001c): *Climate Change 2001: Impacts, Adaptation and Vulnerability*. Cambridge University Press, Cambridge and New York

IPCC (2007): *IPCC AR4 WG1: Climate Change 2007: The Physical Science Basis. Contribution of Working Group I to the Fourth Assessment*

Kalkstein, et al (1993): The impact of climate change on human health: some international implications, *Experientia* 49, p.969-979

Kunst, et al (1993): *J. Epidemiol.*, 137: 331-341

Martens, et al (1997): Sensitivity of malaria, schistosomiasis and dengue to global warming. *Climatic Change*, 35(2):145-156

Meehl, G.A., T.F. Stocker, W.D. Collins, P. Friedlingstein, A.T. Gaye, J.M. Gregory, A. Kitoh, R. Knutti, J.M. Murphy, A. Noda, S.C.B. Raper, I.G. Watterson, A.J. Weaver and Z.-C. Zhao (2007) Global Climate Projections. In: *Climate Change 2007: The Physical Science Basis. Contribution of Working Group I to the Fourth Assessment Report of the Intergovernmental Panel on Climate Change* [Solomon, S., D. Qin, M. Manning, Z. Chen, M. Marquis, K.B. Averyt, M. Tignor and H.L. Miller (eds.)]. Cambridge University Press, Cambridge, United Kingdom and New York, NY, USA.

Murray, et al (1996): *The global burden of disease: a comprehensive assessment of mortality and disability from disease, injuries and risk factors in 1990 and projected to 2020*, Harvard University Press

Nordhaus (1994): *Managing the global commons: The economics of climate change*, MIT Press, Cambridge, MA

Olson, et al (1983): Carbon in Live Vegetation of Major World Ecosystems, Report ORNL-5862, Oak Ridge National Laboratory, Oak Ridge, Tennessee, USA

Parry, et al (1999): Climate change and world food security: a new assessment, *Global Environment Change*, 9, S51-S67

Randall, D.A., R.A. Wood, S. Bony, R. Colman, T. Fichefet, J. Fyfe, V. Kattsov, A. Pitman, J. Shukla, J. Srinivasan, R.J. Stouffer, A. Sumi and K.E. Taylor (2007): Cilmate Models and Their Evaluation. In: *Climate Change 2007: The Physical Science Basis. Contribution of Working Group I to the Fourth Assessment Report of the Intergovernmental Panel on Climate Change* [Solomon, S., D. Qin, M. Manning, Z. Chen, M. Marquis, K.B. Averyt, M.Tignor and H.L. Miller (eds.)]. Cambridge University Press, Cambridge, United Kingdom and New York, NY, USA.

Reiter (2000): BITING BACK, New Scientist, 23 September

Steen (1999): A systematic approach to environmental priority strategies in product development (EPS) Version 2000-General system characteristics, CPM report

Tol(1995): The damage cost of Climate Change Toward More Comprehensive Calculations

Tol (2002):Dynamic Estimates,Environmental and Resource Economics 21:47-73,2002.

Estimates of the Damage Costs of Climate Change. Part 1: Benchmark Estimates, Environmental and Resource Economics, 21 (1), 47-73

United Nations (2003): World Population Prospects : The 2002 Revision, United Nations, New York

WHO (1998): 21st Century, Health, World – World Health Report edited by WHO, Eidensha

WHO (2001): The World Health Report 2000

Wigley & Raper (2001) : Interpretation of High Projections for Global-Mean Warming, Science, 293, No.5529, p.451-454

Wigley (2003) : MAGICC/SCENGEN 4.1:USER MANUAL

World Bank (2001): World Development Indicators 2001(CD—ROM), Washington D.C.

Itsubo, Inaba (2005): Life-Cycle Impact Assessment Method Based on Endpoint Modeling LIME-LCA, Environmental Accounting, Assessment Methods and Databases for Environmental Efficiency, Japan Environmental Management Association for Industry

Environment Agency's Research Group on the Global Warming Problem (edit.) (1990): Prevention of Global Warming, NHK Publishing

Koike (2006): To What Extent Has Global Warming Been Clarified?, Maruzen

Takahashi et al. (1997): Environmental System Study, 25: 121-131

Institute of Energy Economics, Japan (2002): Handbook of Energy & Economic Statistics 2002, Energy Conservation Center

Hayakawa K (1992): Regional Cooling and Heating Systems, Inoueshoin

Matsuoka, et al. (1994): Prospects for Impact of Global Warming on Prevalence of Malaria, National Institute for Environmental Studies

Matsuoka (2005): Integrated Assessment Modeling for the Climate Change Problem: International Economy (2005) Vol. 56: 5-29

2.3 Acidification

(Changes under LIME2)

- Uncertainty analysis of the damage factors for primary production (terrestrial ecosystem) and social assets (fishery production) was carried out.
- With regard to the calculation of the source attribution of sulfur dioxide (SO_2) and nitrogen oxides (NO_x), under LIME1 we calculated a domestic average for terrestrial areas from prediction results of the OPU model and the ratio of total terrestrial area to total marine area within the model region. Under LIME2, however, we divided Japan into six zones, taking into account geographical fluctuation, and calculated the source attribution by zone based on the ratio of terrestrial area and marine area.
- Naturally produced SO_2 was excluded from the amount of emissions used for the calculation of the source attribution of SO_2 to the extent possible.
- While LIME1 used only one type of relational equation for aluminum ion (Al^{3+}) and the dry matter growth rate of trees, LIME2 uses three types by collecting knowledge.

2.3.1 What phenomenon is acidification?

(1) Cause of acidification

For the purpose of this section, acidification means that terrestrial environments and ground water have gradually become acid through long-term continuation of acidic deposition from the air to the ground. Generally known acid rain is included in acidification. However, as described later, the term “acid rain” refers to only a part of acidic deposition.

Acid substances are substances that emit hydrogen ion (H^+) in a water solution (so-called Arrhenius acid). Main acid substances are sulfuric acid (H_2SO_4), nitric acid (HNO_3), hydrochloric acid (HCl), and organic acid (RCOOH). In the atmosphere, ammonia (NH_3), a basic substance, also creates two moles of H^+ when receiving microbes’ nitrification after being deposited to the ground from the atmosphere (Pierzynski et al. 1994) and thereby functions as a net monovalent acid. Therefore, from the viewpoint of acidification, NH_3 must be considered potential acid. For the purpose of this section, acid substances and NH_3 are collectively expressed as acidifying substances. The main causative substances of H_2SO_4 are sulfur oxides (SO_x) (especially, sulfur dioxide (SO_2)), and the main causative substances of HNO_3 are nitrogen oxides (NO_x) (especially, nitrogen monoxide (NO) and nitrogen dioxide (NO_2)). These causative substances, including NH_3 , emerge often, accompanying human activities. The main artificial source of SO_x and NO_x is burning of fossil fuels, while that of NH_3 is stockbreeding and application of fertilizers. Table 2.3-1 shows main acidifying substances and their causative substances.

When causative substances are emitted in the atmosphere, they spread widely by atmospheric currents (advection diffusion process). During this process, various reactions occur (alteration process) – for example, the change of SO_x into H_2SO_4 , the change of NO_x into HNO_3 , and the ion binding of H_2SO_4 and NH_3 into particle ammonium sulfate ($(\text{NH}_4)_2\text{SO}_4$). In parallel with this, deposition on the surface of the ground occurs (deposition process). The deposition process can be roughly divided into two types. One of them is acid load that accompanies precipitation (wet deposition). Acid substances are incorporated into

precipitation, such as rain, snow, and fog, and are deposited on the surface of the ground. In a strict sense, acid rain refers only to acidized rainwater. The other is acid load that accompanies gaseous or particle substances' direct deposition on the surface of the ground (dry deposition). Because this cannot be observed directly, it is hard to recognize. However, because precipitation is high in Japan, it has been thought that the load of substances is almost the same between wet deposition and dry deposition. For the purpose of this document, acidic deposition means both the wet and dry deposition of acid substances.

Table 2.3-1: Typical acid substances and their causative substances

Main acidifying substance	Causative substance (●: contribution of artificial sources is large)	Main source of causative substance	
		Artificial source	Natural source
Sulfuric acid (H ₂ SO ₄)	● Sulfur oxides (mainly, SO ₂)	Burning	Volcanoes
	Deoxidized sulfur oxides (H ₂ S, DMS, etc.)	Drainage	Sea, substratum
Nitric acid (HNO ₃)	● Nitrogen oxides (mainly, NO and NO ₂)	Burning	Lightning
Hydrochloric acid (HCl)	● Direct generation as hydrochloric gas	Burning, chlorine factory	Volcanoes
Organic acid (RCOOH) ^{†1}	Hydrocarbon (HC)	Burning	Vegetation
Ammonia (NH ₃) ^{†2}	● Direct generation as ammonia	Chemical fertilizer, livestock	Soil

†1. Organic acid is the generic term for various substances (R widely refers to organic matters). Main organic acids in the atmosphere are formic acid (HCOOH), acetic acid (CH₃COOH), and oxalic acid ((COOH)₂).

†2. Ammonia itself is a basic substance. However, because ammonia functions as a net monovalent acid due to nitrification after deposition on the surface of the ground, from the viewpoint of acidification, ammonia must be considered latent acid.

The geographical range of acidification is between a regional level (such as the Kanto region) and a transnational level (such as East Asia). In Europe and North America, the cross-border air pollution problem has become an important political issue (Environmental Agency (supervised) 1993). In Asia, where energy and food consumption have been increasing because of economic and population growth, the same problem is highly likely to arise.

There are various impacts of acidification (Figure 2.3-1). Once the environment is acidified, it cannot be recovered easily, with the result that great damage will continue to exist for a long time. Like other global environment problems, it is extremely important to prevent the occurrence of acidification.

There are other effects of acidic deposition in addition to acidification of the environment. Nitrogen (N), which is an element of HNO₃ and NH₃, is an element essential for living things and is generally considered the scarcest element in terms of the amount demanded in forests. Therefore, if the ratio of nitrogenous compounds deposited from the atmosphere to the whole nitrogen circulation is low, they may greatly influence the growth of forests. The state where the amount of nitrogen is greater than the amount demanded by living things is called "nitrogen saturation" (Aber et al. 1989). The effects of nitrogen saturation vary, including not only effects on the ecosystem but also pollution of groundwater due to nitrate-nitrogen, eutrophication of water areas, and an increase in the amount of GHG emitted from forest soil

(Orui 1997, Izuta 2001). Under LIME, although inclusion of nitrogen saturation in the category of “acidification” was considered, it was judged that there is a shortage of knowledge necessary for the quantification of the impact at present and nitrogen saturation was not assessed.

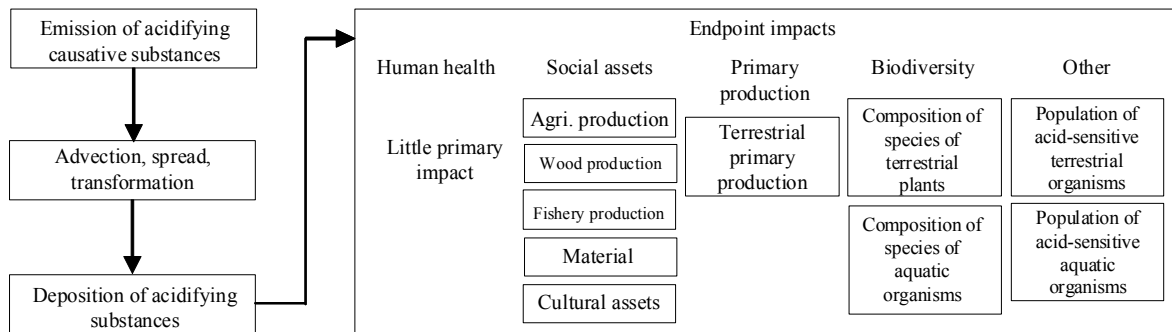


Figure 2.3-1: Causation of acidification

(2) Endpoints of acidification

a Human health

In Japan, acid rain was recognized when stimuli to eyes and throat occurred due to drizzle mainly in the Kanto region during the rainy season in 1973 to 1975 (Okita 1982). This was caused by rain considerably polluted by highly concentrated air pollutants. Because air quality has greatly improved recently, rainfall that gives a stimulus to eyes and throat is unlikely to occur, and there is little fear that acidification gives direct impact to human health. At present, however, there is an increasing fear that pollution of groundwater due to nitrate-nitrogen (Ministry of the Environment (ed.) 2002) might give indirect impact to human health.

b Impact on the ecosystem

Impact on the ecosystem can be roughly divided into impact on the terrestrial ecosystem and impact on the aquatic (land water) ecosystem.

The impact on the terrestrial ecosystem can be divided into direct impact and indirect impact. Direct impact is the direct harmful impact of highly concentrated acid on trees, etc. Usually, the acid level (pH) of rainfall is not so high as to give direct impact to trees. However, in regions where fog easily occurs, there is fear that acid fog might have direct impact. Because, compared with a raindrop, a fog droplet has a far smaller diameter and a larger specific surface area, fog droplets very easily cause pollution. Moreover, because it is hard for fog drops to fall, trees covered by fog are exposed for a long time. It is even said that fog droplets enter leaves through stomata and give harmful effect to the leaves (Murano 1993). On the other hand, indirect impact means that the physical and chemical characteristics of soil change due to the acidification of soil and give harmful effect to growing trees. Acidification of soil makes it easier to cause eluviation of bases, elution of inorganic aluminum (Al), and elution of precious metals, such as manganese (Mn) (Totsuka 1996). Eluviation of bases brings about a shortage of nourishment for plants, and inorganic Al is known to have phytotoxicity (Japan Society of Soil Science and Plant Nutrition (ed.) 1994). Both might hinder the growth of plants and reduce the primary production of plants, the basic

production of the ecosystem. However, general soil has high buffer capacity, and changes in the physical and chemical characteristics of soil due to acidic deposition are extremely slow and hard to detect. In addition, because many factors are involved in indirect impact, it is difficult to prove indirect impact at the field level.

Because acidification of land water is caused through acidification of terrestrial water catchment areas, the contribution of acid substances directly depositing on terrestrial water from the atmosphere is usually small. Therefore, indirect impact is problematic to the freshwater ecosystem. Because, if the load of substances is the same, water quality change becomes more conspicuous as nutrition is poorer, aquatic organisms in an oligotrophic environment are susceptible to the impact of acidification. Both the degree of acidity (= low pH) and inorganic Al have harmful effect on aquatic organisms (Ikuta 1999). However, there is little quantitative information on the impact of inorganic Al.

c Impact on social assets

Because large quantities of fertilizers are scattered on farmland, acidic deposition has extremely little impact on the soil of farmland. Therefore, it can be thought that acidic deposition has direct influence on farm products only through low pH rainfall. However, unless the rainfall pH falls to about 2, it hardly has an effect to farm products (Nouchi 1996). With regard to forestry, because it takes dozens of years to grow trees, it is difficult to quantitatively assess long-term impact of acidification. As for fisheries, acidification has caused serious damage to salmon fishery in lakes and rivers in Northern Europe (Hesthagen et al. 1999).

Acid substances corrode metals and stones. Although they rarely have serious structural impact, they might cause problems related to maintenance, such as an increase in the frequency of repair. In addition, they might impart damage to structures as well as art objects and other cultural assets placed outdoors (Komeiji 1993).

2.3.2 Characterization of acidification

(1) Characterization factor for acidification under the existing LCA method

Acidification potential (AP) has been frequently adopted for LCA as the characterization factor for acidification (Heijungs et al. 1992). AP is calculated by relativizing the amount of H⁺ produced through the emission of a unit amount of causative substances of acidification by the amount of H⁺ produced through the emission of a unit amount of SO₂.

$$AP_1 = (\eta_i / M_i) / (\eta_{SO_2} / M_{SO_2}) \quad (2.3-1)$$

In this equation, η_i is the valence of the substance i serving as an acid, and M_i is the molecular weight of the substance i .

AP (Heijungs et al. 1992) is the characterization factor from the viewpoint of sources. However, the degree of impact of acidification varies where and in what quantity the causative substance emitted at a certain place deposits as an acid substance and the kind of sensitivity of the soil and vegetation of the place of deposition. Recently, therefore, characterization factors that take into account regional characteristics have been drawing

attention. There are four approaches for taking into account regional characteristics: 1) covering only highly sensitive regions (Hogan et al. 1996); 2) setting sensitivity for each region and weighting the amount of emissions (Hauschild et al. 1998); 3) comparing and assessing the maximum scenario and the minimum scenario (Lindfors et al. 1996; Nichols et al. 1996); and 4) introducing a numerical model into atmospheric transport and taking into consideration differences in sensibility among regions (Potting et al. 1997; Huijbregts 1999). Of them, approaches 1) to 3) do not solve the problem because they do not take into consideration fate analysis between emission and deposition. Therefore, we examined two methods that adopt approach 4).

Potting et al. (1998) introduced a characterization factor employing the atmospheric transport model developed according to the European Monitoring and Evaluation Program (EMEP) (Amman et al. 1996; Berrett et al. 1996) and the acidic deposition impact assessment model (Posch et al. 1997).

$$I = \sum_{e \in \text{Europe}} A_{e \in j} \cdot \Theta(D_j - CL_{e \in j}) \quad (2.3-2)$$

$$D_j = \sum_{i \in \text{acid}} \sum_{j \in \text{Europe}} t_{r,i,j} \cdot E_{r,i} \quad (2.3-3)$$

In this equation, I is the total impact of emission of acidifying causative substances; A is the ratio of the ecosystem e (such as spruce forests) in the mesh j ; CL is the critical load of the ecosystem e in the mesh j (Posch et al. 1997); D_j is the amount of acid deposition in the mesh j (amount of load as H^+); Θ is the step function, which is 1 if acidic deposition exceeds the critical load of the ecosystem e or 0; $t_{r,i,j}$ is the ratio of the acidifying substance i emitted in the region r and deposited in the mesh j ; and $E_{r,i}$ is the amount of emissions as the amount of produced H^+ of the acidifying substance i in the region r .

The method adopted by Potting et al. (1998) is better than other approaches in that it takes into consideration both the fate of the emitted substance and differences in sensibility. However, because it uses a step function, the relation between the amount of acidic deposition and the cumulative ratio of the fragile ecosystem becomes a discontinuous function with a slope of 0 or infinity. Therefore, the method is unsuitable for assessing the impact of additional emission of an acidification causative substance to the baseline load.

On the other hand, Huijbregts (1999) used the ratio between the amount of acidic deposition and the critical load and introduced a characterization factor that expresses a change in the total risk of the ecosystem's receiving harmful effect from acidification.

$$I = \sum_{e \in \text{Europe}} A_{e \in j} \cdot D_j / CL_{e \in j} \quad (2.3-4)$$

This method has an advantage in that it can express the total impact by a continuous function, because it uses a concept similar to the characteristic factor obtained from the relation between the amount of exposure and no observed effect level for the purpose of toxic assessment.

(2) Characterization factor for acidification under LIME

Application of the characterization factors developed by Potting et al. (1998) and Huijbregts (1999) to Japan has the following problems: 1) consideration is given only to terrestrial vegetation, excluding impact on aquatic organisms; 2) the results have been obtained in Europe, whose geographical conditions are different from those in Japan; 3) not all the acidifying causative substances to be considered are covered; and 4) because the characterization factors are biased toward endpoints, uncertainty caused by models is large. To cope with these problems, under LIME we developed a characterization factor for acidification with consideration for the geographical characteristics found in Japan. As main acidifying causative substances, we gave consideration to SO₂, NOx (NO and NO₂), hydrochloric acid (HCl), and NH₃. Although it is usually rare to regard HCl as a problematic substance, we gave consideration to it because it is produced during the process of burning substances that contain chlorine (Cl). As described above, we regarded NH₃, which functions as a base in the atmosphere, as a latent acid, because it contributes as a net monovalent acid due to nitrification after deposition from the atmosphere. The geographical extent of emission and deposition was limited to Japan. Figure 2.3-2 shows a flowchart of estimation of the characterization factor.

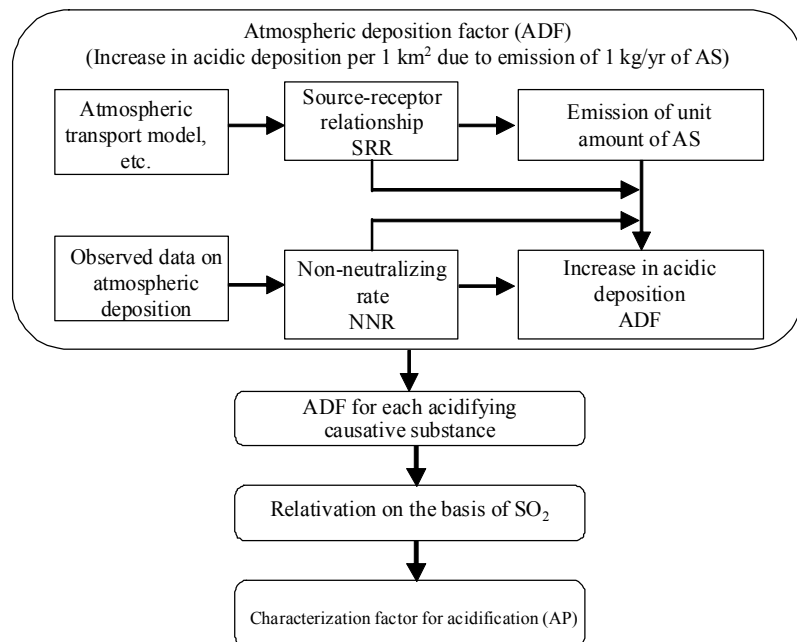


Figure 2.3-2: Flowchart of estimation of characterization factor for acidification

a Source-receptor relationship of acidifying causative substance

Source-receptor relationship (SRR) (Ichikawa 1998) indicates where and to what degree an acidifying causative substance (AS) emitted in a region deposits (example: what percentage of SO₂ emitted in the Kanto region is deposited in the Kanto region and what percentage is deposited in the Tohoku region?).

The SRR of SO₂ and the SRR of NOx were calculated for each of the six zones in Japan based on estimation of SRR in 1991 for each of the six zones (Nakaminami 2000) and the ratio between terrestrial and marine areas for each of them (see Figure 2.3-3). The calculation was based on the results obtained from an atmospheric transport model of Eulerian type (fixed

system of coordinates) developed by Osaka Prefecture University (Ikeda et al. 1997, 2001) (for details of the model developed by Osaka Prefecture University, see Section 2.4) and the results of research on the positional relationships of the grids of the second mesh system. We calculated the domestic average of SRR by averaging each zone's SRR, weighting the area of each zone, and as a result the SRR of SO₂ and the SRR of NO_x were estimated to be 0.166 and 0.150 respectively. The details of SRR of SO₂ and NO_x are shown in Table 2.3-2 and 2.3-3.



Figure 2.3-3: Probability distribution among the emission zones of air polluting substances (1 to 6 are zone numbers) (example: SO₂)

Table 2.3-2: Source-receptor matrix of SRR of SO₂

		receptor						
source	Terrestrial area [km ²]	zone 1	zone 2	zone 3	zone 4	zone 5	zone 6	
	zone 1	53838	0.045	0.005	0.034	0.007	0.003	0.002
	zone 2	23083	0.003	0.076	0.030	0.053	0.027	0.006
	zone 3	78001	0.006	0.019	0.168	0.033	0.007	0.003
	zone 4	73445	0.0006	0.004	0.008	0.153	0.015	0.004
	zone 5	56341	0.0002	0.002	0.001	0.019	0.160	0.017
	zone 6	76973	0.0001	0.0002	0.0002	0.0005	0.002	0.068

Table 2.3-3: Source-receptor matrix of SRR of NOx (NO, NO2)

		receptor						
source	Terrestrial area [km ²]	zone 1	zone 2	zone 3	zone 4	zone 5	zone 6	
	zone 1	53838	0.052	0.007	0.036	0.007	0.003	0.001
	zone 2	23083	0.003	0.046	0.023	0.046	0.024	0.005
	zone 3	78001	0.005	0.014	0.104	0.031	0.007	0.002
	zone 4	73445	0.0007	0.004	0.008	0.141	0.019	0.004
	zone 5	56341	0.0003	0.002	0.001	0.016	0.100	0.016
	zone 6	76973	0.0001	0.0003	0.0003	0.0008	0.005	0.090

Because there was little information on the SRR of HCl, an average SRR in Japan was calculated by estimating the amount of emissions to the atmosphere and the amount of deposition from the atmosphere between 1993 and 1997. It was assumed that the main sources of HCl were incineration of waste and combustion of fossil fuels. The amount of

HCl produced by incineration was calculated by multiplying the amount of incinerated waste (Statistical Bureau of Ministry of Internal Affairs and Communications (ed.) (each fiscal year)) by the volatile Cl content ratio of incinerated waste (Japan Waste Management Association, Japan Waste Research Foundation 1999) and took into consideration the elimination efficiency of exhaust gas treatment systems (Shigaki 1998) to obtain the amount of emissions to the atmosphere. The average amount of emissions between 1993 and 1997 was estimated to be 4.2 GgCl/yr. In addition, we also calculated the amount of emissions to the atmosphere by converting primary energy consumption of oil and coal (Agency for Natural Resources and Energy (ed.) 2000) into weight, multiplying the result by the Cl content ratio (Okita 1982) to obtain the amount of HCl produced by full incineration, and taking into consideration the elimination efficiency at the time of refining and combustion (by applying the elimination efficiency of exhaust gas treatment systems). The average amount of emissions between 1993 and 1997 was 137.4 GgCl/yr for HCl originated in oil and 3.2 GgCl/yr for HCl originated in coal. As a result, the average amount of HCl emissions was estimated to be 144.7 GgCl/yr. Meanwhile, we calculated the average amount of deposition in each urban or non-urban district based on the amount of wet deposition and the amount of dry deposition of chloride ion (Cl^-) at 15 monitoring points in urban zones and 29 monitoring points (excluding 1 point where the value was extremely large) in non-urban zones between 1993 and 1997 obtained from a dataset of the third acid rain monitoring survey (Committee for Acid Rain Measures 2004). After that, we calculated the total domestic amount of Cl^- deposition by multiplying each average amount of deposition by the area of each urban or non-urban district. When calculating the amount of non-seasalt Cl^- deposition by the use of seawater composition, it is assumed that the total amount of sodium ion (Na^+) originates from seawater droplets (seasalt origin).

$$nss\text{Cl}_{dep} = \text{Cl}_{dep} - \text{Na}_{dep} \cdot SW(\text{Cl} / \text{Na}) \quad (2.3-5)$$

In this equation, $nss\text{Cl}_{dep}$, Cl_{dep} , and Na_{dep} are the amounts of deposition of non-seasalt Cl^- , Cl^- , and Na^+ , respectively. $SW(\text{Cl}/\text{Na})$ is the composition ratio of Cl^- to Na^+ in seawater. As a result of the calculation, the average domestic amount of deposition (total amount of dry deposition and wet deposition) between 1993 and 1997 was estimated to be 57.0 GgCl/yr. We divided the estimate by the amount of emissions and obtained 0.394 as the SRR of HCl.

With regard to NH_3 also, because there was little information on SRR, we calculated the average SRR in Japan as in the case of HCl.

According to an existing study (Kannari et al. 2001), we assumed that the amount of emissions in Japan was 430.1 GgN/yr, an estimate for 1994. We calculated the average amount of dry deposition in Japan based on the estimate between 1987 and 1989 at 15 monitoring points obtained from Fujita et al. (2000). Meanwhile, we calculated the average amount of dry deposition in each urban or non-urban zone based on the amount of dry deposition of ammonium ion (NH_4^+) in 1994 at 15 monitoring points in urban districts and 26 monitoring points (excluding 4 points where the value was extremely large) in non-urban districts obtained from a dataset of the third acid rain monitoring survey (Committee for Acid Rain Measures 2004). After that, we calculated the total domestic amount of NH_4^+ deposition by multiplying each average amount of deposition by the area of the respective urban or non-urban district. As a result of the calculation, the average domestic amount of deposition (total amount of dry deposition and wet deposition) was estimated to be 190.9 GgN/yr. We divided the estimate by the amount of emissions and obtained 0.444 as the SRR of NH_3 .

b Degree of neutralization in the atmosphere

Atmospheric acid substances are neutralized by coexisting basic substances. It is assumed herein that additionally emitted acid also is neutralized by the same degree as at present. The effective amount of acid load divided by the latent amount of acid load was defined as the non-neutralizing ratio. The effective amount of acid load was calculated by adding the amount of H^+ produced by nitrification of NH_4^+ to the amount of deposited H^+ . Because two moles of H^+ are produced from one mole of NH_4^+ through nitrification:

$$Acid_{eff} = H_{dep} + 2 NH_{4dep} \quad (2.3-6)$$

In this equation, $Acid_{eff}$ is the effective amount of acid load [eq]; and H_{dep} and NH_{4dep} are the observed amounts of atmospheric deposition of H^+ and NH_4^+ respectively (wet + dry) [eq]. Additionally, NH_4^+ contributes to the observed deposition of H^+ as a monovalent basic substance. If the production of H^+ as a result of nitrification of NH_4^+ (in this sense, a bivalent acid substance) is taken into account, NH_4^+ is regarded as a net monovalent acidifying substance (a monovalent base and a bivalent acid). Meanwhile, the latent amount of acid load indicates the total amount of an acidifying substance before neutralization - that is, the total amount of non-seasalt sulfate ion (SO_4^{2-}), nitrate ion (NO_3^-), non-seasalt Cl^- , and NH_4^+ . Non-seasalt substances are excluded, because a negative ion originated from sea salt has alkali metal or alkali earth metal as a counter ion and does not function as an acid. NO_3^- and NH_4^+ originated from sea salt are ignored because they are extremely scarce.

$$Acid_{ini} = nssCl_{dep} + NO_{3dep} + nssSO_{4dep} + NH_{4dep} \quad (2.3-7)$$

In this equation, $nssCl_{dep}$, NO_{3dep} , and $nssSO_{4dep}$ are the amounts of atmospheric deposition of non-seasalt Cl^- , NO_3^- , and non-seasalt SO_4^{2-} respectively. The amount of non-seasalt ion was calculated by the use of the ratio of Na^+ and the precursor ion in seawater as in the case of Equation 2.3-5.

The non-neutralizing rate (NNR) can be calculated by Equation 2.3-8.

$$NNR = Acid_{eff} / Acid_{ini} \quad (2.3-8)$$

In this equation, the average NNR in each urban or non-urban zone was calculated based on the amount of deposition between 1993 and 1997 at 15 monitoring points in urban zones and 30 monitoring zones in non-urban zones obtained from a dataset of the third acid rain monitoring survey (Committee for Acid Rain Measures 2004). We calculated the domestic average NNR by averaging the NNRs in the two zones, weighting the area of each zone. The result was 0.769.

c Atmospheric deposition factor

An increase in the amount of H^+ deposited due to the emission of 1 kg/yr of an acidifying causative substance [eq/km²/yr] was defined as the atmospheric deposition factor (ADF).

$$ADF(j) = SRR(j) \cdot MW(j)^{-1} \cdot VA(j) \cdot LA^{-1} \cdot NNR \cdot 10^3 \quad (2.3-9)$$

In this equation, j is each acidifying causative substance; MW and VA are the molecular

weight and acid valence of j respectively; and LA is land area [km^2].

Table 2.3-4: DAP, ADF, and parameters used for these calculations

Causative substance	Emission unit	Characterization factor			Parameter used for calculation				
		DAP	ADF	Zone	SRR	MW	VA	LA (km^2)	NNR
SO_2	$\text{kgSO}_2 / \text{yr}$	1.00	1.10 E-5	Av. in Japan	0.166	64.1	2	361,680	0.769
		0.34	3.79 E-6	Zone 1	0.009			53,838	
		1.04	1.15 E-5	Zone 2	0.011			23,083	
		1.57	1.73 E-5	Zone 3	0.056			78,001	
		1.64	1.80 E-5	Zone 4	0.055			73,445	
		0.72	7.93 E-6	Zone 5	0.019			56,341	
		0.46	5.10 E-6	Zone 6	0.016			76,973	
NOx	kgNO / yr	0.97	1.06 E-5	Av. in Japan	0.150	30.0	1	361,680	0.769
		0.50	5.48 E-6	Zone 1	0.012			53,838	
		0.94	1.04 E-5	Zone 2	0.009			23,083	
		1.23	1.42 E-5	Zone 3	0.043			78,001	
		1.87	2.06 E-5	Zone 4	0.059			73,445	
		0.72	7.94 E-6	Zone 5	0.017			56,341	
		0.29	3.20 E-6	Zone 6	0.010			76,973	
NO_2	$\text{kgNO}_2 / \text{yr}$	0.63	6.93 E-6	Av. in Japan	0.150	46.0	1	361,680	0.769
		0.32	3.57 E-6	Zone 1	0.012			53,838	
		0.62	6.78 E-6	Zone 2	0.009			23,083	
		0.84	9.25 E-6	Zone 3	0.043			78,001	
		1.22	1.34 E-5	Zone 4	0.059			73,445	
		0.47	5.18 E-6	Zone 5	0.017			56,341	
		0.19	2.09 E-6	Zone 6	0.010			76,973	
HCl	kgHCl / yr	2.02	2.23 E-5	Av. in Japan	0.394	36.5	1	372,798	
NH ₃	$\text{kgNH}_3 / \text{yr}$	4.89	5.38 E-5	Av. in Japan	0.444	17.0	1	372,798	

Zones 1 to 6 are six divisions in Japan used for the source-receptor matrix used for the calculation of source contribution of an acidifying causative substance (see Figure 2.4-7).

- DAP: Deposition-oriented acidification potential (the quotient of ADF of each substance to ADF of SO_2)
- ADF: Atmospheric deposition factor (see Equation 2.3-9)
- SRR: Source-receptor relationship (see Section 2.3.2)
- MW: Molecular weight
- VA: Valence in the case of functioning as acidifying substance
- LA: Land area (in the case of SO_2 and NO_x , estimated terrestrial areas included in grids to be calculated under Osaka Prefecture University's model; in the case of HCl and NH₃, statistical values in 1995)
- NNR: Non-neutralizing rate (see equations 2.3-6 to 2.3-8)

d Characterization factor for acidification (deposition-oriented acidification potential)

“Deposition-oriented acidification potential” (DAP) that took SRR into account can be obtained by dividing ADF of each acidifying causative substance by the average ADF of SO₂ in Japan. Under LIME, DAP was recommended as the characterization factor for acidification for the following reasons: 1) DAP took into account the SRR of each acidifying causative substance in Japan; 2) taking SRR into account enables assessment not on the side of emission but on the side of deposition; and 3) DAP covers four main substances that can become acidifying causative substances. Table 2.3-4 shows DAP, ADF, and parameters used for these calculations. DAP and ADF of HCl and NH₃ are larger than those of SO₂ and NOx, main causative substances for acidification, largely because the SRRs of HCl and NH₃ are high. With regard to NH₃ especially, because its molecular weight is light, the number of molecules is larger in relation to the emission of 1 kg. DAP is the characterization factor that has taken into account the processes between the emission of a causative substance and its deposition, but has not taken into account the sensitivity of the zone that undergoes deposition. However, the impact on the zone has been taken into account for the damage factor.

2.3.3 Damage assessment of acidification

(1) Basic policies for damage factor calculation and uncertainty assessment

LCA so far has mainly been based on the midpoint approach that uses AP (Heijungs et al. 1992) and other characterization factors for the impact assessment of acidification. However, because the midpoint approach cannot concretely calculate damage, under LIME we developed a method of assessing the impact of acidification by the use of the endpoint approach.

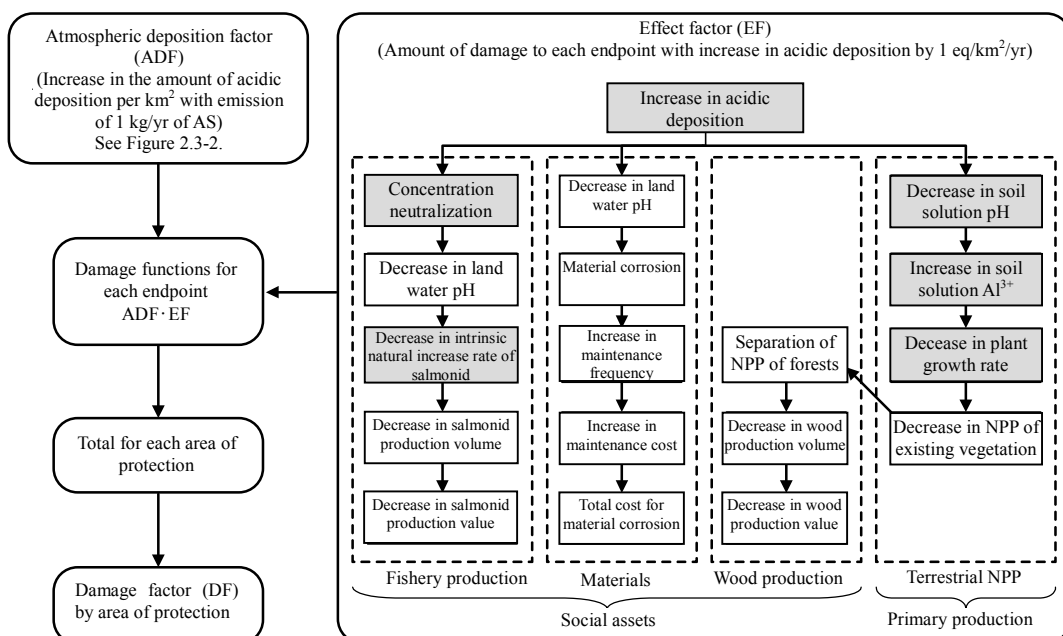
Under LIME, what quantitatively expresses the relation between inventories and the impact on each category endpoint is defined as a damage factor, and a set of damage functions in each area of protection is defined as a damage factor. Table 2.3-5 shows category endpoints for acidification and items used for the calculation of damage functions. The table covers almost all important category endpoints. In addition, Figure 2.3-4 shows the flowchart of calculation of damage functions and factors.

The damage function for acidification indicates how much the amount of latent damage increases with additional emission of a unit amount of an acidifying causative substance. For example, it indicates how much the production of forests latently decreases if 1 kg of SO₂ is emitted. As in the case of characterization, under LIME, we covered only zones of emission of acidifying causative substances, zones of acceptance of the impact, and Japan.

In addition, we extracted causes of uncertainty during the calculation of the damage functions for acidification and establish probability distributions mainly for the items predicted to be highly uncertain. Table 2.3-6 shows main causes of uncertainty in the damage functions for acidification and policies for dealing with them, and Table 2.3-7 shows details of the items for which probability distributions were established.

Table 2.3-5: Category endpoints for acidification and object of damage function calculation

Area of protection	Category endpoint		Object of damage function calculation	
Human health	While secondary impact of NO_3^- and Al^{3+} may occur via drinking water, primary impact is rare in Japan.		-	Not available
Social assets	Agri. production	Decrease in production of farm products, etc.	-	Hard for impact to occur in the current situation
	Wood production	Impact of decrease in primary production of trees	○	Net primary productivity (NPP) of forests
	Fishery production	Impact on freshwater fish with high acid sensitivity	○	Catch of salmonidae
	Material	Reduction in quality, reduction in durability, etc.	△	Maintenance cost
	Cultural assets	Loss of value, etc.	×	Hard to quantify impact
Primary production	Terrestrial ecosystem	Decrease in primary production of terrestrial plants	○	NPP of existing vegetation
Bio-diversity	Terrestrial ecosystem	Decrease in the number of terrestrial species, changes in species structure	×	Scarce qualitative information
	Aquatic ecosystem	Decrease in the number of aquatic species, changes in species structure	×	Scarce qualitative information
Other	Terrestrial ecosystem	Existing amount of terrestrial organisms	×	Scarce qualitative information
	Aquatic ecosystem	Existing amount of aquatic organisms	×	Scarce qualitative information

**Figure 2.3-4: Flowchart of calculation of acidification damage functions and factors**

The shaded items are those for which an uncertainty distribution has been established. Dotted lines encircle the items for which a variability distribution has been established.

Table 2.3-6: Policies for treating main causes of uncertainty in acidification damage functions

No	Endpoint	Main possible cause of uncertainty	Policy for uncertainty assessment
1	Common to acidification	Regional variations are not taken into account for the source-receptor relationship of SO ₂ and NO _x , and a uniform average is used all over Japan.	Adopt a probability distribution to selection of emission zones and use the source-receptor relationship by zone.
2		Based on a national average from actual data at two or more points, the amounts of wet and dry deposition of NH ₄ ⁺ were fixed.	Establish a probability distribution based on the amount of statistics on two or more sets of actual data.
3		Based on a national average from actual data at two or more points, the amounts of wet and dry deposition of Cl ⁻ were fixed.	Establish a probability distribution based on the amount of statistics on two or more sets of actual data.
4		Based on a national average from actual data at two or more points, the atmospheric non-neutralizing rate was fixed.	Establish a probability distribution based on the amount of statistics on two or more sets of actual data.
5	Primary production (Terrestrial primary ecosystem)	Each soil's pH was fixed based on the median of the soil pH dataset corresponding to FAO/UNESCO soil classification of ISRIC.	Establish a probability distribution together with data on the minimum and maximum values of soil pH entered in the dataset.
6		Uncertainty exists in the equations (approximate equation, linear function equation) of pH and Al ³⁺ concentration calculated based on actual values.	Establish a probability distribution concerning parameters for each approximate equation.
7		As a relation equation between Al ³⁺ concentration and the plant growth rate (quadratic function equation), the relation equation for red pine has been adopted to all kinds of vegetation.	The relation equations for cedar and Japanese cypress were newly added. Regarding the relation equations formulated for some types of trees, there were some cases where a probability distribution was established as to which equation to adopt.
8		Uncertainty exists in the equation (quadratic function equation) of Al ³⁺ concentration and the plant growth rate calculated based on actual values.	Conduct uncertainty assessment by use of the boot strap method concerning parameters for each approximate equation.
9	Social assets (Fishery production)	Uncertainty is included in preconditions for the calculation of an acid neutralization rate for each surface geological type in water catchment areas.	Because the uncertainty of this assumption is very high, this should be reflected in establishment of a probability distribution.
10		It is assumed that the decrease rate of frequency of female salmonid's digging due to decrease in pH is the same as the decrease in spawning rate.	Because no data are available on quantitative relation, uncertainty should be widely reflected in establishment of a probability distribution.
11		Uncertainty exists in the relation equation (log approximate equation) between pH and the intrinsic natural increase rates of various salmonidae calculated based on actual values.	Establish a probability distribution concerning parameters for each approximate equation.
12		Life history of salmonidae has been estimated based on existing materials.	If values entered in existing materials vary widely, establish a probability distribution based on them.

Table 2.3-7: Uncertainty of acidification, details of establishment of probability distribution

No	Item	Unit	Probability distribution	Value (Rep. value)	Parameter (standard deviate)	Parameter setting method
1	Source-receptor relationship of SO ₂ , NO _x	-	Custom distribution	-	-	From the result of atmospheric model prediction by Ikeda et al. (1997, 2001) and the result of estimation of natural SO ₂ emissions by Fujita et al. (1992)
2	Wet deposition of NH ₄ ⁺	eq/km ² /yr	Normal distribution	34.22 (Av.)	Standard deviation: 1.23	From the result of measurement of Fujita et al. (2000)
	Dry deposition of NH ₄ ⁺ (urban zones)	meq/m ² /yr		3.50 (Av.)	Standard deviation: 0.53	From dry deposition data of the Committee for Acid Rain Measures (2004)
	Wet deposition of NH ₄ ⁺ (non-urban zones)	meq/m ² /yr		2.49 (Av.)	Standard deviation: 0.60	
3	Dry and wet deposition of Cl ⁻ (urban districts)	meq/m ² /yr	Normal distribution	9.97 (Av.)	Standard deviation: 4.07	From dry deposition data of the Committee for Acid Rain Measures (2004)
	Dry and wet deposition of Cl ⁻ (non-urban districts)	meq/m ² /yr		4.03 (Av.)	Standard deviation: 1.54	
4	Atmospheric non-neutralizing rate (urban districts)	-	Normal distribution	0.636 (Av.)	Standard deviation: 0.03	From dry deposition data of the Committee for Acid Rain Measures (2004)
	Atmospheric non-neutralizing rate (non-urban districts)	-		0.778 (Av.)	Standard deviation: 0.02	
5	pH of each soil	-	Triangular distribution	- (Med.)	Max. likelihood value:- Max. value:- Min. value:-	From median, minimum, and maximum values of pH of each main soil entered in the soil pH dataset corresponding to the FAO/UNESCO soil classification of ISRIC
6	Relation equation between pH decrease and Al ³⁺ concentration	Power of μmol/L	t-distribution	- (Partial regression coefficient)	Standard:- Latitude:-	From measurement data on pH, eluted Al ³⁺ concentration, or exchangeable acidity of black humic soil, brown forest soil, red yellow soil, crystalline clay minerals, and podsol soil (So et al. 1999, Shioiri 1934, Kitagawa 1966, Yamatani 1968, Umemura 1968, Ministry of Agriculture, Forestry and Fisheries' Forestry Experiment Station, Maruyama 1995)
				- (Constant term)		
7	Relation equation between Al ³⁺ concentration and plant growth rate	-	Custom distribution	-	-	Adopt the relation equation for red pine to the vegetation classes other than "cedar and Japanese cypress." Adopt the ratio between the area of artificial cedar forests and the

						area of artificial Japanese cypress forests in each zone (Forest Agency) to “cedar and Japanese cypress.”
8	Relation equation between Al ³⁺ concentration and the plant growth rate	-	Boot strap method	-	-	Actual measurement data on Al ³⁺ concentration in soil solution and dry increment of red pine seedling (Ri et al. 1997) and actual measurement data on Ca concentration and Al concentration in soil solution and increment of cedar and Japanese cypress seedling (Kono et al. 1998)
9	Acid neutralization rate by surface geological type in water catchment areas	-	Triangular distribution	- (Representative value)	Max. likelihood value:- Max. value:1.0 Min. value:0.0	From measurement data on the amount of eluted base due to consumption of proton (Kozuki et al. 1997)
10	Relation equation between pH and decrease in the spawning rate of salmonid	-	Triangular distribution	- (Calculated value)	Max. likelihood value:- Max. value:1.0 Min. value:0.0	From measurement data on decrease in pH and frequency of female red salmon's digging of spawning beds (Ikuta et al. 2000)
11	Relation equation between pH and each salmonid type's intrinsic natural increase rate	-	t-distribution	- (Partial regression coefficient) - (Constant term)	Standard:- Latitude:-	From measurement data on median lethal time in relation to salmonid (Ikuta et al. 1992) (Rombough 1983)
12	Life history time of salmonid	hr	Uniform distribution	- (Intermediate value)	-	From data on each salmonid type's accumulated temperature and life history time (Miyaji et al. 1976, Masuda et al. 1984, Ochiai et al. 1986, Nagata et al. 1997, Japan Fisheries Resource Conservation Association 1981)

(2) Primary production: damage functions for terrestrial primary production

a Object of calculation of damage functions for terrestrial primary production

Acidic deposition is a phenomenon that occurs in all terrestrial areas, and vegetation covering the ground surface is an important receptive field.

Under LIME, we considered indirect impact on plant growth through soil acidification due to acidic deposition and calculated the damage function for terrestrial net primary productivity (NPP). Although the causes of indirect impact of acidification vary, we focused on the phytotoxicity of Al – that is, the impact of an increase in the concentration of inorganic aluminum ion (Al³⁺) due to soil acidification (for details of methodology, see Hayashi et al. (2004)).

Under LIME, to obtain the damage function for terrestrial primary production, we calculated

the effect factor (EF), which gives damage when the amount of H⁺ deposition increases by 1 eq/km²/yr, and multiplied the result by ADF obtained through calculation of the characterization factor – that is, an increase in the amount of H⁺ deposition per unit area when 1 kg/yr of an acidifying causative substance is emitted [eq/km²/yr]. The calculation of EF requires geographical information, such as vegetation distribution and climate conditions. Under LIME, we used geographical information on the second mesh system (10-km meshes; latitude 5' × longitude 7.5').

b Relation between acidic deposition and soil acidification

We assumed that the entire increase in the amount of H⁺ deposition as a result of additional emission of an acidifying causative substance contributes to soil acidification.

Q [mm/yr], the annual quantity of water that penetrates from soil vertically downward, is annual precipitation less the annual quantity of evaporation. Annual precipitation was calculated as that in each 10-km mesh by averaging the normal values between 1961 and 1990 by the use of the mesh climate values prepared by the third mesh system (1-km meshes; latitude 30' × longitude 45') (Japan Meteorological Agency 1996). Annual evaporation was estimated by the Thornthwaite method (edited by the Japan Institute of Construction Engineering, 1993). The monthly average temperature necessary for the Thornthwaite method was obtained from the mesh climate values (Japan Meteorological Agency 1996).

An increment in H⁺ concentration in soil solution can be calculated by dividing an increase in H⁺ deposition by Q .

$$[H^+]_{inc} = H_{add-dep} \cdot Q^{-1} \cdot 10^{-6} \quad (2.3-10)$$

In this equation, $H_{add-dep}$ is an increment in H⁺ deposition [eq/km²/yr], and $[H^+]_{inc}$ is an increment in H⁺ concentration in soil solution [eq/L].

Next, the main soil type for each 10-km mesh was selected based on a one-millionth soil map (Group of Japanese Pedologists, Committee for Soil Classification and Nomenclature 1990). We establish a probability distribution (triangular distribution) based on the minimum, maximum, and median values obtained from the soil pH dataset (Batjes 1995) corresponding to the legend of FAO-UNESCO World Soil Map (FAO-UNESCO 1990) as soil pH for each soil type. Assuming that soil pH is equal to soil solution pH, we calculated soil solution pH after an increase in H⁺ in soil solution.

$$pH_1(lea) = -\log (10^{-pH_0(lea)} + [H^+]_{inc}) \quad (2.3-11)$$

In this equation, pH_1 (lea) and pH_0 (lea) are soil solution pH after an increase in H⁺ concentration and early soil solution H⁺, respectively.

c Relation between soil acidification and inorganic aluminum ion concentration

Based on observed data from existing research cases (So et al. 1999; Shiori et al. 1934; Kitagawa 1966; Yamatani 1968; Umemura 1968; Ministry of Agriculture, Forestry and Fisheries' Forestry Experiment Station 1968; Maruyama 1995), for each soil type (podsol soil, brown forest soil, black humic soil, red yellow soil and others), we prepared an index

approximation equation (in the case of podsol soil, we used a primary expression, taking into account the excessive uncertainty of an index approximation equation) that gave inorganic Al^{3+} concentration in soil solution [$\mu\text{mol/L}$], using soil solution pH as the explanatory variable. With regard to parameters for the prepared equation, we established a probability distribution (*t*-distribution) based on the result of variance analysis of observed data. We carried out uncertainty analysis of a linear function equation, converting the y-axis of the basic index approximation equation into an index and the x-axis into pH (except in the case of podsol soil).

d Relation between inorganic aluminum ion concentration and plant growth

Based on the results of experiments on red pine, cedar, and Japanese cypress (Li et al. 1997; Kono et al. 1998), we examined the relation between inorganic Al^{3+} and the growth of trees in Japan. After that, we prepared a quadratic approximation equation that gives a dry growth rate, using Al^{3+} concentration as an explanatory variable. With regard to parameters for the prepared approximation equation, we established an uncertainty distribution by the boot strap method based on observed data.

e Net primary productivity for existing vegetation

We calculated the average NPP per 10-km mesh [kg/ha/yr] as follows (see Section 2.10):

We extracted examples of existing vegetation in units of 100-m mesh (100 m × 100 m) from Natural Environment Information GIS (Ministry of the Environment 1999). After that, we rearranged vegetation information on about 900 examples into 30 examples where NPP was calculated concerning main vegetation and land use (Iwaki 1981). However, examples of 100-m meshes that fall under building sites or highways in the Dataset of Numerical Information on National Land Use (Ministry of Land, Infrastructure, Transport and Tourism 2002) are included in “Other.”

In the vegetation information, both cedar forests and Japanese cypress forests are included in the division “Cedar and Japanese cypress forests,” but are not subdivided further. On the other hand, a relation equation between inorganic Al^{3+} concentration and the growth of trees in Japan exist for both cedar and Japanese cypress. Because of this, with regard to which equation to adopt, herein a probability distribution (custom distribution Figure 2.3-5) was established for each of zones 1 to 6 based on the Forest Agency’s data by type of tree and by age group, using the meshes of “cedar and Japanese cypress forests.”

Because the NPP values of 30 examples offered by Iwaki (1981) were fixed values, we revised them to reflect climate differences. Using a dataset of the normalized difference vegetation index (NDVI) obtained through satellite observation (Center for Global Environmental Research 2000), we calculated an average of the NDVI values of all the relevant 100-m meshes by type of example. In addition, we corrected the NPPs by multiplying the fixed NPPs by a correction coefficient – that is, the ratio between the NDVI value of each 100-m mesh and the average NDVI value of the relevant examples.

It was assumed that the average of the corrected NPP values of all the 100-m meshes within a 10-km mesh was the average NPP of the mesh [kg/ha/yr].

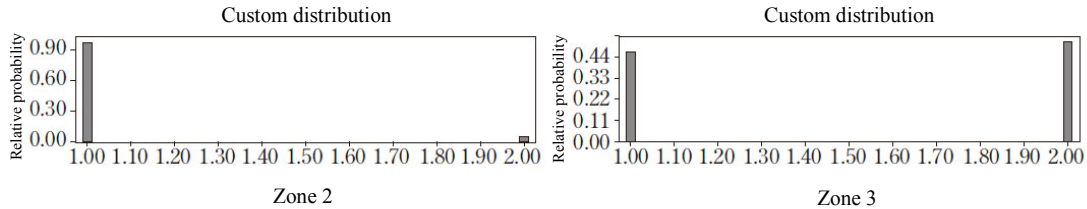


**Figure 2.3-5: Probability distribution for selection of a relation equation concerning growth of trees in the division “cedar and Japanese cypress forests” by zone
(examples: Zone 2 at left, Zone 3 at right)**

If [1] is selected, use the relation equation for cedar forests; if [2] is selected, use the relation equation for Japanese cypress forests.

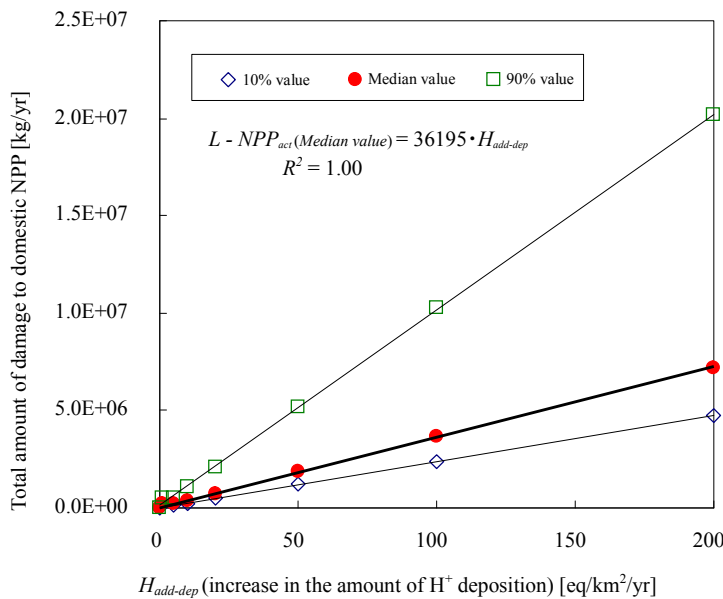


Figure 2.3-6: Relation between an increase in the amount of H⁺ ion deposition and an increase in the total amount of damage to domestic NPP

f Damage function for terrestrial primary production

The amount of damage to NPP in each 10-km mesh can be calculated by Equation 2.3-12:

$$L-NPP_{act} = NPP_{act} \cdot A (GR_0 - GR_1) / GR_0 \quad (2.3-12)$$

In this equation, $L-NPP_{act}$ is the amount of damage to NPP in a 10-km mesh [kg/yr]; NPP_{act} is the average NPP in a 10-km mesh [kg/ha/yr]; A is the area of a 10-km mesh [ha]; GR_0 is the early growth rate [%]; and GR_1 is the growth rate [%] after additional emission of an acidifying causative substance.

The total amount of damage to all the 10-km meshes in Japan indicates the total amount of damage in Japan.

$$L-NPP_{act}(tot) = \sum_i^n L-NPP_{act}(i) \quad (2.3-13)$$

In this equation, $L-NPP_{act}(tot)$ and $L-NPP_{act}(i)$ are the amount of damage to NPP [kg/yr] in Japan and the amount of damage to NPP [kg/yr] in the i th 10-km mesh, respectively.

In this equation, assuming that the acidifying causative substance has been averagely deposited all over Japan, we calculated $L-NPP_{act} (tot)$ in the case where the average amount of deposition $H_{add-dep}$ was changed from 0 to 200 eq/km²/yr. It is assumed herein that the slope of the resultant median value, 36195, is the EF of the terrestrial primary production. However, because the calculation of the damage function and factors is based on uncertainty analysis of zones where the acidifying causative substance is emitted, the damage function is not the same as the product of ADF and EF as described above.

Table 2.3-8 shows statistical amounts obtained from the calculation of the acidification damage function for terrestrial primary production accompanied by uncertainty assessment, and Figure 2.3-7 shows the probability density distribution of the damage function for SO₂ as an example. In addition, Table 2.3-9 shows the rank correlation coefficients of the acidification damage function for terrestrial primary production, and Figure 2.3-8 shows the result of comparison between LIME1 and LIME2 concerning the damage function.

Table 2.3-8: Statistical amounts of acidification damage functions for terrestrial primary production

Division	SO ₂	NO	NO ₂	HCl	NH ₃
Unit	kgDW/kg	kgDW/kg	kgDW/kg	kgDW/kg	kgDW/kg
No. of trials	50,000	50,000	50,000	50,000	50,000
Average value	0.417	0.481	0.314	1.267	3.120
Median value	0.301	0.365	0.238	0.853	2.091
Standard deviation	0.565	0.578	0.377	1.534	3.442
Dispersion	0.320	0.334	0.142	2.355	11.846
Kurtosis	143.443	198.269	198.228	49.797	45.791
Variation coefficient	1.355	1.202	1.202	1.211	1.103
10 percentile value	0.134	0.149	0.097	0.409	1.344
90 percentile value	0.674	0.810	0.529	2.329	5.707
Average standard error	0.003	0.003	0.002	0.007	0.015

Table 2.3-9: Rank correlation coefficients of acidification damage function for terrestrial primary production (example: SO₂)

Coefficient	Correlation coefficient
Linear coefficient of relation equation between pH and Al ³⁺ (podsol soil)	- 0.28
Relation equation between Al ³⁺ concentration and plant grown rate (red pine)	0.28
Soil pH (typical podzolic soil)	0.26
Zone of SO ₂ emissions	0.26
Soil pH (typical gley soil)	0.19
Soil pH (typical gray paddy field soil)	0.09
Relation equation between Al ³⁺ concentration of “cedar and Japanese cypress forests” and plant growth rate in Zone 3	0.08
Linear coefficient of relation equation between pH and Al ³⁺ concentration (gley soil)	0.06
Relation equation between Al ³⁺ concentration and plant growth rate (cedar)	0.05

- Variable numbers with a coefficient of correlation value of 0.05 or more were extracted.

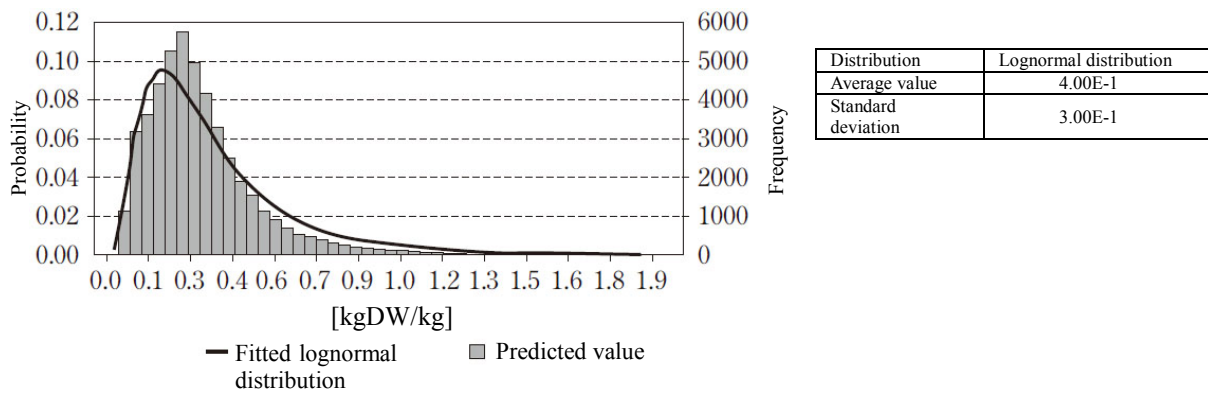


Figure 2.3-7: Probability density distribution of acidification damage functions for terrestrial primary production (example: SO2)

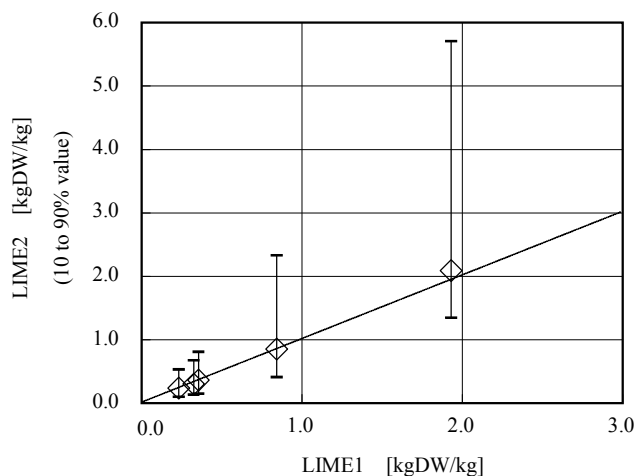


Figure 2.3-8: Comparison between LIME1 and LIME2 (acidification (terrestrial primary production))

Column 2.3-1

Method to assess the impact of soil acidification on plant growth

With progress in soil acidification, base cation (BC) – especially, potassium ion (K^+), magnesium ion (Mg^{2+}), and calcium ion (Ca^{2+}) – decreases and facilitates a decline in trees, while Al and heavy metals become soluble. Al hinders the growth of plant roots and reduces their efficiency in absorption of Ca and other nutrients, causing harmful effects.

Under LIME, based on data on the growth of red pine, cedar, and Japanese cypress actually measures by Li et al. (1997) and Kono et al. (1998), a quadratic approximation equation was formulated by the use of Al^{3+} as the explanatory variable and the growth rate of trees as the dependent variable to assess the impact of soil acidification on plant growth.

Meanwhile, because, as described above, plant growth is influenced by heavy metal concentration and BC concentration in soil solution, recently the ratio between BC concentration and Al^{3+} concentration in soil solution has been frequently used as the index of the impact of acidification on plants. Sverdrup and Warfvinge (1993) used existing materials for arranging differences in plant growth rate according to the pH change and

concentration change of Ca, Mg, K, and Al in soil solution, and proposed “(Ca + Mg + K) / Al ratio (converted into moles)” as the most suitable impact index for vegetation. Based on this index and the actually measured growth rate, they created a model of calculation of the critical load of acidic deposition to the growth of each type of tree (Figure 2.3-A) and, with regard to some types of trees, proposed the relation equation between leaf loss rate and trunk growth rate and the relation equation between root growth rate and plant survival rate. In Japan also, the Committee for Acid Rain Measures (2004) presented “the ratio of Ex-BC (total of exchangeable Ca, Mg, and K) and Al (exchangeable Al)” as the index of soil acidification. Hayashi et al. (2003) have developed a screening method for zones where soil acidification due to acidic deposition may cause forest decline. This method also has adopted the assessment index “(K + Mg + Ca) / Al ratio.”

Although their use as indices requires information on BC concentration in soil solution, data for analysis of constituents of soil solution are not sufficient to cover every type of soil. In addition, because the geographical fluctuation of BC concentration in soil solution is large, BC concentration is highly likely to fluctuate greatly even by a slight difference in location. Because of this, there are many problems concerning the application of LIME and other LCIA models that cover all of Japan.

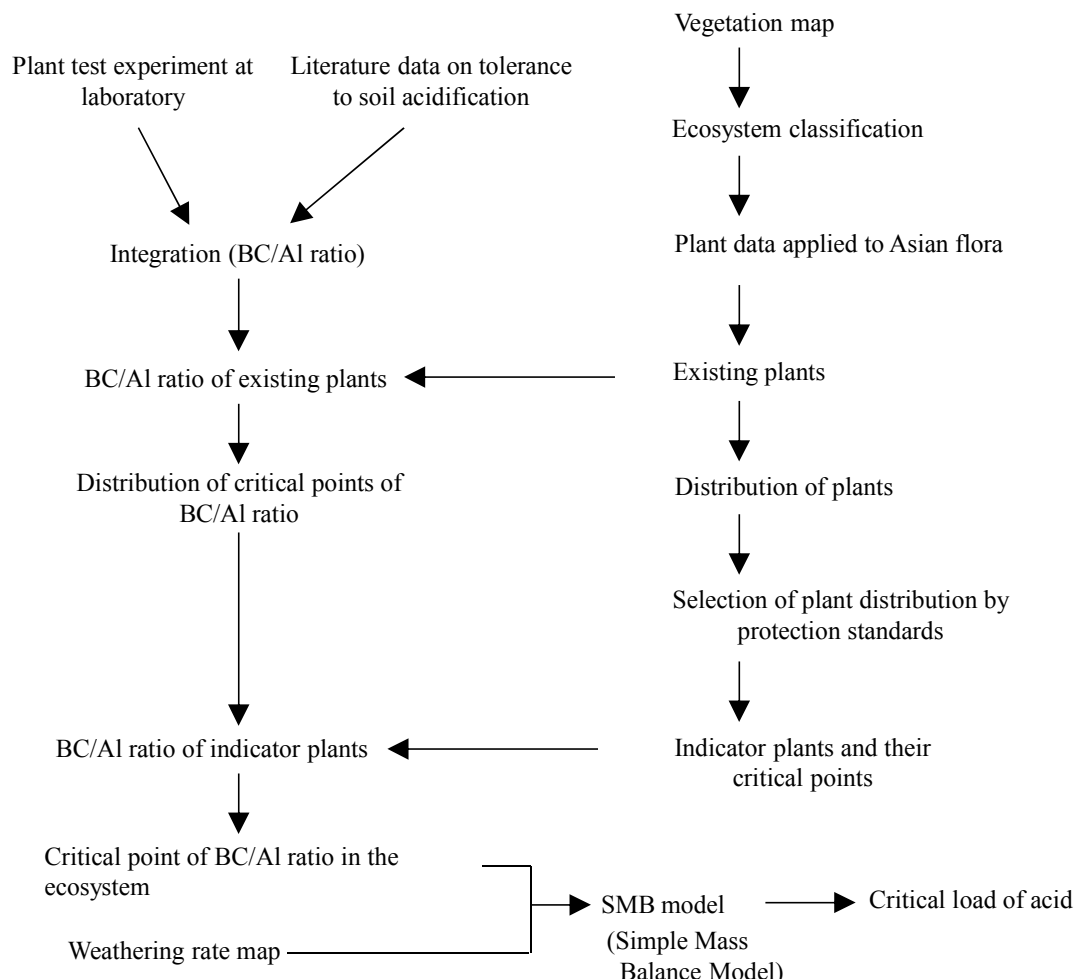


Figure 2.3-A: Flowchart of calculation of critical load of acidified soil on plant growth (Sverdrup et al. 1993)

The critical point of the BC/Al ratio is a value when the plant growth rate becomes 80% during an experiment.

(3) Social assets: damage function for fishery production

a Object of calculation of damage function for fishery production

With progress in terrestrial acidification, land water may be acidified in areas that serve as water catchment areas. In North Europe and North America, a problem arose about the disappearance of fishes due to acidification of lakes and marshes. Acidification of land water has impact on all the organism species constituting the terrestrial ecosystem. However, because tolerability for acid and Al differs among the organism species, it is difficult to quantify the impact on the whole ecosystem.

Meanwhile, some organisms constituting the terrestrial ecosystem have important values as food for human beings. Among of them, salmonidae are valuable as aquatic resources, spend the time from egg to juvenile (or adult) in rivers, lakes, or marshes so oligotrophic as to be relatively susceptible to the impact of the load of acidifying substances, and are known to be highly sensitive to acid.

Under LIME, a damage function of acidification for salmonidae production was calculated from the aspect of social assets. This can be said to indirectly take into account the impact of acidification on the terrestrial ecosystem. The salmonidae covered by LIME are white-spotted char (including char), dolly varden, chum salmon (so-called salmon), pink salmon, cherry salmon (including seema; broadly including red-spotted trout), and sockeye salmon (including kokanee). The basic unit of geographical distribution necessary for the calculation of damage function is 10-km mesh as in the case of the terrestrial ecosystem.

b Relation between acidic deposition and land water pH

Because soil percolation water is fully neutralized until leaching into land water, the pH of river water in Japan usually exceeds 7. Therefore, if the amount of acidic deposition increases a little, land water pH will hardly change. Herein, however, thinking that a part of H⁺ whose amount of deposition has increased due to additional emission leaches into rivers, it is assumed that the degree of neutralization depends on the nature of surface soil in the zone in question.

The legend of the Geological Map of Japan (Geological Survey of Japan (ed.) 1995) was reclassified into seven classes in order of latent acid neutralization capacity: 1) ultramafic rock; 2) mafic rock; 3) limestone; 4) basalt; 5) felsic rock; 6) debris/cherst; and 7) sedimentary rock (Okazaki). With regard to the neutralization rate for each class, by reference to experimental calculation of soil's H⁺ consumption by base material (Kozuki et al. 1997), a triangular probability distribution was formulated with a minimum value of 0%, a maximum value of 100%, and an apex of 1) 95%, 2) 65%, 3) 45%, 4) 30%, 5) 20%, 6) 15%, and 7) 5%. The non-neutralizing rate NR of river leachate was calculated by subtracting 1 from the neutralizing rate.

It is assumed that the quantity of river leachate is the same as the quantity of percolation water Q and that the baseline leachate pH is the same as river pH. The annual average at the river pH monitoring points was extracted from the Public Water Quality Monitoring Data in 1997 (Environment Agency (supervised) 1998). If two or more monitoring points exist within a 10-km mesh, the arithmetic average is used as the river pH in the mesh. If there is no monitoring point in a 10-km mesh, the average in the first mesh (40' latitude, 1' longitude) is

used as the river pH in the mesh.

The river pH after an increase in acidic deposition can be calculated by Equation 2.3-14.

$$pH_1(river) = -\log (10^{-pH_0(river)} + NR [H^+]_{inc}) \quad (2.3-14)$$

In this equation, $pH_1(river)$ and $pH_0(river)$ are the river pH after additional emission of an acidifying causative substance and the baseline river pH, respectively. $[H^+]_{inc}$ is an increment on H^+ concentration after additional emission of the acidifying causative substance (Equation 2.3-10).

c Relation between a decrease in pH and the cumulative mortality rate and reproduction rate of salmonidae

Female sockeye salmon's digging a spawning bed is remarkably controlled by a decrease in pH (Ikuta et al. 2000). On the assumption that a decrease in the frequency of digging a spawning bed directly indicates a decrease in the spawning rate, the relation between pH and the frequency of digging was standardized through approximation by a logistic curve and division by the maximum value, and a regression equation for the calculation of a spawning rate ($NestR$, 0 - 1) was formulated by the use of river pH (pH_{river}) as the explanatory variable. Moreover, for the purpose of uncertainty assessment, a triangular probability distribution was formulated with an apex of the calculated $NestR$, a minimum value of 0, and a maximum value of 1.

$$NestR = \frac{1}{1 + 1.794 \cdot 10^{21} \exp(-7.503 pH_{river})} \quad (2.3-15)$$

During the life history of salmonidae, their sensitivity to acid becomes especially high in the period between hatched fry and surfacing fry – that is, the period between hatching and beginning to go down a river (Ikuta et al. 1992). Under LIME, a damage function was formulated with consideration for each of the life history stages: egg, hatched fry, surfacing fry, and young fish (land water). By the use of results of observation of pH to salmonidae and the median lethal time (T_{50} : hr) (Ikuta et al. 1992, Rombough 1983), an index approximation equation for the calculation of a cumulative mortality rate was formulated by the use of pH as the explanatory variable at each stage of life history. Moreover, for the purpose of uncertainty assessment, with regard to the parameters for the formulated equation, a probability distribution (t-distribution) was formulated based on the result of dispersion analysis of observed data.

$$MR = 1 - \exp(-\ln 2 \cdot t / T_{50}) \quad (2.3-16)$$

In this equation, MR and t are a cumulative mortality rate (0 - 1) during a life history and the number of hours passed from the beginning of the life history [hr], respectively.

d Estimation of spawning areas and life history time of salmonidae

The damage function is calculated for a 10-km mesh where salmonidae live. However, it is difficult to estimate spawning areas themselves. In addition, there is another problem: although salmonidae exist near spawning beds from the egg stage to the hatched fry stage,

they spread downstream after surfacing (that is, they move beyond a mesh). Because it is extremely difficult to estimate them strictly, the existence of spawning in each 10-km mesh was estimated by the use of water temperature as an index, but without consideration for diffusion after surfacing.

By reference to information on the distribution areas and spawning period of each type of salmonid (Miyaji et al. 1976; Masuda et al. 1984; Ochiai et al. 1986; Japan Fisheries Resource Conservation Association 1981; Sapporo Salmon Museum), the existence of spawning in each 10-km mesh was estimated from the geographical position of the mesh and the daily average temperature and water temperature during the spawning period. The daily average temperature was calculated by creating a temperature model where a cosine function was applied to the normal monthly average temperature of the Mesh Climate Value (Japan Meteorological Agency 1996). The daily average temperature was calculated by creating a model for the calculation of water temperature fluctuation by multiplying the temperature fluctuation fixed through the temperature model by the ratio of difference in the monthly average water temperature (maximum water temperature – minimum water temperature) to the monthly average temperature by the use of a case where the annual average water temperature was expressed as an annual average temperature function (Kitano et al. 1995). After that, with regard to each of the 10-km meshes judged as spawning areas, the time of each life history was calculated by deducting the estimated time of each life history obtained from existing materials (Miyaji et al. 1976; Masuda et al. 1984; Ochiai et al. 1986; Nagata et al. 1997; Japan Fisheries Resource Conservation Association 1981) by the above-described model for the calculation of daily average water temperature.

Moreover, for the purpose of uncertainty assessment, with regard to the ratio of difference in the monthly average water temperature to the monthly average temperature and the estimated time of each life history, a probability distribution (normal distribution) was formulated based on the obtained annual average temperature data, if possible.

e Changes in intrinsic natural increase rate due to changes in the cumulative mortality rate and reproduction rate of salmonidae

Given the whole population, TI_{pH} (0 - 1), the total impact of pH on avoidance of spawning and an increase in the mortality rate during the period between the egg stage and the young fish stage can be expressed by the product of impact at each stage. If the impact on the spawning rate is expressed by the spawning avoidance rate $NAR = 1 - NestR$ to indicate the total impact:

$$TI_{pH} = 1 - \prod_{i=0}^4 a_i = 1 - (1 - NAR) (1 - MR_0) \quad (2.3-17)$$

In this equation, a_0 , a_1 , a_2 , a_3 , and a_4 are the spawning rate of adult fish ($= 1 - NAR$), the egg survival rate, the fry survival rate, the surfacing fry survival rate, and young fish survival rate, respectively.

The intrinsic natural increase rate r refers to the population increase rate per unit time and is a function for the increase potential P (the average number of descendants that a new individual leaves during its lifetime). The estimation of the amount of damage requires a decrease in r – that is, the difference in r before and after an increase in the amount of H^+ deposition. It is known that r can be approximated by P (Tanaka et al. 1998).

$$r = \ln P / \bar{T} \quad (2.3-18)$$

In this equation, \bar{T} is the average generation time expressed by Equation 2.3-19.

$$\bar{T} = \sum_{t=0}^{\infty} t \cdot l_t \cdot m_t \Bigg/ \sum_{t=0}^{\infty} l_t \cdot m_t \quad (2.3-19)$$

In this equation, l_t is the survival rate at the age of t , and m_t is the number of eggs laid at the age of t . The average generation time (weighted average of age that weights the product of the survival rate of egg-laying females and the number of laid eggs) of each type of salmonid was estimated by reference to existing materials (Miyaji et al. 1976; Masuda et al. 1984; Ochiai et al. 1986; Nagata et al. 1997; Japan Fisheries Resource Conservation Association 1981).

If the baseline pH is pH_0 , and the pH after additional emission of an acidifying causative substance is pH_1 , the impact on r , r_{damage} can be expressed by Equation 2.3-20.

$$r_{damage} = r_{pH_0} - r_{pH_1} = \ln \left\{ (1 - TI_{pH_0}) / (1 - TI_{pH_1}) \right\} / \bar{T} \quad (2.3-20)$$

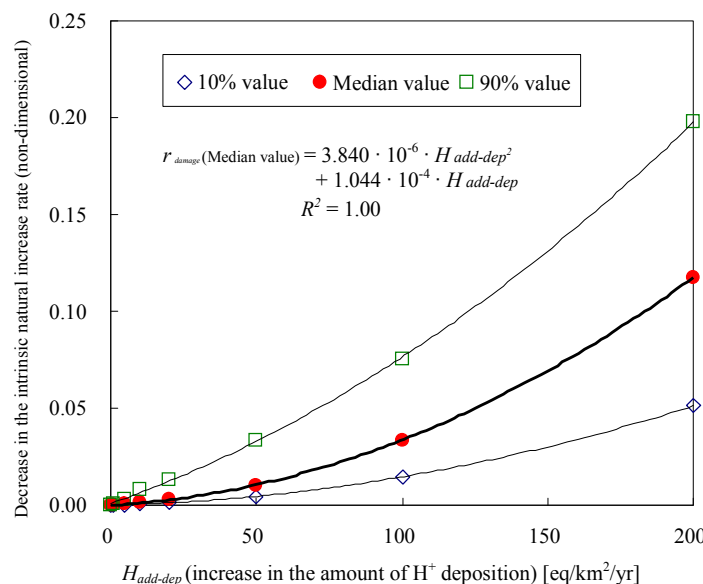


Figure 2.3-9: Relation between an increase in the amount of H⁺ deposition and the impact on the intrinsic natural increase rate of salmonid (example: chum salmon)

f Estimation of catch of salmonidae

Although grasping the current amount is ideal for assessing the impact on fishery resources, it is extremely difficult to estimate the current amount. Therefore, the catch (weight and monetary amount) of salmonidae was grasped based on the Fisheries Statistics (Statistics and Information Department of Ministry of Agriculture, Forestry and Fisheries).

g Damage function for fishery production

With regard to each type of salmonid, EF of fishery production in each 10-km mesh can be calculated by Equation 2.3-14 to Equation 2.3-20. The total amount of damage to fishery production can be obtained by calculating r_{damage} in each 10-km mesh in areas where salmon lay eggs, averaging the r_{damage} by weighting the area of each terrestrial area, and multiplying the result by the catch in Japan.

On the assumption that an acidifying causative substance averagely deposits all over Japan, r_{damage} per 10-km mesh concerning each type of salmonid was calculated in the case of a change in the average deposition $H_{add-dep}$ from 0 to 200 eq/km²/yr, and a weighted average was calculated by weighting the area. After that, a quadratic approximation equation was prepared by plotting the average value of r_{damage} corresponding to $H_{add-dep}$ (Figure 2.3-9), and the approximation equation was multiplied by the catch to obtain the EF of fishery production. However, because the calculation of damage functions and factors are based on uncertainty analysis, it is necessary to note that it is not the same as the product of ADF and EF as described above.

Table 2.3-10 shows statistical amounts obtained from the calculation of the acidification damage functions for fishery production accompanied by uncertainty assessment, and Figure 2.3-10 shows the probability density distribution of the damage functions for SO₂. In addition, Table 2.3-11 shows the rank correlation coefficients of the acidification damage functions for fishery production, while Figure 2.3-11 shows the result of comparison with LIME1 concerning damage function values.

Table 2.3-10: Statistical amounts of acidification damage functions for fishery production

Division	SO ₂	NO	NO ₂	HCl	NH ₃
Unit	Yen/kg	Yen/kg	Yen/kg	Yen/kg	Yen/kg
No. of trials	5,000	5,000	5,000	5,000	5,000
Average value	234.3	288.2	188.8	562.5	1,359.9
Median value	97.9	121.2	77.6	212.9	520.4
Standard deviation	679.1	651.9	529.0	1,365.1	3,784.8
Dispersion	461,226.6	425,006.9	279,803.8	2,673,497	14,324,720
Skewness	23.8	8.6	15.8	16.3	17.7
Kurtosis	1,017.8	128.6	398.4	407.9	532.8
Variation coefficient	2.9	2.3	2.8	2.9	2.8
10 percentile value	13.6	27.8	17.6	74.1	240.2
90 percentile value	447.4	607.5	368.5	1,085.8	2,609.3
Average standard error	9.6	9.2	7.5	23.1	53.53

- With regard to the calculation of damage functions for fishery production, because of the complicatedness of the model, the number of trials is fixed at 10,000 for the purpose of uncertainty assessment.
- In this table, damage functions are calculated by dividing the amount of damage from the emission of 1,000 kg of each acidifying substance by 1,000.

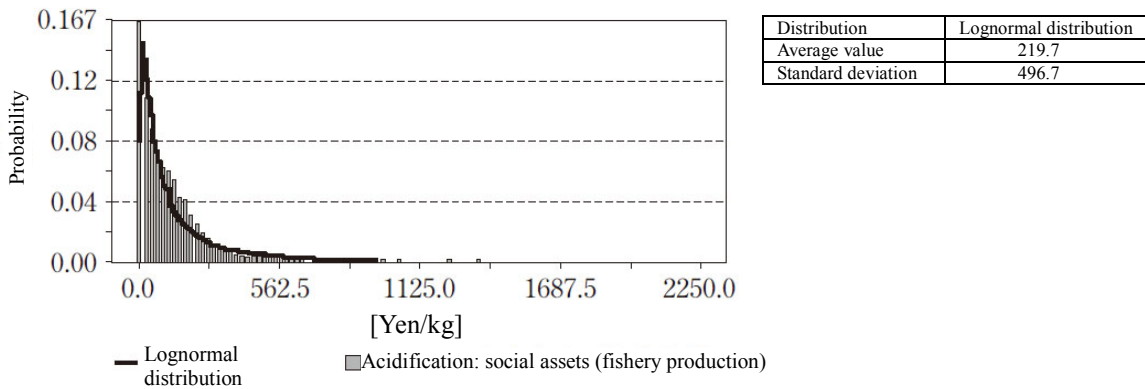


Figure 2.3-10: Probability density distribution of acidification damage functions for fishery production (example: SO₂)

Table 2.3-11: Rank correlation coefficients of acidification damage factors for fishery production (example: SO₂)

Coefficient	Correlation coefficient
SO ₂ emission zone	0.69
Linear coefficient of relation equation between pH and inner natural increase rate of salmonidae (salmon; hatch stage; when pH is high)	0.32
Linear coefficient of relation equation between pH and inner natural increase rate of salmonidae (salmon; surfacing stage)	0.19
Acid neutralization rate by type of surface soil in water catchment area (sedimentary rock)	-0.18
Acid neutralization rate by type of surface soil in water catchment area (felsite)	-0.06
pH – female salmonid's spawning rate (a mesh)	0.06
pH – female salmonid's spawning rate (a mesh)	0.06
pH – female salmonid's spawning rate (a mesh)	0.05
pH – female salmonid's spawning rate (a mesh)	0.05

Variables with a correlation coefficient of 0.05 or more are extracted.

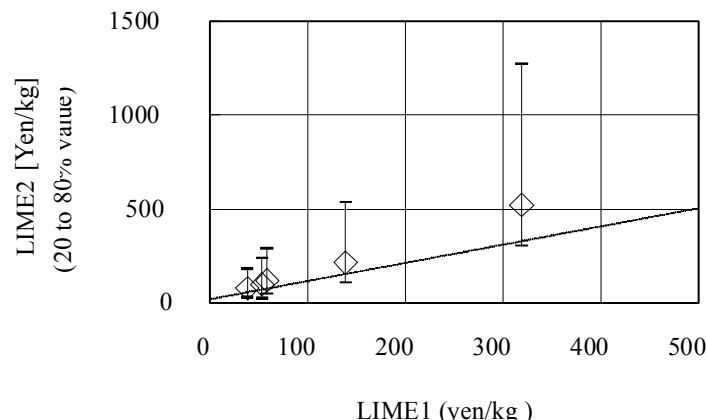


Figure 2.3-11: Comparison between LIME1 and LIME2 (acidification (fishery production))

(4) Social assets: damage functions for wood production

Acid damage to primary production of the terrestrial ecosystem is also damage to social assets, because it causes a decrease in the amount of resources as wood. Based on an NPP dataset on the existing vegetation in a 10-km mesh prepared in the section on the terrestrial ecosystem, the total NPP value of the part of legend corresponding to forests and the total NPP value of the whole legend, and the EF of the terrestrial ecosystem was multiplied by 0.715, the ratio between the two NPP values, to obtain the EF of the forest NPP. It was assumed that the forest NPP can be divided into trunks and branches and that damage to the forest NPP indicates damage to wood production. On this assumption, the EF of the forest NPP was multiplied by the average wood density of 500 kg/m³ and the wood producer's unit price (Statistics and Information Department of Ministry of Agriculture, Forestry and Fisheries 2001) [yen/m³] to obtain the EF of wood production.

Table 2.3-12 shows the statistical amounts obtained from the calculation of acid damage functions for wood production accompanied by uncertainty assessment. The probability density distribution, rank correlation coefficients, and other factors related to damage functions were omitted because their forms, variants, etc. are the same as those for terrestrial primary production.

**Table 2.3-12: Statistical amounts of acidification damage functions for wood production
(example: SO₂)**

Division	SO ₂	NO	NO ₂	HCl	NH ₃
Unit	Yen/kg	Yen/kg	Yen/kg	Yen/kg	Yen/kg
No. of trials	5,000	5,000	5,000	5,000	5,000
Average value	9.84	11.35	7.30	29.15	70.67
Median value	7.08	8.62	5.55	19.76	48.17
Standard deviation	14.88	13.32	8.15	34.20	72.05
Dispersion	221.50	177.33	66.36	1,169.66	5,191.20
Skewness	14.94	8.71	7.91	5.48	4.36
Kurtosis	419.59	124.50	123.32	54.06	28.94
Variation coefficient	1.51	1.17	1.12	1.17	1.02
10 percentile value	3.16	3.46	2.28	9.52	31.29
90 percentile value	15.90	19.13	12.23	54.08	131.82
Average standard error	0.21	0.19	0.12	0.48	1.02

(5) Social assets: damage functions for materials

Of the materials used for buildings and other structures, some types of metals and stones are susceptible to the impact of acidification. LIME used the dose-response function (ICP 2001) obtained from the Europe International Co-operative Programme (ICP). This function is used for calculating the amount of corrosion of materials due to the impact of the dry deposition of SO₂ and the wet deposition of H⁺.

Under LIME, only the impact of wet deposition was considered. On the assumption that the dry deposition item of the dose-response function (ICP 2001) does not change before and after an increase in the amount of H⁺ deposition, an increase in the degree of corrosion of

each material due to an increase in the amount of H⁺ deposition was replaced with a function of the amount of H⁺ deposition and a function of time. With regard to time, based on the thinking that maintenance would be required when corrosion progresses to some extent (metal: 50 µm; stone; 4 mm), the wet deposition item of the dose-response function was transformed to the time when maintenance would be required. The time was multiplied by the repair cost (metal: 3,000 yen/m²; stone; 30,000 yen/m²) to obtain an equation for the calculation of the annual repair cost per unit area. However, because it was extremely difficult to estimate the exposed area of materials in Japan, it was impossible to calculate the EF and damage function of materials. Under LIME, no consideration was given to materials as cultural assets.

(6) Damage factors for acidification

The damage functions obtained at each endpoint were added up for each area of protection (social assets and primary production), and the total was used as the damage factor for acidification for each area of protection. That is, the total of damage functions for fishery production and wood production is the damage factor for social assets, and the damage function for the terrestrial NPP is the damage factor for primary production as it is.

Table 2.3-13 shows the statistical amounts obtained from the calculation of the acidification damage factor for social assets, accompanied by uncertainty assessment. Figure 2.3-12 shows the probability density distribution of the damage factor of SO₂ as an example. Table 2.3-14 shows the rank correlation coefficients of acidification damage factors for social assets. Figure 2.3-13 shows the result of comparison with LIME1 concerning the damage factor. In addition, the damage factors for primary production are as shown in Table 2.3-8, Figure 2.3-7, Table 2.3-9, and Figure 2.3-8.

Table 2.3-15 shows the damage factor for each area of protection. Uncertainty assessment was conducted for both social assets and primary production, and the median value of the statistical amounts was used as the representative value.

Table 2.3-13: Statistical amounts of acidification damage factors for social assets

Division	SO ₂	NO	NO ₂	HCl	NH ₃
Unit	Yen/kg	Yen /kg	Yen /kg	Yen /kg	Yen /kg
No. of trials	5,000	5,000	5,000	5,000	5,000
Average value	244.2	299.6	188.8	591.6	1,430.6
Median value	108.5	134.4	77.6	243.7	602.8
Standard deviation	679.2	652.4	529.0	1,636.9	3,785.2
Dispersion	461276.3	425,580.4	279,803.8	2,679,345	14,327,548
Skewness	23.8	8.6	15.8	16.2	17.7
Kurtosis	1,017.1	128.2	398.4	405.9	532.4
Variation coefficient	2.78	2.18	2.80	2.77	2.65
10 percentile value	22.9	35.8	17.6	93.1	299.3
90 percentile value	457.7	617.2	368.5	1,124.4	2,706.9
Average standard error	9.6	9.2	7.5	23.1	53.5

- With regard to the calculation of the damage function for social assets, because of the complicated nature of the model, the number of trials is fixed at 10,000 for the purpose of uncertainty assessment.
- In this table, the damage factor was calculated by dividing the amount of damage from the emission of 1,000 kg of each acidifying substance by 1,000.

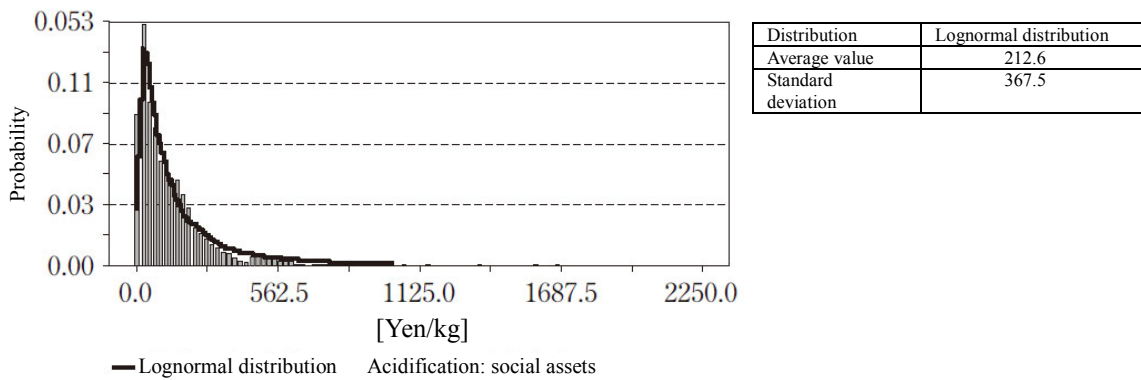


Figure 2.3-12: Probability density distribution of acidification damage factors for social assets (example: SO₂)

Table 2.3-14: Rank correlation coefficients of acidification damage function for social assets (example: SO₂)

Coefficient	Correlation coefficient
SO ₂ emission zone	0.67
Linear coefficient of relation equation between pH and inner natural increase rate of salmonidae (salmon; hatch stage; when pH is high)	0.32
Linear coefficient of relation equation between pH and inner natural increase rate of salmonidae (salmon; surfacing stage)	0.19
Acid neutralization rate by type of surface soil in water catchment area (sedimentary rock)	-0.18
Acid neutralization rate by type of surface soil in water catchment area (felsite)	-0.06
pH – female salmonid's spawning rate (a mesh)	0.06
pH – female salmonid's spawning rate (a mesh)	0.05
pH – female salmonid's spawning rate (a mesh)	0.05
pH – female salmonid's spawning rate (a mesh)	0.05

Variables with a correlation coefficient of 0.05 or more are extracted.

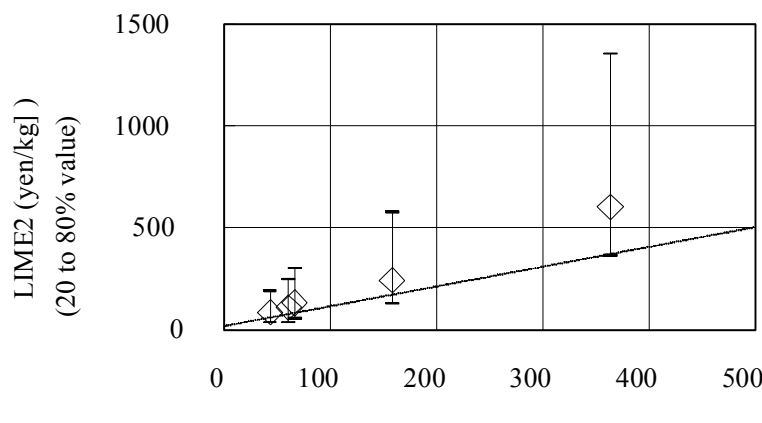


Figure 2.3-13: Comparison between LIME1 and LIME2 (acidification (social assets))

Table 2.3-15: Acidification damage factors

Acidifying causative substance	SO ₂	NO _X		HCl	NH ₃
		NO	NO ₂		
Damage factor	Social assets (Yen/kg)	108.5	134.4	85.8	243.7
	Primary production (kgDW/kg)	0.301	0.365	0.238	0.853
Because a damage calculation model that combines amounts of damage to wood production and fishery production is used for uncertainty analysis concerning social assets, the total representative value of damage functions for wood production and fishery production is not the same as the representative value for social assets.					

2.3-4 Procedure for impact assessment of acidification

Concretely, the procedures for characterization and impact assessment of acidification can be carried out as described below.

Users can select what is suitable for their purpose from among characterization, damage assessment, and integration, and use it for LCA.

The characterization result $CI^{Acidification}$ can be obtained from $Inv(X)$, the inventory of an acidifying causative substance X , and $CF^{Acidification}(X)$, the characterization factor.

$$CI^{Acidification} = \sum_X CF^{Acidification}(X) \cdot Inv(X) \quad (2.3-21)$$

There are several lists of the characterization factor $CF^{Acidification}(X)$. Under LIME, the characterization factor DAP was recommended because it is based on the environmental conditions in Japan and has been obtained through quantitative linkage from occurrence and deposition. $CI^{Acidification}$ is regarded as the total emissions of the acidifying causative substance converted into SO₂, a typical causative substance.

In addition, the damage assessment result $DI(Safe)$ can be obtained from $Inv(X)$ of each acidifying causative substance and $DF^{Acidification}(Safe, X)$, the damage factor for each area of protection $Safe$.

$$DI(Safe) = \sum_X DF^{Acidification}(Safe, X) \cdot Inv(X) \quad (2.3-22)$$

$DI(Safe)$ means the potential amount of damage to each area of protection $Safe$ due to emissions of the acidifying causative substance. This equation enables damage assessment concerning social assets and primary production. With regard to common areas of protection, comparison and integration with amounts of damage that occur through different impact categories are possible.

$IF^{Acidification}(X)$, the factor that integrates impacts on social assets and primary production, is used for integration. The single index SI can be obtained from each acidifying causative substance's $Inv(X)$ and the integration factor $IF^{Acidification}(X)$. The obtained result can be directly compared and added with the assessment results of other impact categories.

$$SI = \sum_X \{IF^{Acidification}(X) \cdot Inv(X)\} \quad (2.3-23)$$

Appendices A1, A2, and A3 show the characterization factor $CF^{Acidification}(X)$, the damage factor $DF^{Acidification}(Safe, X)$, and the integration factor $IF^{Acidification}(X)$, respectively.

[References for Section 2.3]

- Aber JD, Nadelhoffer KJ, Steudler P, Melillo JM (1989): Nitrogen saturation in northern forest ecosystems, BioScience, 39: 378-386
- Amman, et al (1996): Cost-effective control of acidification and ground-level ozone. Second interim report to European Commision, DG-XI, IIASA, Luxembourg
- Batjes, N.H. (1995): A Global Data Set of Soil pH Properties. Technical Paper 27, International Soil Reference and Information Centre (ISRIC)
- Berrett, et al (1996): Transboundary Air Pollution in Europe. Research Report 32, EMEP/MSC-W, Report 1/96, Oslo
- FAO-UNESCO (1990): Soil Map of the World
- Hayashi K, Okazaki M, Itsubo N, Inaba A (2004): Development of Damage Function of Acidification for Terrestrial Ecosystems Based on the Effect of Aluminium Toxicity on Net Primary Production. Int J LCA, 9: 13-22
- Hauschild M, Wenzel H (1998): Environmental Assessment of Products. Volume 2: Scientific background. Chapman & Hall, London
- Heijungs R, Guinee J, Huppes G, Lankreijer RM, Udo de Haes HA, Wegener Sleeswijk A, AMM Ansems, PG Eggels, R van Duin, HP de Goede (1992): Environmental Life Cycle Assessment of products. Guide and Backgrounds. CML, Leiden University, Leiden
- Hesthagen T, Sevaldrud IH, Berger HM (1999): Assessment of Damage to Fish Populations in Norwegian Lakes Due to Acidification, Ambio, 28: 112-117
- Hogan LM, Beal RT, Hunt RG (1996): Threshold Inventory Interpretation. Methodology - A Case Study of Three Juice Container Systems, Int. J. LCA, 1: 159-167
- Huijbregts MAJ (1999): Life cycle impact assessment of acidifying and eutrophying air pollutants: Calculation of equivalency factors with RAINS-LCA, Interfaculty Department of Environ., Sci., Faculty of Environ., Sci., Univ. of Amsterdam
- ICP Materials (2001): Main Centre web page, Swedish Corrosion Institute, <http://www.corr-institute.se/ICP-Materials/>
- Ikuta K, Yada T, Kitamura S, Ito F, Yamaguchi M, Nishimura T, Kaneko T, Nagae M, Ishimatsu A, Iwata M (2000): Recent Studies on the Effects of Acidification on Fish in Japan, Global Environ. Res., 4: 79-87
- Lindfors LG, Christiansen K, Hoffman L, Virtanen Y, Juntilla V, Leskinen A, Hansen OJ, Ronning A, Ekwall T, Finnveden G (1995): LCA-NORDIC Technical Reports No. 1-9, Nordic Council of Ministers, Copenhagen

Nichols, et al (1996): In Towards a Methodology (Udo de Haes ed.), SETAC—Europe, Brussels

Pierzynski GM, Sims JT, Vance GF (1994): Soil Nitrogen and Environmental Quality, In Soils and Environmental Quality, CRC Press, p.55-102

Posch M, Hettelingh J-P, de Smet PAM, Downing RJ (1997): Calculation and Mapping of Critical Thresholds in Europe, CCE Status Report 1997, RIVM, Bilthoven

Potting J, Hauschild M (1997): Predicted Environmental Impact and Expected Occurrence of Actual Environmental Impact Part II: Spatial Differentiation in Life-Cycle Assessment via the Site-Dependent Characterization of Environmental Impact from Emissions, Int. J. LCA, 2 (4): 209-216

Rombough, P.J. (1983): Effects of Low pH on eyed embryos and Alevins of Pacific Salmon . Can.J.Fish.Aquat.Sci., 40: 1575-1582

Sverdrup, H., Warfvinge, P.(1993): The effect of soil acidification on the growth of trees, grass and herbs as expressed by the (Ca+Mg+K)/Al ratio, Reports in ecology and environmental engineering, Lund, Sweden, p. 177

Ikuta K (1999): Impact of Land Water Acidification on Fishes, Journal of Japan Society on Water Environment, 22: 181-185

Ikuta K, Kashima T, Oda S, Okumoto N (1992): Acid-Resistance Assessment of the Eyed Eggs and Fry of Salmonidae, Bulletin of National Research Institute of Aquaculture, 21: 39-45

Ikeda Y, Higashino H (1997): Measurement of Deposition of Acidifying Droppings in East Asia (ii), Journal of Japan Society for Atmospheric Environment, 32 (3): 175-186

Ikeda Y et al. (2001): Establishment of a Comprehensive Method for Control of Emissions of Air Polluting Substances in the Whole East Asia, Report on Research Results for FY1997 to FY2000 Scientific Research Subsidies (Basic Research (B) (1))

Ichikawa Y (1998): Long-Distance Transportation of Acid Substances, Journal of Japan Society for Atmospheric Environment, 33: A9-18

Izuta T (2001): Nitrogen Saturation in the Forest Ecosystem and Its Impact on Trees, Journal of Japan Society for Atmospheric Environment, 36: A1-13

Iwaki H (1981): Regional Distribution of Phytomass Resources, Environment Information Science, 10: 54-61

Umemura H (1968): Podsol Soil on the Central High Mountain Range in Japan, Pedologist, 12 (2): 110-117

Okita T (1982): Atmospheric Conservation Science, Sangyo Toshō

Ohrui K (1997): Nitrogen Saturation in the Forest Ecosystem, Forest Environment, 39: 1-9

Okazaki M: private letter

Ochiai A, Tanaka M (1986): Ichthyology (New Edition) (Vol. 2), Koseisha Koseikaku, p. 1140

Ministry of the Environment (1999): Natural Environment Information GIS, CD-ROM

Ministry of the Environment (edit.) (2002): Handbook of Groundwater Pollution Measures by Nitrate Nitrogen, Environmental Research and Control Center

Ministry of the Environment (supervised) (1993): Acid Rain Science and Measures, Maruzen

Ministry of the Environment (supervised) (1998): Yearbook of National Water Quality 1998, Fuji Research Institute

Kannari A, Baba T, Hayami H (2001): Estimation of Ammonia Emissions in Japan, Journal of Japan Society for

Atmospheric Environment, 36: 29-38

Japan Meteorological Agency (1996): Normal Values (Mesh Statistical Values) Observed by Japan Meteorological Agency, CD-ROM

Kitagawa Y (1966): Clay Mineral in Podsol Soil in Sarufutu, Hokkaido, Pedologist, 10: 11-17

Kitano F, Nakano S, Maekawa K, Ono Y (1995): Impact of Water Temperature on the Stream Distribution of River Dolly Varden and Prediction of Shrinkage of Biotope due to Global Warming, Wildlife Conservation, 1: 1-12

Kozuki S, Higashi T (1997): Typification of Forest Soil in Japan from Soil Organic and Inorganic Ingredient Amounts by Use of Multivariate Analysis and Evaluation of Each Component of Proton Consumption of Forested Soil in Japan, Journal of Japanese Society of Soil Science and Plant Nutrition, 68 (3): 272-284

Kawano Y, Umezawa T, Morakoshi M (1998): Impact and Critical Point of Ca/Al on the Growth of Cedar, Japan Cypress, and Spanish Mackerel under the Condition of Inference Cultivation, Journal of Japan Society for Atmospheric Environment, 33 (6): 335-343

National Land Development Technology Center (ed.) (1993): Groundwater Research and Observation Guidelines (draft), Sankaido, p. 110-111

Ministry of Land, Infrastructure, Transport and Tourism (2002): National Land Numerical Information Land Use, National and Regional Planning Bureau of Ministry of Land, Infrastructure, Transport and Tourism

Komeji T (1993): Impact of Air Pollution on Cultural Assets, Journal of Japan Society for Atmospheric Environment, 28: A103-111

Sapporo Salmon Museum

Committee for Acid Rain Measures (2004): Comprehensive Report on Acid Rain Research, CD-ROM

Shioiri M (1934): Chemical Research on Gelatinous Substance of Clay in Soil, Japan Academic Association Report, 10 (3): 694-699

Shigaki M (edited and written) (1998): Illustrated Waste Incineration Technology [2nd Revision], Ohmsha, p. 86

Planning and Research Division, Director-General's Secretariat, Agency for Natural Resources and Energy (ed.) (2000): General Energy Statistics, Tsusho Sangyo Kenkyusha

Japan Waste Management Association, Japan Waste Management Research Foundation (1999): Guide to Planning and Designing of Waste Disposal Facilities, p. 138

Statistics Bureau of Management and Coordination Agency (ed.) (each fiscal year): Statistics in Japan, Japan Statistical Association

So Y, Kohira T, Oakazaki M (1999): Case Study on the Impact of Acidic Deposition of Acidifying Droppings on Cedar, Japanese Cypress, and Quercus Serrata on Kazusa Hills, 13th Anthology of Environment Information Science Treatises, Center for Environmental Information Science, p. 263-268

Tanaka Y, Nakanishi J (1998): Application of Ecological Models to Ecological Risk Analysis – Effectiveness of Extrapolation and Life History Sensitivity Analysis, Journal of Water and Environment Technology, 21: 616-623

Center for Global Environmental Research (2000): Monthly Mosaic Diagram of Vegetation Indices in East Asia, CD-ROM, National Institute for Environmental Studies

Geological Survey of Japan (ed.) (1995): One-Millionth Geological Map of Japan, CD-ROM

Totsuka M (1996): Impact of Acid Droppings on the Forest Ecosystem, Acid Rain – Compound Effect and Impact of the Ecosystem – (new edition) (supervised by Okita), Hakuyusha, p. 163-181

Nagata Y, Hosoya K (ed.) (1997): Current Situation and Systematic Conservation of Rare Freshwater Fishes in Japan (supervised by Ichthyological Society of Japan), Midoro Shobo, p. 379

Nakaminami H (2000): Study on Measures to Control the Transportation and Emissions of Sulfur Compound in East Asia – Centering on China's Control Measures, Master's Thesis, Graduate School of Environmental Science and Technology, Osaka Prefecture University

Japan Fisheries Resource Conservation Association (1981): Material on Ecology of Aquatic Organisms, p. 361

Japan Society of Soil Science and Plant Nutrition (ed.) (1994): Low pH Soil and Plants, Hakuyusha

Nouchi I (1996): Impact of Acid Rain on Farm Products, Acid Rain – Compound Effect and Impact of the Ecosystem – (new edition) (supervised by Okita), Hakuyusha, p. 233-251

Forestry Research Institute of Ministry of Agriculture and Forestry (1968): Collection of Cross-Section Drawings of Forest Soil 2, p. 84

Statistics and Information Department of Ministry of Agriculture, Forestry and Fisheries (each fiscal year): Annual Statistics of Fishery and Fish Culture 2003, Norin Tokei Kyokai

Statistics and Information Department of Ministry of Agriculture, Forestry and Fisheries (2001): Report on Supply and Demand of Lumber 2000

Hayashi K, Okazaki M (2003): Development of a Regional Screening Method by the Use of the BC/Al Ratio as the Index Concerning the Possibility of Forest Decline due to Acidic Deposition – Case Study in South Kanto, Journal of Society of Environmental Science, 16: 377-392

Fujita S, Sotooka Y, Ohta I (1992): Estimation of Emissions of Sulfur Dioxide from Volcanoes in Japan, Journal of Japan Society for Atmospheric Environment, 27 (6): 336-343

Fujita S, Takahashi A, Hayami H, Sakurai T (2000): Wet Deposition of Nitrate Ion and Ammonium Ion in Japanese Islands, Journal of Society of Environmental Science, 13: 491-502

Group of Japanese Pedologists, Committee for Soil Classification and Nomenclature (1990): One-Millionth Soil Map of Japan

Masuda H, Amaoka K, Araga C, Ueno T, Yoshino T (ed.) (1984): Illustrated Guide to Japanese Fishes <Explanation>, Tokai University Press, p. 448

Maruyama A (1995): Comparison of Soil Properties between Sloping Terrains and Sharp Sloping Terrains in Tertiary Areas – Example Seen in Mamurogawa-cho, Yamagata, Pedologist, 35 (1): 12-25

Miyaji H, Kawanabe H, Mizuno N (1976): Illustrated Color Guide to Japanese Waterproof Fishes (fully revised new version), Hoikusha, p. 462

Murano K (1993): Acid Rain and Acid Fog, Shokabo Publishing

Yamatani K (1968): Podsol Soil in Forests in Japan – Centering on the Tohoku Region, Pedologist, 12 (1): 2-11

Li T, Izuta T, Aoki M, Totsuka M (1997): Sole and Multiple Impact of Al and Mn on the Growth and Nutrition of Hydroponically-Cultured Red Pine Seedlings, Journal of Japan Society for Atmospheric Environment, 32 (5): 371-382

Current Situation of Forest Resources, Website of Forestry Agency (as of March 31, 2002)